GEOLOGICAL MODELING IN GIS FOR PETROLEUM RESERVOIR CHARACTERIZATION AND ENGINEERING:

A 3D GIS-ASSISTED GEOSTATISTICS APPROACH

by

Diego A Vasquez

A Thesis Presented to the
FACULTY OF THE USC GRADUATE SCHOOL
UNIVERSITY OF SOUTHERN CALIFORNIA
In Partial Fulfillment of the
Requirements for the Degree
MASTER OF SCIENCE
(GEOGRAPHIC INFORMATION SCIENCE AND TECHNOLOGY)

March 2014

DEDICATION

I wish to dedicate this project to all of the citizens who wish to solve the most challenging scientific problems by implementing cross-disciplinary research and that are determined to make the world a better place.

I would also like to dedicate this to my friends and family who've supported me throughout the project.

ACKNOWLEDGMENTS

I would like to thank all of my committee members for their guidance and support: Dr. Jennifer Swift and Dr. Su Jin Lee from the Spatial Sciences Institute, Dr. Behnam Jafarpour from the Petroleum Engineering Department and Dr. Doug Hammond from the Earth Sciences Department.

I would also like to thank the engineering and geology consultants who have helped provide the necessary data for performing this work and who've provided assistance in the field.

In addition, I would also like to send a big thank you to SPE as well as my fellow colleagues in the Petroleum Engineering, Geology and Geography Departments at USC.

TABLE OF CONTENTS

LIST OF TABLES

LIST OF FIGURES

LIST OF ABBREVIATIONS

3D	Three-Dimensional
AAPG	American Association of Petroleum Geologists
CA	(state of) California
CIPA	California Independent Petroleum Association
DEM	Digital Elevation Model
DOGG	(CA) Division of Oil, Gas and Geothermal Resources
EIA	(U.S.) Energy Information Administration
GIS	Geographic Information Systems
GPS	Global Positioning System
GSA	Geological Society of America
IPAA	Independent Petroleum Association of America
MATLAB	Matrix Laboratory Software
MMbbl	One Million Barrels (of oil)
NSWA	National Stripper Well Association
OCR	Optima Conservation Resources
R	Resistivity
SGeMS	Stanford Geostatistical Modeling Software
SGS	Sequential Gaussian Simulation
SP	Spontaneous Potential
SPE	Society of Petroleum Engineers
SSI	Spatial Sciences Institute
USC	University of Southern California

ABSTRACT

Geographic Information Systems (GIS) provide a good framework for solving classical problems in the earth sciences and engineering. This thesis describes the geostatistics associated with creating a geological model of the Abacherli reservoir within the Mahala oil field of the Los Angeles Basin of Southern California using a variogram-based two-point geostatistical approach. The geology of this study area features a conventional heterogeneous sandstone formation with uniformly inclined rock strata of equal dip angle structurally trapped by surrounding geologic faults. Proprietary electrical well logs provide the resistivity and spontaneous potential at depth intervals of 10' for the thirteen active wells in the study area. The dimensions and shape of the reservoir are inferred from geological reports. An isopach map was georeferenced, digitized and used to generate a 3D point-set grid illustrating the boundaries and the volumetric extent of the reservoir. Preliminary exploration of the input data using univariate and bivariate statistical tests and data transformation tools rendered the data to be statistically suitable for performing ordinary kriging and sequential Gaussian simulation. The geological and statistical characteristics of the study area ensure that these interpolations are appropriate to employ. Three variogram directions were established as part of the variogram parameters and then a best-fit statistical function was defined as the variogram model for each of the two electrical log datasets. The defined variogram was then used for the kriging and simulation algorithms. The data points were interpolated across the volumetric reservoir resulting in a 3D geological model displaying the local distribution of electrochemical properties in the subsurface of

the study area. Data is interchanged between separate modeling programs, Stanford Geostatistical Modeling Software (SGeMS) and Esri ArcGIS, to illustrate the interoperability across different software. Validation of the predictive geostatistical models includes performing a leave-one-out cross-validation for each borehole as well as computing a stochastic model based on the sequential Gaussian simulation algorithm, which yielded multiple realizations that were used for statistical comparison. The reservoir characterization results provide a credible approximation of the general geological continuity of the reservoir and can be further used for reservoir engineering and geochemical applications

CHAPTER ONE: INTRODUCTION

1.1 Background

Geographic Information Systems (GIS) are a very useful way to integrate geology with engineering. Geostatistics in particular is an inherently interdisciplinary branch with direct applications to geology, geography and petroleum engineering practices (Myers 2013). Since geostatistics involves quantitative analysis, modeling and simulation of field data using numerical and analytical techniques it is a core component of petroleum engineering (Dubrule and Damsleth 2001). Due to the focus on modeling of spatial and spatiotemporal datasets measured at geographical locations, geostatistics is also a widely used approach in geography and GIS (Burrough 2001). When geostatistics is applied to petroleum (or hydrology) the focus is on modeling the subsurface environment constrained to the local geology, thus geostatistics is also an important discipline in the earth sciences (Journel 2000). Therefore this research provides a good interdisciplinary opportunity to combine the earth and spatial sciences with petroleum engineering.

1.1.1 Global Objective

A global effort within the scientific community has begun which acknowledges the need for greater capabilities in information management to: 1) satisfy the continuously increasing demand for the discovery, management and sustainability of natural resources, and 2) provide solutions in forecasting natural phenomena for addressing societal challenges (Sinha et al. 2011*)*. One of the main objectives of this research is to promote and contribute to the relatively new but rapidly evolving interdisciplinary field of

geoinformatics. Geoinformatics is the science that uses spatially related information and computational technology systems to address complex problems in the earth, environmental, geographical and related engineering disciplines with the future goal to provide greater availability of data and tools for serving the needs of the public (Awange and Kiema 2013). When GIS-assisted approaches are used to acquire, manage and analyze geo-information in combination with advanced computational techniques, geoinformatics becomes a powerful tool to efficiently integrate different data and improve the way scientific information is processed and presented (Krishna et al. 2010).

The development and implementation of information and computing technology as well as cyberinfrastructure for the earth sciences is expected to help transform the next generation of interdisciplinary research. The shift to the information age (known as the "Digital Revolution") has very significantly affected academia in which earth scientists increasingly rely more on digital data instead of hard copy. Hence the emergence of evolving fields such as geoinformatics will be very important for data-intensive research, especially with the global exchange of information (i.e. the onset of "big data"). Geographic information systems are complex systems that are comprised of different components which have separate functions including data, software/hardware and personnel. When used collectively the components allow for broader approaches to spatial problem solving. GIS usage specializations relevant to this research include remote sensing, programming, global navigation and positioning systems, spatial analysis and modeling, as well as other spatial science disciplines dealing with data visualization and optimization (Wilson and Fotheringham 2008). The data management system of a GIS is typically managed via the use of integrated spatial databases that allow for the

organization of information and the determination of relationships between the data and topology. An illustration of the database which was used as a model for the database for this research and for optimizing field activities, and which contains information about the study area input data and individual oil reservoir wells, is shown in Figure 1. Additional more complex programs that can perform GIS geoprocessing functions (e.g. ModelBuilder) can be used to automate workflows for improving production activities encountered in day-to-day field work.

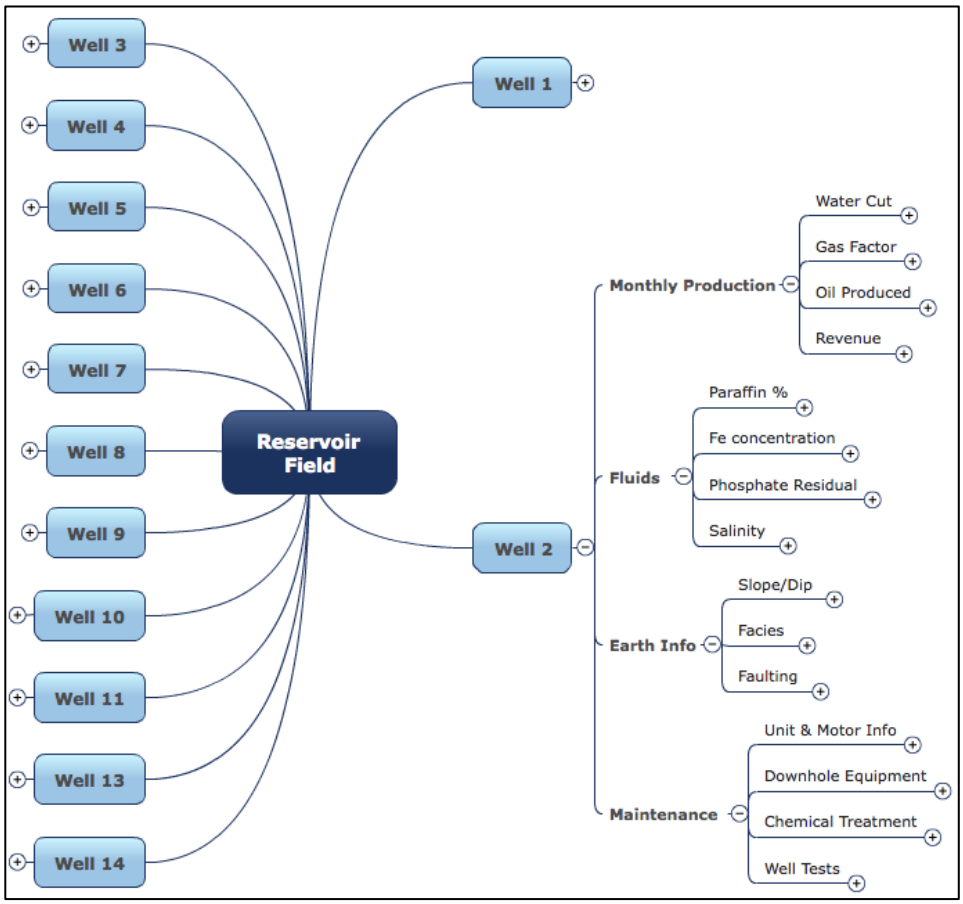

Figure 1: Database design utilized for field services by lease operators (OCR 2014).

1.1.2 Thesis Objective

The primary objective of this thesis project was to develop a volumetric 3D geological model of the petroleum reservoir in the study area using GIS to visualize the subsurface distribution of rock properties shown in Figure 2, the Abacherli reservoir within the Mahala oil field of the Los Angeles Basin of Southern California.

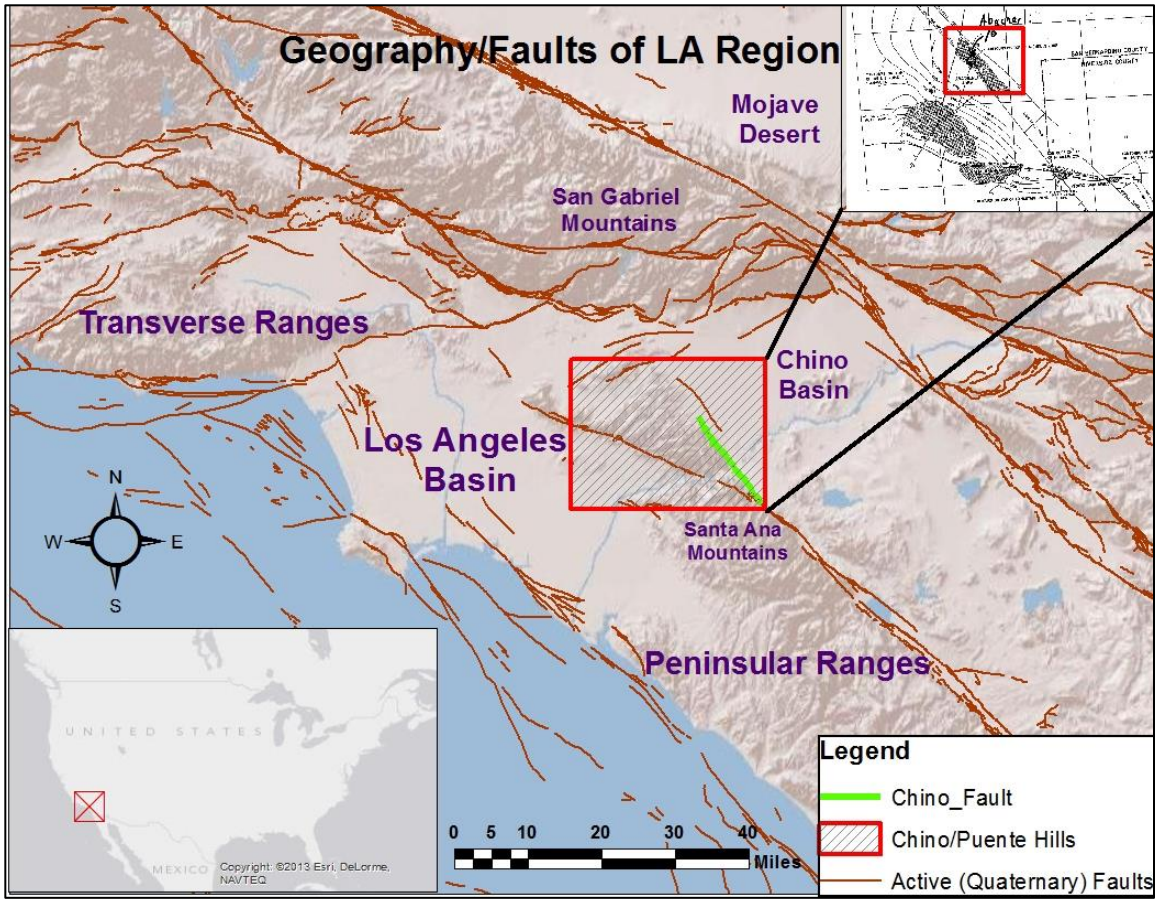

Figure 2: DEM of study area region with active geological faults (based on USGIN 2011)

Interpolation of drilled well or wellbore data involves predicting values of specific variables at unknown locations based on the measurements obtained from known locations using statistical principles, thereby creating a continuous surface of the subsurface field. Earth systems are inherently complex, dynamic and contain various

characteristics that can make reservoir characterization a very burdensome task (Caumon 2010). The inclusion of geological features depends mainly on the depositional environment and defines the overall geological architecture of a given reservoir (Kelkar and Perez 2002). Different geological settings may require different geostatistical approaches (e.g. object-based modeling or variogram-based modeling) in order to construct an appropriate model that honors the form of the reservoir as closely as possible. Stationarity, defined in practice as local data averages within a spatial domain that are approximately constant, is the most important assumption for estimation in geostatistics. Assuming stationarity in a particular region requires that the model developed from the sampled data be applicable within the specified study area. In reservoir analyses this assumption is necessarily subjective because of the inherent uncertainties in the subsurface and the scarcity of data which prevents researchers from being absolutely certain about the subsurface geology of a region in which there is limited wellbore data. In the context of this study, a region of stationarity defines the continuity boundaries for the study area subsurface or "field".

Geostatistics is the discipline concerned with determining the extent of that continuity within the region of assumed stationarity by taking advantage of the notion that values that are closer to one another are more similar than values further away (i.e. as the distance between any two values increases the similarity between the two measurements decreases) (Kelkar and Perez 2002). Following this assumption, geostatistical techniques are aimed at identifying spatial relationships between variables, such as how neighboring values are related to each other, in order to estimate values at separate locations. Provided that field conditions meet the criteria, one reliable approach to define this variability is

through a statistical correlation as a function of distance, known as a variogram. In many cases where geological structures are assumed continuous throughout the reservoir, even if a few discontinuous lithological layers act as baffles, it is appropriate to assume that the reservoir can be modeled as a whole by the use of variogram-based modeling. Figure 3 illustrates a typical petroleum deposit scheme in which oil and gas are generated at the source, migrate in direction of least resistance and are subsequently trapped and accumulated to form petroleum reservoirs.

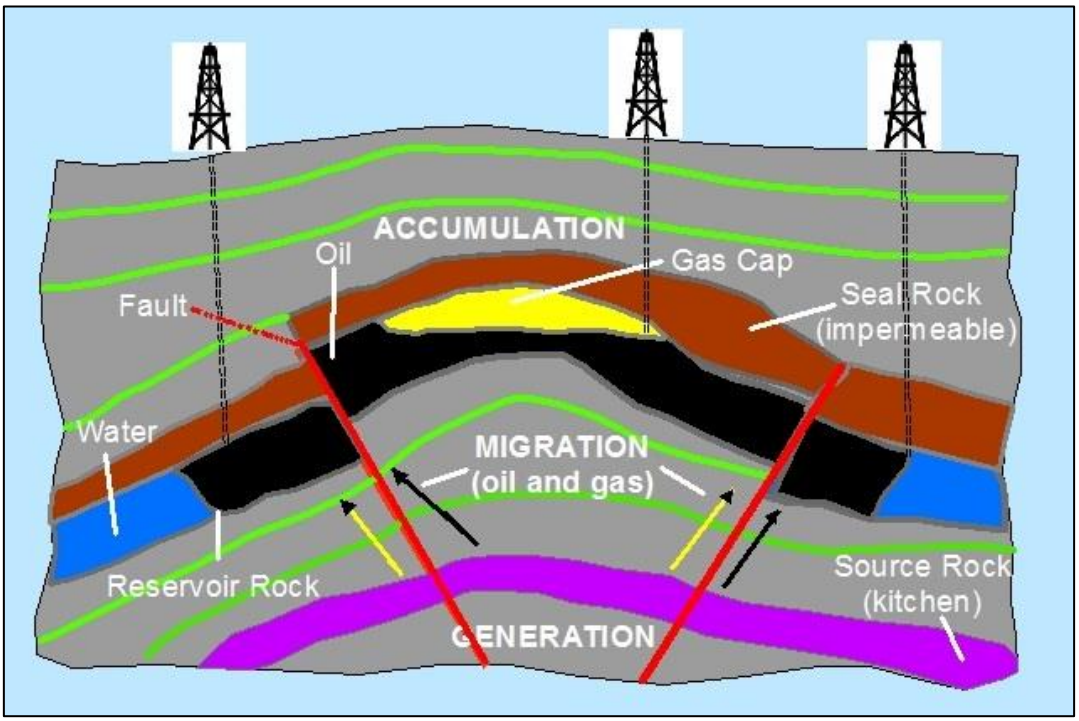

Figure 3: Digitized hydrocarbon deposit system (based on AAPG UGM SC 2011)

1.2 Analysis Review

1.2.1 Kriging Review

Kriging is a widely used conventional estimation technique that is based on a linear estimation procedure expected to provide accurate predictions of values within a volume, over an area or at an individual point within a specified field. In earth science, kriging is a favored interpolation approach compared to other methods because of its ability to include the anisotropy that rock layers of a sedimentary material exhibit in geological formations, thus the models that are obtained via the use of kriging have more resemblance to the true field geology (SPE PetroWiki 2013). This is in part because the linear-weighted averaging methods used in kriging techniques depend on direction as well as orientation, instead of only depending on distance as other interpolation methods do. The fundamental principle in any kriging technique is that an unknown value at an unsampled point is estimated by the product of a weighted average of neighboring values, as explained by the following simplified expression:

$$X^*(\vec{u}_0) = \sum_{i=1}^{n} \lambda_i X(\vec{u}_i) \qquad \text{(Equation I obtained from Kelkar and Perez 2002)}$$

Where $X(\vec{u}_i)$ = value at neighboring location $(\vec{u}_i)$, λ_i = weight of neighboring value and $X^*(\vec{u}_0)$ = estimated value at unsampled location. The estimation procedure calculates the weights (λ_i) assigned to neighboring locations, which depend on the spatial relationship between unsampled points and neighboring values as well as the spatial relationship between neighboring points (Kelkar and Perez 2002). The relationships are obtained via the use of a variogram model.

Variations between the different types of variogram-based kriging methods available are different depending by how the mean value is determined and used in the interpolation (SPE PetroWiki 2013). Ordinary kriging is by far the most commonly used kriging approach that allows for the local mean to vary and be re-estimated based on nearby (local) values thereby easing the assumption of first-order stationarity (Kelkar and Perez 2002). Ordinary kriging is better suited for this type of analysis because a true stationary global mean value for data in a reservoir is typically unknown and it cannot be assumed that the sample mean is the same as the global mean. This is due to the fact that in any real reservoir the local mean within a neighborhood in the field can easily vary over the spatial domain.

Ordinary kriging is deemed appropriate and used as the estimation technique in this analysis. Nevertheless, it is important to consider three other types of kriging techniques, which include simple kriging, universal kriging and cokriging. As the name suggests simple kriging is the mathematically simplest technique where a known stationary mean must be assumed over the entire spatial domain or study area. However, it is unrealistic to assume that we know the exact mean for all the data locations in the field given the degree of uncertainty in the subsurface geology, therefore this technique was not applied in this study. The universal kriging model assumes that there is a general polynomial trend. However the data is not known to exhibit a trend in a particular direction and there is no scientific justification to describe a potential trend, so universal kriging was not deemed to be more appropriate either. Cokriging is a type of kriging technique that uses spatial correlations from different data variable types to estimate the values at unsampled locations. In addition to estimating the values at unsampled locations

with surrounding samples of the same variable type (e.g. porosity), cokriging also uses the surrounding samples from different variables (e.g. permeability) provided the assumption that both variable types are spatially correlated to each other (Kelkar and Perez 2002). Taking advantage of the covariance between two or more spatially related variables, and in theory providing a greater ability to make better predictions, cokriging is an attractive as well as commonly used approach. Nevertheless, the applicability of cokriging to a particular field depends on if the objective is to provide a stronger prediction of a more undersampled variable relative to a more well-sampled variable given a strong correlation between the two variables. For example, if permeability values were derived from core samples for only a few wells, say 4 or 5, but electrical log values were obtained for all of the 13 wells and assuming spatial relationships between the cores and logs, then it would be most appropriate to "cokrige" the permeability samples with the resistivity/spontaneous potential to provide a better permeability distribution model. But because both electrical properties in this study, spontaneous potential and resistivity ("SP" and "R"), are adequately sampled, it was decided that cokriging analysis would not be included. Nevertheless performing cokriging between SP and R as an additional analysis in the future may provide useful results and information.

1.2.2 Simulation Review

Another approach besides conventional estimation techniques such as kriging to characterize heterogeneous reservoirs is the use of geostatistical conditional simulation techniques. One of the primary differences between the two is that simulation methods preserve the variance observed in the data by relaxing some of the constraints of kriging,

as opposed to only preserving the mean value. Conditional simulation is a type of variation of conventional kriging and is a stochastic modeling approach that allows for the calculation of multiple equally probable solutions (i.e. realizations) of a regionalized variable by simulating the various attributes at unsampled locations, instead of estimating them (SPE PetroWiki 2013). A "conditional" simulation is conditioned to prior data, or in other words the hard or raw data measurements and their spatial relationships such as a variogram are honored. By providing several alternate equiprobable realizations this approach helps represent the true local variability thereby helping to characterize local uncertainty. This is one of the most useful properties of a simulation because all models are subject to uncertainty, in particular geological models because they are based on partial sampling. This is especially true of reservoir models due to the several different sources of uncertainty.

Provided that the true value of a geological attribute is a single number but that exact value is always unknown because of the uncertainty in the field, the practice in statistical modeling is to transform the single number into a random variable, a variate, which is a function that specifies its probability of being the true value for every likely outcome. The two main types of conditional simulation methods are either grid-based (a.k.a pixel-based) which operate one cell (or point) at a time, or are object-based which operate on groups of cells arranged within a discretized geologic shape (SPE Petrowiki 2013). During each individual run the corresponding realization starts with a unique random 'navigational path' through the discretized volume providing the order of cells (or points) to be simulated. Because the 'path' differs from each realization-to-realization the results provide differences throughout the unsampled cells which yield the local

changes in the distribution of rock properties throughout the reservoir that are of interest for accurate geological representations. For example, in this study running several realizations produced several values per variate, which then allowed for a graphical representation of the results and an approximation of the variates (Olea et al. 2012). The method used in this study is the grid-based approach because of the geological assumption that the geologic facies vary smoothly enough across the reservoir (typical depositional setting of shallow marine reservoirs) as opposed to sharp changes in the shape of the sedimentary body. Furthermore, there are different types of simulation methods including annealing simulation, truncated Gaussian simulation, turning bands simulation and sequential simulation. Sequential simulation methods are some of the most widely used in practice and are kriging-based methods where unsampled locations are sequentially and randomly simulated until all points are included. The order and the way that locations are simulated determine the nature of the realizations. There are three types of sequential-simulation procedures, including Bayesian indicator, sequential Gaussian, sequential indicator. These are based on the same algorithm but with slight variations. Sequential Gaussian Simulation (SGS) is one of the most popular, it assumes the data follow a Gaussian distribution. Because SGS is best suited for simulating continuous petrophysical variables (e.g. resistivity, spontaneous potential, porosity, permeability) it is deemed most appropriate for this study and thus was used as the simulation method, detailed in Chapter 4.

1.2.3 Interpolation Comparison

Both conventional estimation (kriging) and stochastic modeling (sequential Gaussian simulation) techniques are well proven, but slightly different, approaches to describe the natural processes and attributes of geological phenomena, in this case the characterization of a petroleum reservoir. A useful addition is to use both of them in a study to compare and contrast. To recap the main differences between the two: 1) kriging provides an estimation of the mean value and its standard deviation at an individual point given that the variate is represented as a random variable that follows a Gaussian distribution, and 2) SGS selects a random deviate from the same Gaussian distribution instead of estimating the weighted mean at each point where the simulation is selected according to a uniform random number that represents the probability level (Halliburton-Landmark Software 2011). When including the simulation approach the natural variability of the local geology counters the blunt smoothing effects of kriging. From the multiple equiprobable realizations obtained it is possible to characterize uncertainty by comparing a large number of realizations. Assuming the model is representative of the field then the true value is expected to fall within the bounds of the probability. Quantification in terms of probability can be made, for example finding the mean value of the distribution which corresponds to the highest probability. Both approaches complement each other and are used in the analysis performed as part of this thesis research. The mathematical details of these methods are extensive and beyond the scope of this report. More detailed information on the mathematical and statistical expressions can be accessed from additional text available in the literature (e.g. McCammon 1975; Chiles and Delfiner 1999; Kelkar and Perez 2002).

1.3 Motivation

1.3.1 Applicability to Petroleum Engineering and Petroleum Geology

Applied geostatistics for geological modeling and simulation is essential for successful oil and gas production. Reservoir characterization includes determining the distribution, or the closest possible approximation, of subsurface properties of a geologic system in a petroleum field. This is essential information for improving resource management, production development and field operations (Gorell 1995). Geologic outputs obtained from geostatistical models are used in a variety of important applications for petroleum and similarly for groundwater resources, including exploration, reservoir engineering and environmental remediation (Nobre and Sykes 1992). Having a thorough geostatistical model is very important when it is used in reservoir simulators, inverse models and geochemical models. Reliable geological models based on geostatistics can be used for specific practices such as calculating oil production rates, remediating contaminated aquifers, estimating the recoverable reserves (i.e. oil, gas or water), drilling new boreholes and determining hydrocarbon migration (Deutsch 2006). The combined use of geostatistical, simulation and inverse models enable effective reservoir engineering. This provides the opportunity to predict field performance and further understand reservoir behavior, which in turn furthers the ultimate goal of optimizing production and maximizing hydrocarbon recovery (Coats 1969). Reservoir engineering as a sub-discipline has grown exponentially with the onset of digital technologies and computers capable of performing larger and more complex sets of calculations. Because of this "reservoir simulation revolution" and the increasing demand for energy, geostatistical

modeling will remain a key engineering tool in natural resource development (Stags and Herbeck 1971).

The schematic diagram provided in Figure 4 illustrates the general workflow cycle of the "field" from a reservoir engineering perspective. First a geostatistical model (geological continuity) is developed and input into a fluid flow model (reservoir simulator) that predicts field production, then an objective function (inverse model) is developed to integrate dynamic data (field observations) and adjust the necessary parameters (history match) until the simulations are reasonably close to the observations. The complete process assists in the validation of all model(s) included in a given analysis, thus providing the opportunity to achieve a validated decision-making tool ensuring that optimal field performance is achieved in the future.

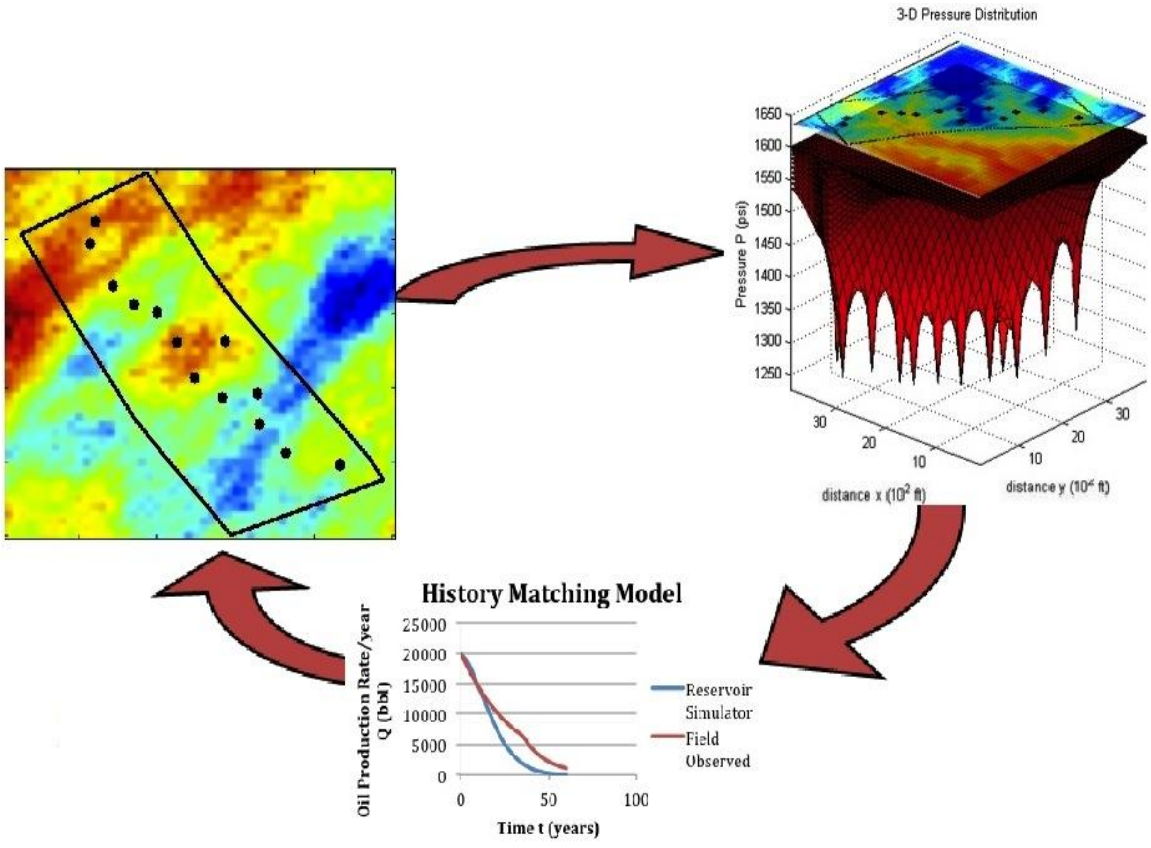

Figure 4: Reservoir engineering results illustrating reservoir characterization/simulation scheme.

1.3.2 Importance of the Energy Industry

The energy industry is an extremely important part of the Unites States economy and will remain a key component for economic growth in the following decades. Petroleum is currently the most important player in the energy industry and is expected to continue to be the main source of energy throughout our human timescale. Petroleum affects virtually every aspect of the industrialized world and is found in most synthesized materials in use today, from the fuel we use (cars, jets, boats) to our electronics and beauty products. Therefore, control of this resource is imperative for the development and stabilization of human well-being (Ranken Energy 2014). In 2011 the U.S. consumed an estimated 18.8 MMbbl/day plus around 19.1 MMbbl/day of refined petroleum products, or around 22% of the global production, making it the largest consumer in the world (EIA 2012). Recent resurgence in domestic oil and gas production has led to a remarkable oil boom, in great part due to the use of advanced recovery technologies for the extraction from unconventional resources. This is dramatically transforming the nation's energy market and has put the U.S. on the verge of becoming the world's largest oil producer (Thompson 2012). In 2012 the U.S. experienced the largest increase in the world of crude oil and natural gas production, providing extraordinary opportunities for independent producers in the upstream industry (Bell, Julia 2013). Independent oil companies operate most of the national oil production, accounting for around 42% offshore and 72% onshore (averaging 68%) (PolitiFact 2014). Approximately 80% of the domestic oil wells in the U.S. are classified as stripper wells (i.e. wells yielding $\leq$ 10 bbl./day), and production from stripper wells makes up about 20% of the total domestic production (NSWA 2014). Furthermore the U.S. is the only country with significant stripper well

output. The production from independent companies in California alone comprises around 70% of total oil and 90% of gas production in the state with a fair share coming from small to midsized companies (CIPA 2014). Therefore crude oil production from independent sources will continue to play an imperative role on the road to energy independence and economic stability. It is important to mention that the amount of oil extracted during primary oil recovery, especially with outdated practices used in the mid-20th century, typically only ranges between 5-15% of the total recoverable oil. When combined with secondary or tertiary recovery production may only reach between 40-60% of the total oil reserves (Tzimas et al. 2005). Since mature oil fields such as the Abacherli reservoir in the Mahala field have only been subjected to primary recovery using outdated technology, much interest and investment is focused on reviving these old fields, which are guaranteed to retain most of their extractable reserves still intact. With innovative solutions and growing technology, mature oil fields including the Mahala have the potential to become significant contributors to the national oil and gas boom, especially with the use of functional operations such as: horizontal drilling, hydraulic fracturing, gas injection and other enhanced oil recovery techniques. Mature reservoirs produce more than 80% of the world oil production. In addition, the rate of production from new (non-mature) discoveries has consistently dropped since the turn of the century (Alvarado and Manrique 2010; Delshad, Mojdeh 2013; EOIR 2013). Therefore mature reservoirs and associated stripper wells comprise an essential part of the energy industry, so increasing production from these assets is very important for ensuring economic security and meeting the growing energy demand. As part of an old large oil field with the vast majority of its recoverable reserves still in play, the Abacherli reservoir in the

Mahala oil field is a good candidate for evaluation and revival. The social motivation of this work and contribution to society is providing computational results for the management of an indispensable natural resource, petroleum. Because of the interconnection between the energy industry with the economy as well as public and political interests, this research project could have a significant impact on the economy. Information derived from this study will be used to take action and make substantial improvements in oil reservoir extraction from the Abacherli reservoir in the Mahala oil field in the future. Lastly, the academic motivation of this work is to help contribute to the rapidly evolving cross-disciplinary research between the natural and applied sciences.

CHAPTER TWO: STUDY AREA

2.1 Geography

2.1.1 Physical Geography Overview of Study Area

This project evaluates the Abacherli reservoir within the Mahala oil field of the Los Angeles Basin of Southern California, shown in Figure 2. Situated between the intersection of Los Angeles, Riverside, Orange and San Bernardino county lines, the reservoir is part of the Chino Hills highlands and immediately connected to the Chino Hills State Park. Based on distance calculations obtained from field observations using GPS/GIS tools, the Abacherli lease is estimated to have a total surface area measuring approximately 1.0 km^2 and a rugged terrain with variable elevation ranging from 500' to 1,200' above sea level, consisting of hills dissected by deep canyons. The study area field is geographically located on the southern Californian pacific coast of the North American Cordillera, which is the major mountain chain extending throughout the western continent.

Along the American west coast are numerous major mountain ranges known collectively as the pacific mountain system. In southern California, more specifically, there are collections of different mountain ranges including the Peninsular Ranges and the Transverse Ranges. The ecology of this region is typical of terrestrial ecosystems of southern California, transitioning from coastal to the desert environments and consisting mostly of shrubland (e.g. chaparral) and woodlands (Schoenherr 1992). The Santa Ana Mountains, part of the Peninsular Ranges, are a north-south trending range that geographically and geologically divide Los Angeles, marking the easternmost border of

the LA basin and county. Within these mountains, the Chino Hills highlands mark the beginning of the Santa Ana range from the north. The Chino Hills are the foothills to the southern section of the east-west trending San Gabriel Mountains of the Transverse Ranges and act as a bridge connecting the Peninsular Ranges to the south, with the Transverse Ranges to the north immediately adjacent to the Puente Hills (California State Parks 2013). The location of Chino Hills is of geographic importance because of its relation to major metropolitan cities and its connection to mountain ranges, ecosystems and local watersheds. In fact, the southeastern part of the study area extends into the Santa Ana River valley. The map provided in Figure 2 displays the major geologic faults of the region overlain on a digital elevation model (DEM) that further illustrates the topography of the study area. Figure 5 illustrates the oil fields within the Los Angeles Basin of southern California. The significant deposits of petroleum in the region can be attributed to the deposition of organic-rich sediments in the basin and their effective accumulation in part due to the major geologic forces at work, such as faulting, folding.

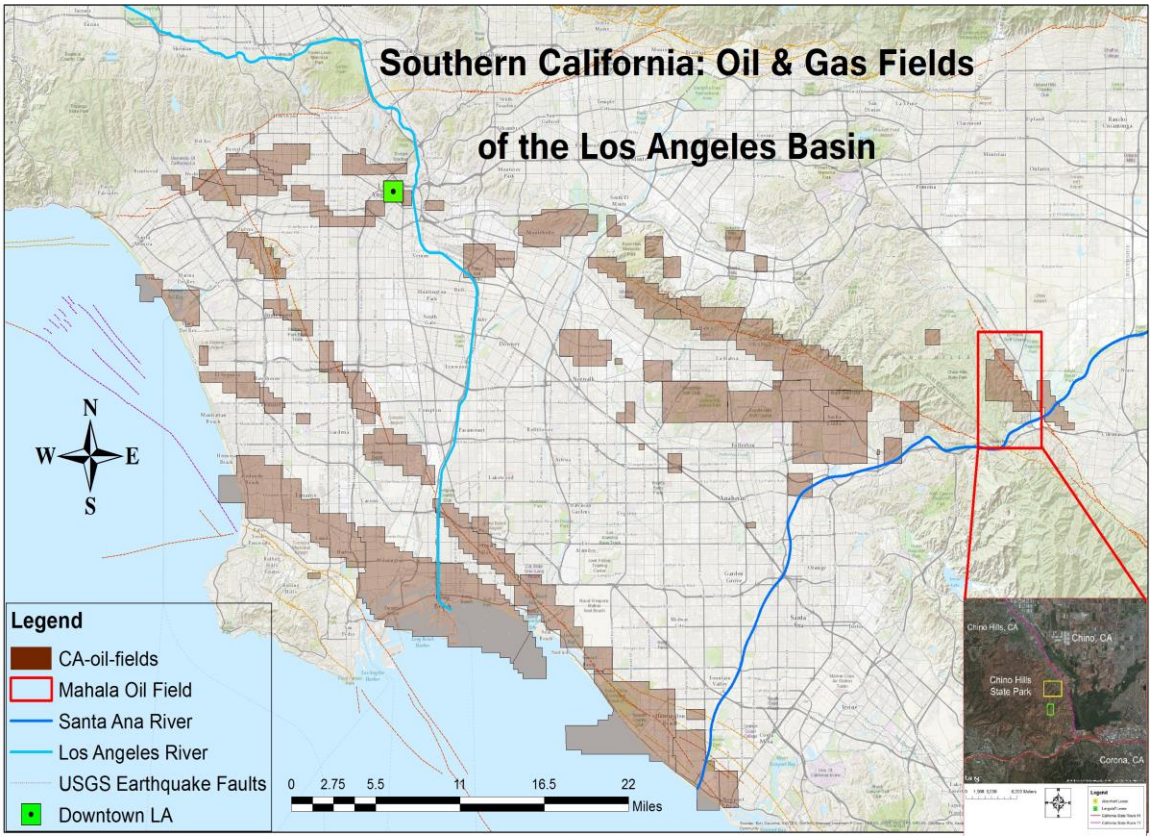

Figure 5: Oilfields of the Los Angeles basin (based on DOGG 2013)

2.2 Geology

2.2.1 Geological Setting

The following geologic map, Figure 6, of Southern California illustrates some of the overall bedrock and lithology of the region.

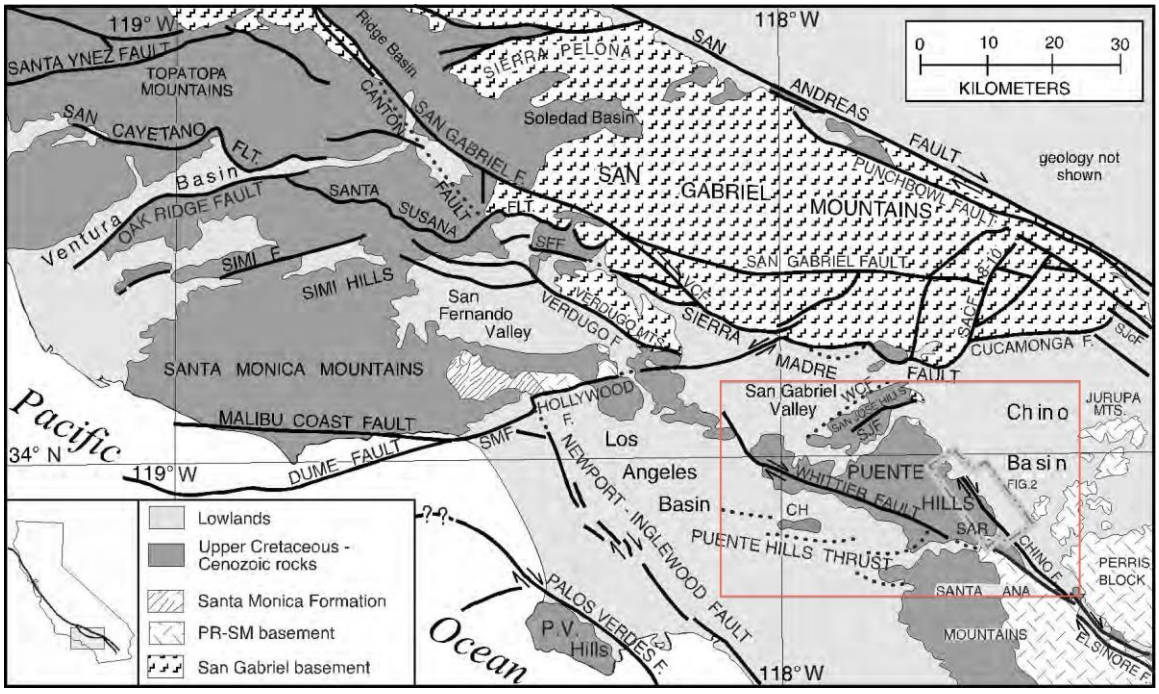

Figure 6: Geology of Southern California study area region (Madden and Yeats 2008)

Regional geographic features and landscapes are shaped by California's complex but young and active geology. Active tectonic forces have resulted in dominant fault zones where structural formations have allowed for the large accumulation of hydrocarbons. Southern California in particular is in a pivotal location where a great continental transform fault (San Andreas) divides two of the world's major tectonic plates. Energy released from geological activity along these plates has resulted in massive stress fields that have triggered the generation of several faulting and folding mechanisms (Wright, Thomas 1987). The two most important structural mechanisms that are responsible for the formations of the Mahala oil field are the Whittier and Chino faults; these are the two upper segments that branch off of the major Elsinore Fault Zone, which is part of the trilateral split of the intercontinental San Andreas Fault system (Figure 2). There are four known and producing reservoirs in the Mahala oil field, listed as follows:

Mahala, West Mahala, Prado Dam and Abacherli, and there are an additional three known reservoirs in the vicinity of the field as shown in Figure 7.

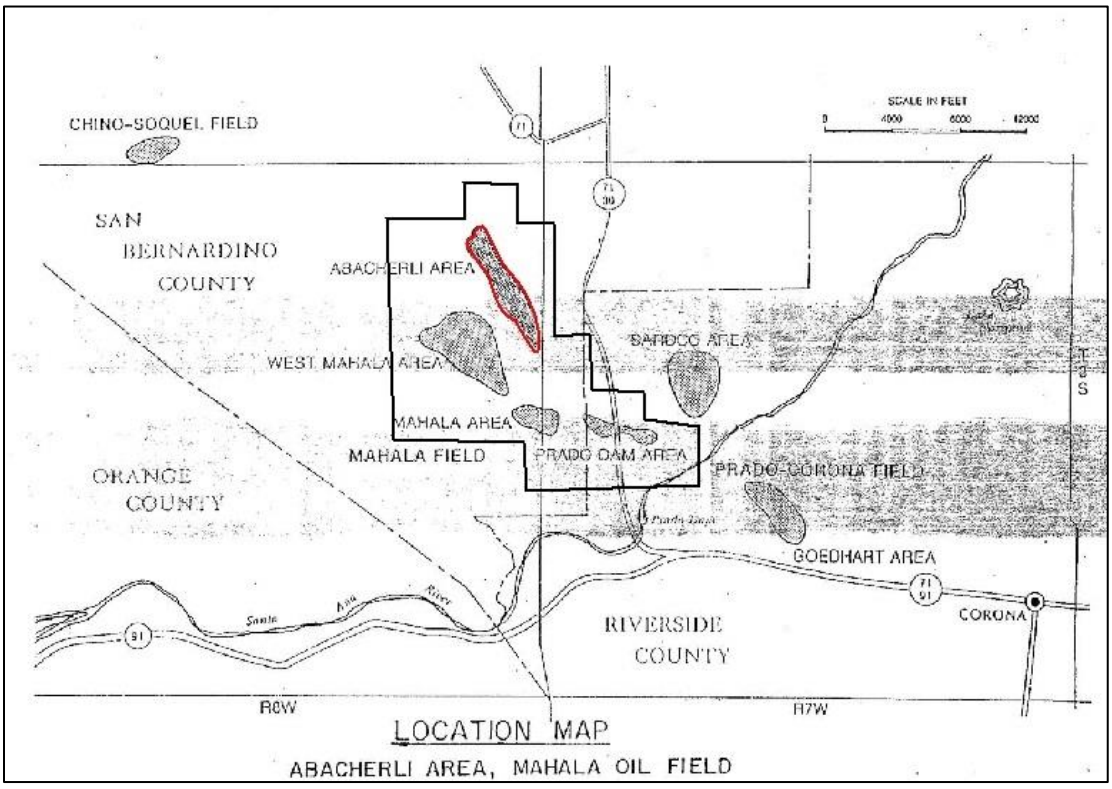

Figure 7: Reservoirs in the Mahala oilfield study area (Olson 1977)

2.2.2 Geological Structure

Compressional forces from the Whittier and Chino faults have resulted in deformation in the area, including large anticline-syncline folding structures between these two faults, such as the Mahala anticline. Located on the geographic extreme eastern edge of the Puente Hills/Chino Hills and located on the geologically extreme eastern edge of the LA basin, the Mahala anticline is an asymmetric northwest-trending breached anticline extending over three miles in length (Dorsey, Ridgely 1993). The anticline is thrust-faulted by the chino fault, which is directly responsible for the uplift of the region

and is the primary structural feature of the Abacherli reservoir. The chino fault trends to the northwest and has a dip range between 50-70 to the southwest (dipping ≤ 50° at depths less than 1,000' and around 70° at depths exceeding 3,0000') (Olson, Larry 1977). The Chino fault thrust segmented the northeastern-most limb of the Mahala anticline fold dividing the area into a hanging wall above the fault and a footwall below the fault. It is estimated that movement along the fault occurred during the Pleistocene epoch (Olson, Larry 1977). This local mechanism is responsible for setting up the updip fault trap for the oil accumulation of the Abacherli reservoir, such as the footwall block in the segmented limb of the faulted Mahala anticline within the Chino fault zone. The reservoir itself is a tilted homocline with steeply but uniformly dipping beds to the northeast with an approximate strike of 315°. The reservoir dip angle ranges between 40-70° with an average of 60°, and the dip angle is largest closer to the fault and decreases with distance from the fault. There are two unnamed northeast-southwest trending sealing faults which merge southwest of the Abacherli area that cap the reservoir at its northern and southern edges, effectively serving as the boundaries of the reservoir.

Figure 9 is a cross-section of line E-E' from Figure 8 below. Both Figures illustrate some of the local lithology and main structures of the chino fault zone within the chino fault area. The column on the right of Figure 9 is the legend for both Figures, providing a reduced version of the stratigraphic column. Figure 10 is an additional cross-section for the location of interest helping to illustrate the local stratigraphy. The "Michelin Zone" in the cross-section is the primary sandstone formation that produces most of the oil in the lease. Appendix I and II illustrates additional information on the stratigraphic sequence.

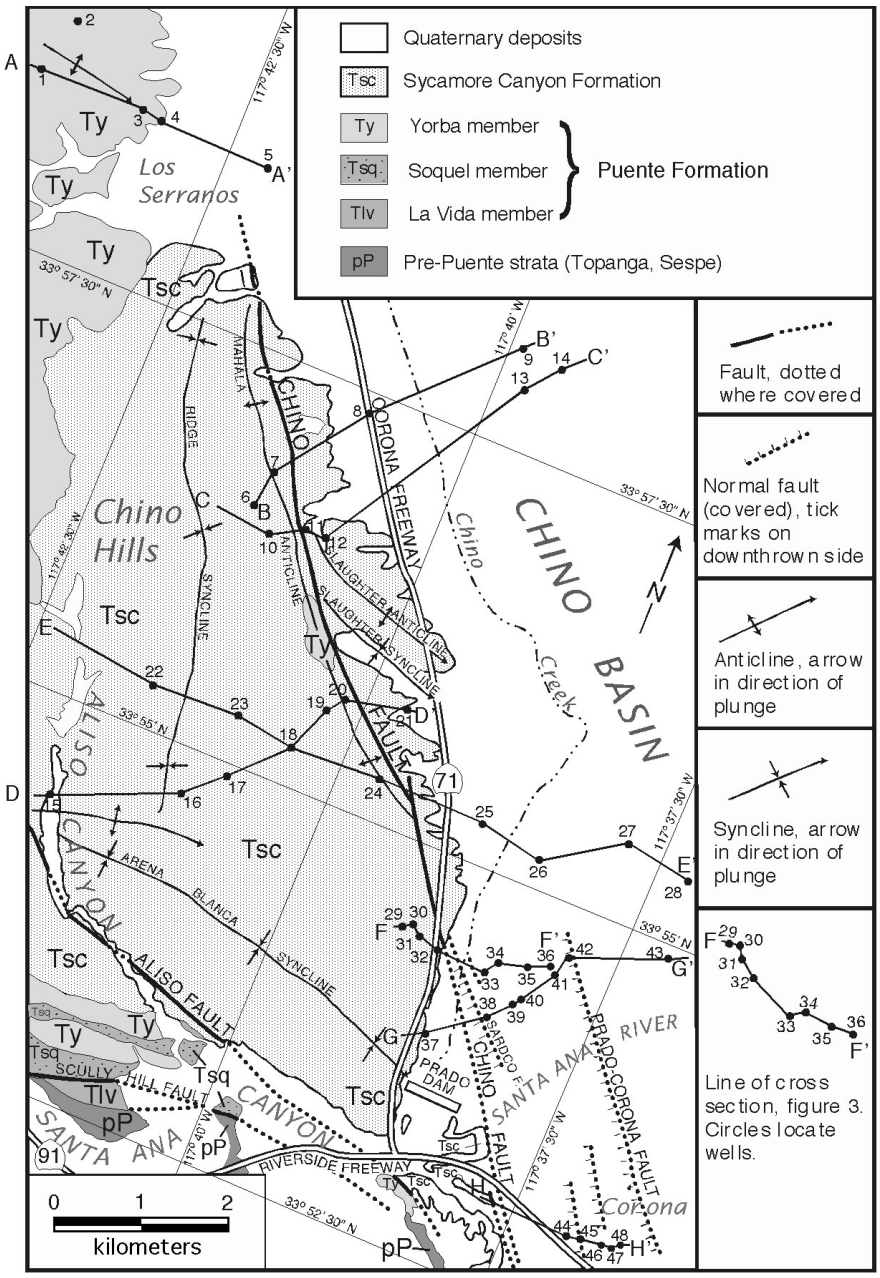

Figure 8: Geological map of study area (Madden and Yeats 2008)

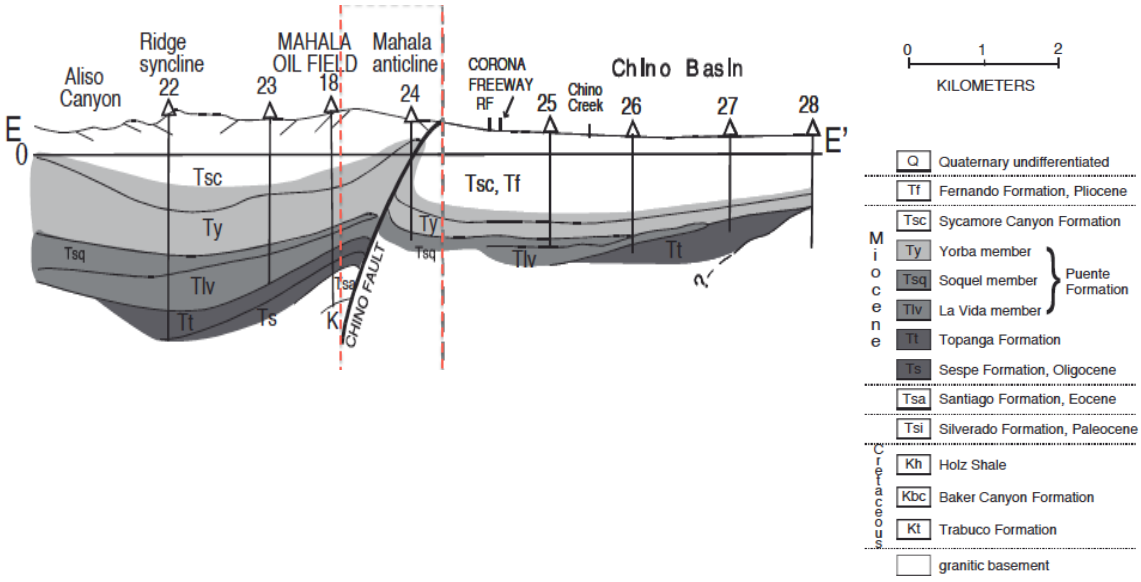

Figure 9 (above): Cross-section of Chino fault zone for line E-E' of Figure 8. Stratigraphic Legend (right) applies to both Figures 8 and 9. (Madden and Yeats 2008)

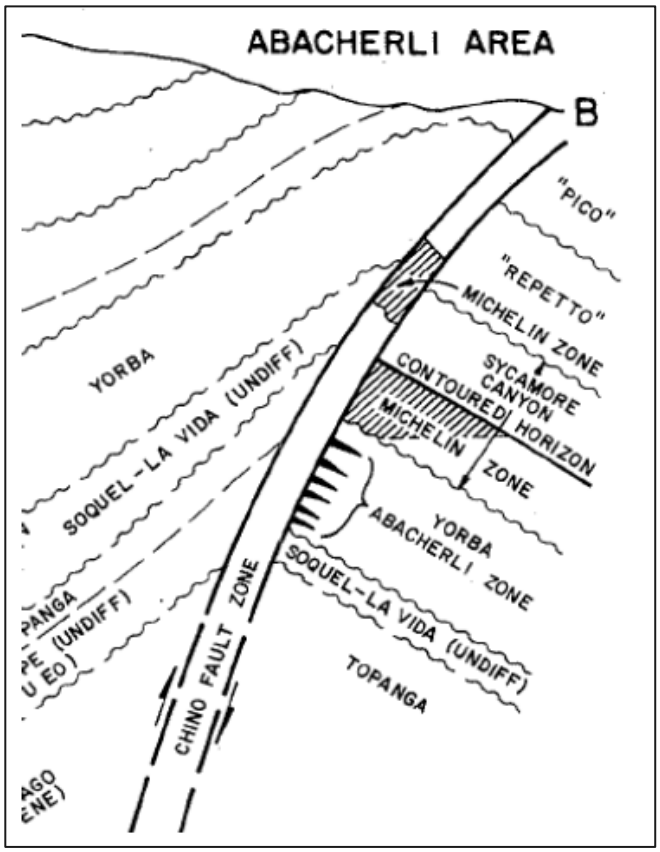

Figure 10: Idealized cross-section of Chino fault zone (DOGG 1992)

2.2.3 Sedimentary History Overview

Part of the greater Los Angeles Basin, the Mahala field is on par with the geological history of the rest of the basin. Basin formation occurred during the Neogene period (approximately 15 million years ago) with major subsidence and deposition occurring between the Upper Miocene until the Lower Pleistocene epochs (approximately between 11.5 to 2.5 million years ago) (Mayuga, 1970). The depositional environment is known to be a marine to moderately deep marine environment with sediment being deposited via the transport mechanisms of the sea and rivers which allowed for the accumulation of large sediment deposits to be further transformed into hydrocarbons. The United States Geological Survey (USGS) report by Durham and Yerkes 1964 estimates the water depth of the Mahala field vicinity at the time of deposition to have been approximately 2,000', with turbidity currents as the main transport method (Dorsey, Ridgely 1993).

2.2.4 Lithology and Stratigraphy

The strata in the area are first divided into series depending on their age, then the series are divided into separate formations according to their sequence. Then the formations are further divided into members according to their producing intervals, such as production zones and lithology. Appendix II illustrates the full stratigraphic column for the Mahala area and surrounding vicinity. Based on the known well penetrations the strata in the field range from Late Cretaceous to Holocene, with the oldest (lowest) Cretaceous section supposedly underlain by a basement of Mesozoic age consisting of granodiorite and associated plutonic rocks of the Southern California batholith from a

depth of 5,000’ to 7,000’ (Olson, Larry 1977). Following the law of superposition we expect that the layering order of the sedimentary rocks will follow the sequence on the stratigraphic column (i.e. oldest on bottom and youngest on top). However, the movement of the thrust fault has reversed the normal order by pushing up rocks of a lower layer over rocks of a higher layer, so older strata southwest of the Chino fault, such as the Yorba shale member, are thrust over younger strata to the northeast, for example the Sycamore Canyon sand member. Therefore the overthrust hangingwall block above the fault contains the lower permeability shale member, and the footwall block including the Abacherli reservoir oil field contains the higher permeability oil-rich sand member (Olson, Larry 1977).

The “Michelin Zone” of the ‘Sycamore Canyon’ member within the Upper Miocene ‘Puente’ formation is the only stratigraphic layer analyzed in this study. Therefore this is the only zone discussed herein. Additional information on the entire stratigraphic column and other associated strata is available in the literature (e.g. Madden and Yeats 2008). The Michelin Zone is predominantly a sandstone facies with some interbedded thin layers of silty and shaly sands underlain by poorly consolidated basal conglomerates (Dorsey, Ridgely 1993). Observations on the lithology include:

- Sand- tan to brown color with fine to coarse grain size
- Shale and Siltstone – white to buff to light gray and dark gray ultrafine grain size
- Conglomerates- Pebble to cobble size, hard, poorly consolidated by calcareous matrix

- Key foraminifera identified – *Rotalia garveyensis*, *Bolivina barbarana* and *Bolivina Hughesi* (biostratigraphy of Upper Miocene foraminiferal fauna of California)

Figure 11 is a geologic contour map of adjacent reservoirs illustrating their areal extent in the field. Additional structural contour maps are included in Appendix III, IV and V.

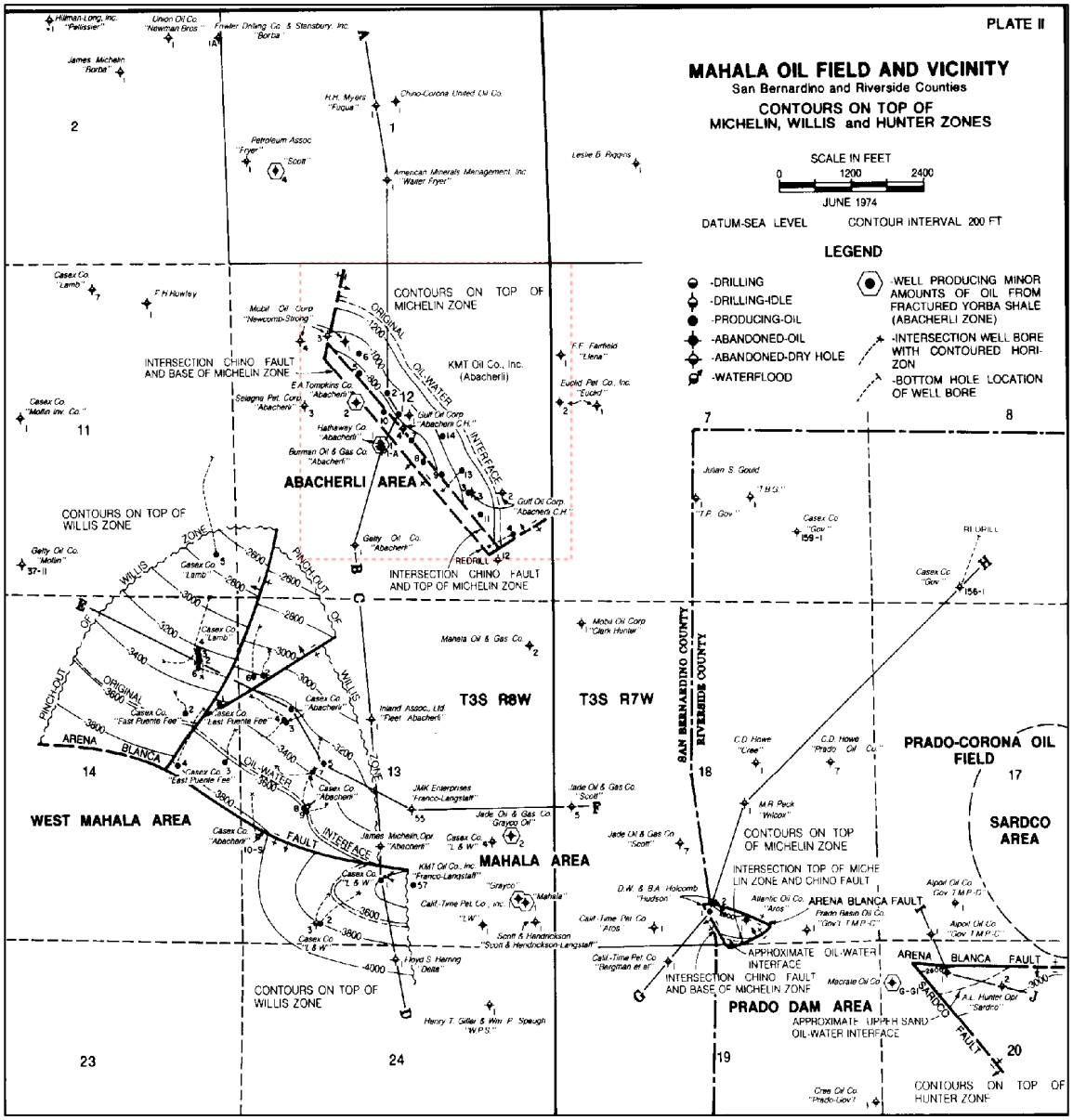

Figure 11: Structural and geological contour map of Mahala oil field (Olson 1977)

Figure 12 is an isopach map, the contours of which help detail the thickness of the stratigraphic formation of interest. This map was subsequently digitized for use in this study to establish the boundaries of the reservoir, to compile the point set shown in Figure 22, and the areal outline shown in Figure 23, all utilized in this analysis.

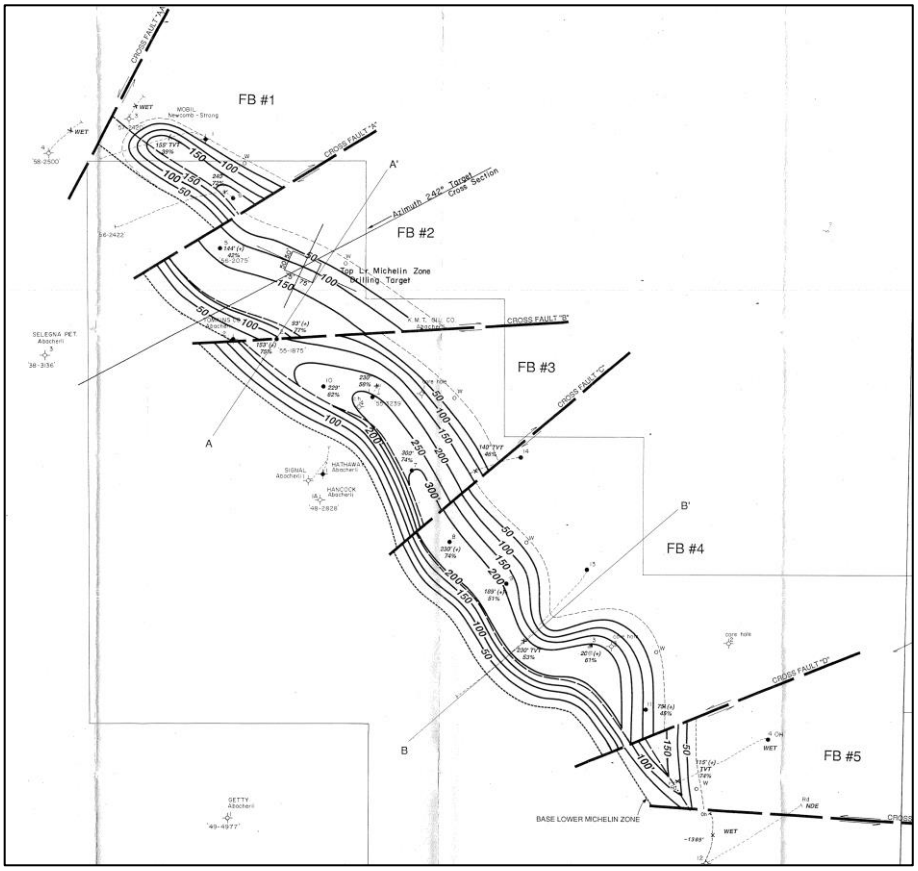

Figure 12: Isopach map of Abacherli reservoir (Dorsey 1993)

Due to very limited core data, values for the production sand characteristics are rough estimates. Dorsey's 1993 study provides estimates of an average permeability of 500 md and an average porosity of 27% (Dorsey, Ridgely 1993). Although the values are

probably overestimated, the sand characteristics are expected to be well within the characteristic sand range favorable for conventional crude oil production.

2.2.5 Remark on Previous Studies and Field Observations

Most of the information obtained from previous geological work for the Mahala oil field is endorsed as true geological characteristics, conditions and representations of the field including the Abacherli reservoir. The necessary geological assumptions are made for the continuation of the analysis, however the only major exception is the suggestion of cross-faults within the reservoir as shown in Figure 12. Dorsey's (1993) geological review suggests that there are at least six cross-faults that divide the reservoir into separate fault blocks. However, in this study this interpretation is deemed rather unsuitable based on direct field observations and the analysis conducted. The existence of these cross-faults is questionable mainly because of the general continuity across the whole reservoir apparent from the geostatistical analysis discussed in this thesis, as well as the synchronous field observations of well pressures on either side of a given proposed cross-fault. In the case of these well pressures, change in one well causes a pressure change in another well across a proposed fault signifying that there must be connectivity between the wells. Even if cross-faults are present and do affect the local geology, the geostatistical analysis performed in this study assumes pre-fault conditions in which the entire reservoir is modeled as a single unit in order to make an overall study viable. Most geological interpretations are subject to case-specific interpretations. The objective of this project is not to refute previous geological work but to model the strata as accurately as possible in the analyses performed. More detailed information on previous geological

work conducted in the study area is available in the literature, for example in Olson, Larry 1977, Dorsey, Ridgely 1993, and Madden and Yeats 2008.

CHAPTER THREE: DATA

3.1 Hard Data Sources

The primary data used in this report consists of well logs located at specific coordinate locations displaying the electrical properties of rocks and their fluids in the borehole. This data represents a geophysical exploration test that provides information on the lithology and other geological characteristics at different points within the reservoir. When combined with additional physical and chemical information of the subsurface a useful description and better evaluation of the field can be made. Electrical properties are given as resistivity values ('R') measured in ohms (Ω) and spontaneous potential values ('SP') measured in millivolts (mv) for the active wells in the field.

The entire Mahala oil field has had several dozens of wells drilled since its initial discovery. All of the thirteen wells drilled within the Abacherli reservoir are still in good production today, and their log values are used as the hard data in this report. Several other dry, unproductive wells were drilled in the immediate vicinity around the reservoir that helped define the extent of the reservoir area and confirm the presence of no-flow boundaries (OCR, LCC 2014). Because the reservoir consists of a single small to medium-sized geological unit comprised of the same sand facies throughout, the wellbore data within the known reservoir boundaries are expected to show coherent statistical properties throughout the field. Thus in order to conduct the statistical analyses performed in this study, stationarity within the boundaries of the Michelin sand layer of the reservoir must be assumed in order for this study to be viable.

For any type of computational analysis it is imperative to know and understand the integrity of the data. Schlumberger Limited performed the borehole logging of the

thirteen wells used in this study (OCR, LLC 2014). Log values are measurements obtained from borehole equipment which consists of wireline instruments directed down into the subsurface of the earth that record the measurements at depth via direct contact of electrical sensors with rocks and their fluids (Schlumberger 2014). The wireline services produced a continuous dataset (recorded as a log) for each of the drilled wells, and this raw data was used as the hard data points utilized in this analysis. Snapshots of sections of different well logs are shown in Figure 13 a through c. Vertical quantitative data values were obtained for 10’ intervals to depths ranging down to 3,050’ from surface.

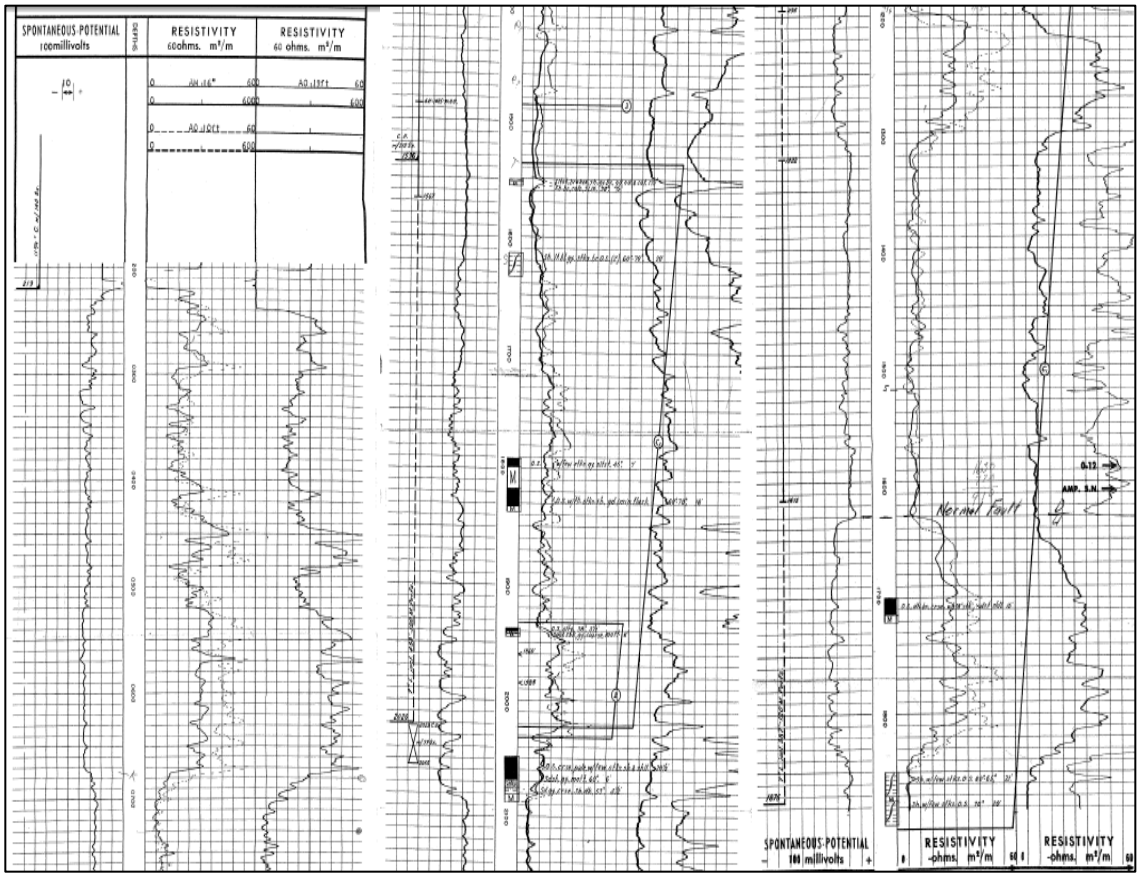

a b c

Figure 13(a-c): Electrical well logs from the Mahala field (KMT Oil Co., Inc 2013)

3.1.1 Electrical Data Boring

Spontaneous Potential ('SP') measures the differences in static electrochemical potential and ionic concentration in pore fluids of rocks that is caused by the charge separations due to the diffusion of ions (Radhakrishna, I. and Gangadhara, T. 1990). Ions in porous and permeable media diffuse differently than ions in impermeable media. The difference in voltages between a reference electrode and the ground electrode is caused by the electric current given off by the sensor at depth as a response to its electric charge. The charge depends on the buildup of ions. This ionic concentration can be high, low, positive or negative depending on the characteristics of the rock material including its mineralogy, permeability and porosity. Greater ion exchange occurs in porous and permeable rock media causing a higher response in the SP log (SPE PetroWiki 2013). Similarly the concentration of ions in connate water depends on the mineral components of the formation rocks Generally, large and negative deflections in SP indicate the presence of permeable beds, thus SP values have been extensively used to help detect permeable and porous formation beds, for instance to identify the location of reservoir rocks (Schechter, David 2014). Figure 14 illustrates how the distribution of an electric current changes between beds of different permeability due to the behavior of ions in separate geologic media, and how it affects the SP electrical measurements in a well log.

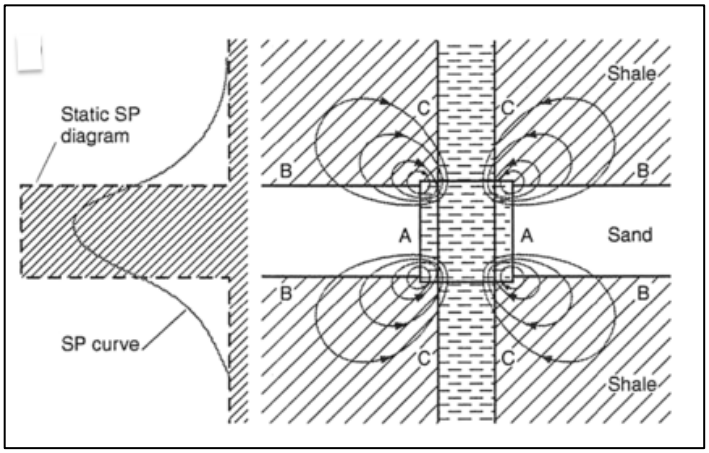

Figure 14: Spontaneous Potential illustration (PetroWiki 2013)

Resistivity (‘R’) measures the electrical resistance of the fluid in the pores of the rock. It is the inverse of electrical conductivity and quantifies how strongly a material readily opposes (or resists) the movement of electric current (William, Lowrie 2007). Rocks, sediments, and their fluids within a borehole will have different properties that cause the resistivity in the materials to vary. By measuring the degree of resistivity down a borehole it is possible to characterize the formation downhole. Although most rocks are insulators, the fluids within their pores are conductors, however the big exceptions are hydrocarbon fluids, which do not conduct electricity. When a formation contains oil, the resulting resistivity will be high and recorded as a “spike” in the log, thus resistivity these logs have been extensively and efficiently used to detect the presence of hydrocarbons. Both the SP and R values combined provide a good tool to characterize geological formations. Large positive R deflections and large negative SP deflections are clear indicators of permeable hydrocarbon-containing formations (a.k.a “pay zones”). Figure 18 is an illustration of a pay zone that has been logged showing the spikes in R and the

opposite spikes in SP. Resistivity values range from 0 to 60 (6mV intervals) and Spontaneous Potential values range from -50 to 50Ω (1ohm intervals).

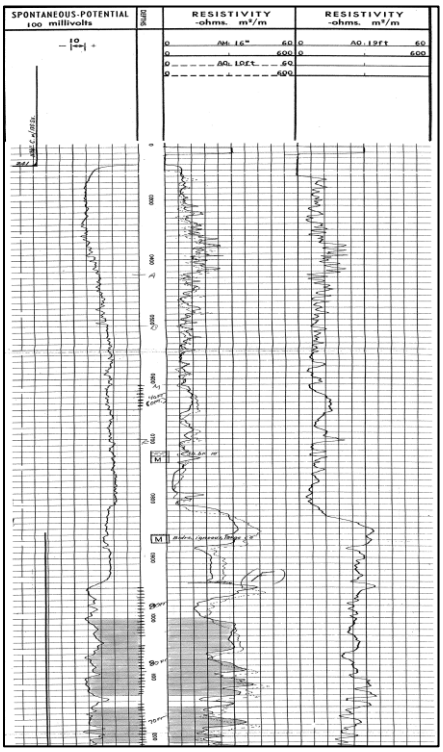

Figure 15: Pay zone electrical log (KMT Oil Co., Inc 2013)

3.2 Software

3.2.1 Modeling Software Interoperability

This study provided a good opportunity to showcase the interoperability between different geographic and modeling software. The transfer of data via common exchange formats allows for data to be inputted and outputted between separate computing programs, including popular systems such as Stanford Geostatistical Modeling Software (SGeMS), Esri ArcGIS, Microsoft Excel and Mathworks MATLAB. The two primary software used for the geostatistical modeling done in this thesis research include SGeMS

2.0 and ArcGIS 10.1. As the most popular Geographic Information System in the world, ArcGIS has several integrated applications including ESRI ArcScene for 3D analysis and modeling, ArcMap for 2D analysis and modeling, ArcCatalog for database management and ArcGlobe for 2D and 3D mapping and visualizing larger datasets (Esri 2012). Since SGeMS is specifically designed for geostatistical modeling it was used for the 3D variogram-based modeling and conditional simulation performed in this study, then these data output were transferred to ArcGIS. ArcGIS and its functional components were used for organizing, georeferencing, digitizing, visualizing and managing most of the field data. Besides electrical well logs other sources include remote sensing, GPS and additional geological information.

3.3.1 Remote Sensing DEM

Remote sensing data obtained from the USGS national map viewer platform was downloaded to provide a DEM of the oil field study area. Geographic coordinates of the oil field were input into the USGS server and the elevation information was then downloaded and georeferenced in ArcGIS (USGS 2014*)*. The DEM grid set, consisting of grid blocks of about 1-arc second resolution (or 30 meters), was imported into ArcScene and converted to a 3-D elevation map of the field. An aerial map was then draped on top of the DEM to provide a realistic visualization model of the topography for the area of interest (Appendix VI). Figure 16 illustrates a close-up 3D DEM representation for the area of interest draped over a full spectrum color ramp to better illustrate the variable elevation.

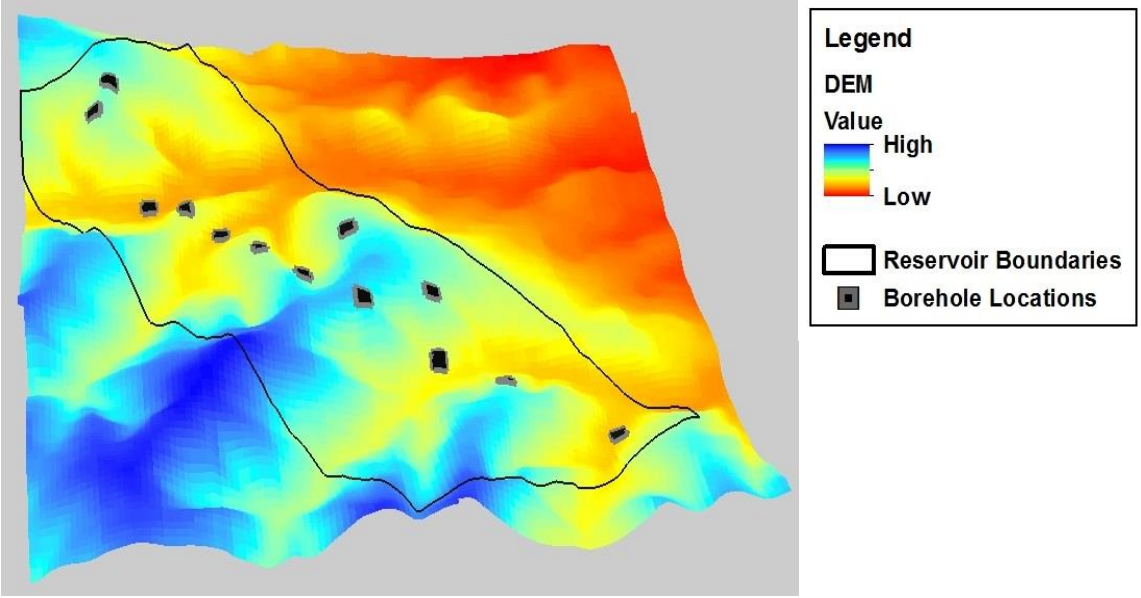

Figure 16: DEM of study area with legend (based on USGS 2014)

3.2.2 3D Stratigraphic Cross-section

As previously discussed, significant deflections in the logs indicate zones of high and low values; these changes in rock properties indicate the interfaces between different geological facies. With this information it is possible to determine the thickness of individual rock units and thus determine the local stratigraphic boundaries. Knowing the facies and thicknesses of geological units at specific depths and coordinate locations within the reservoir makes it possible to develop a cross-section for the area. ArcScene allows for creating and mapping 3D models, thus it is a useful tool to create and maintain the volumetric models used in this study.

The depths of the tops and bottoms of the rock strata were interpreted from the logs at each respective borehole and were input into ArcScene. A continuous surface was created connecting all of the 13 points on the top of each formation and a separate continuous surface was created connecting all of the 13 points at the bottom of each

formation for all of the facies. Next a volume within each formation was generated resulting in a 3D geologic cross-section illustrating the local lithological boundaries of the strata in the field. For visualization purposes, Figure 17 illustrates the stratigraphy of the reservoir as well as the log values for all of the wells. Appendix VI provides illustrations of the cross-section at different angles as well as processed models transferred from SGeMS and MATLAB and integrated into ArcScene.

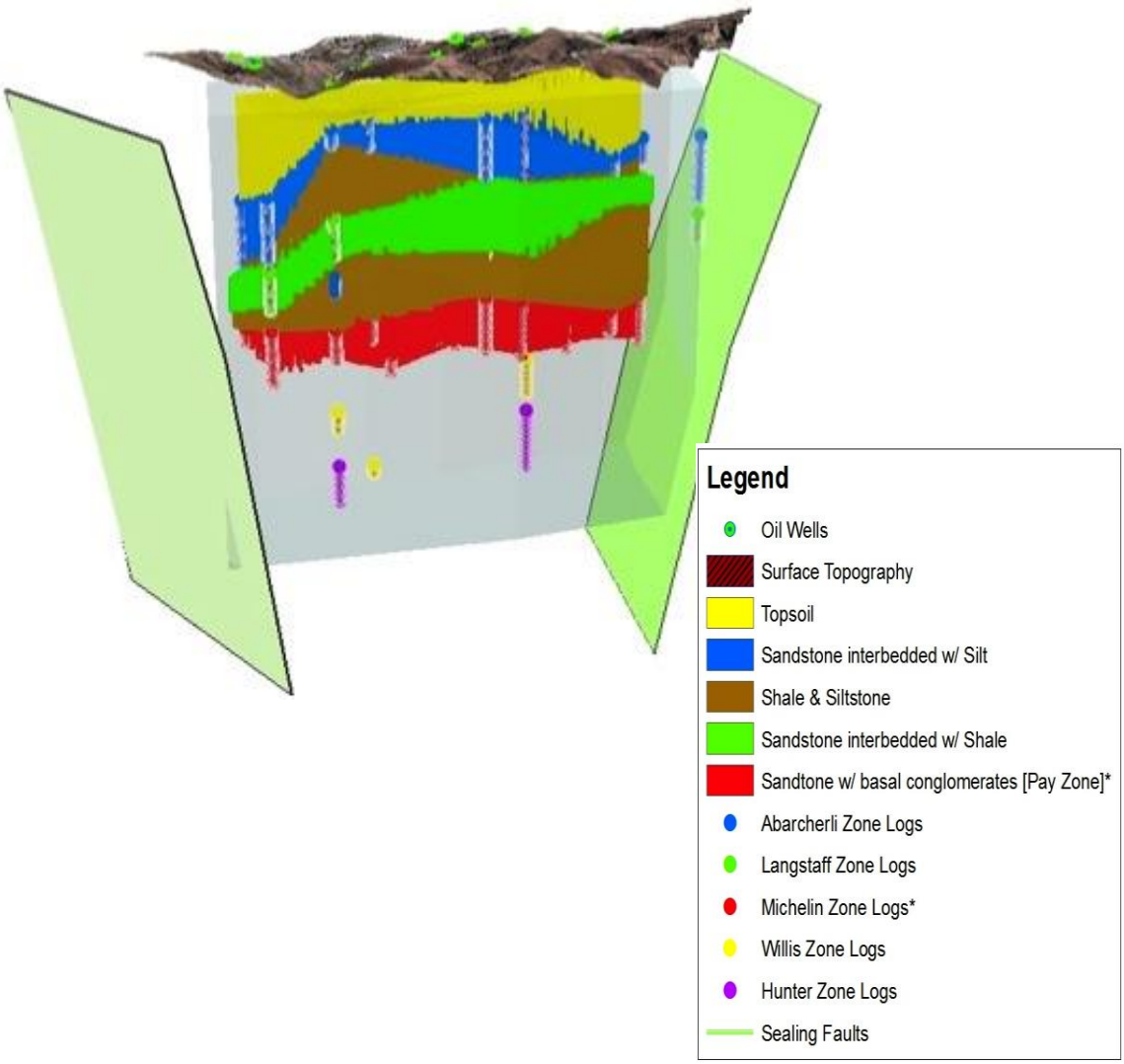

Figure 17: 3D cross-section

3.3.3 Data Point Set

Figure 18 is an image of the point set grid used in the interpolation. After georeferencing the isopach map (Figure 12) and digitizing the dimensions of the reservoir, ArcGIS tools were used to create an ultra-high resolution point data set with the specified volumetric dimensions of the field. The blank point set served as the interpolation medium where each of the individual points were populated after running the ordinary kriging and conditional simulations. One of the drawbacks of performing simulations on an ultra-high resolution point set is the time required to run all of the simulations. Due to the large size of the data point set (> 1.5 million points) running all of the simulations was computationally demanding, taking a total time of over one month for completely performing all 101 realizations to run on a Dell XPS-8300 desktop with a Windows 7 professional 64-bits operating system.

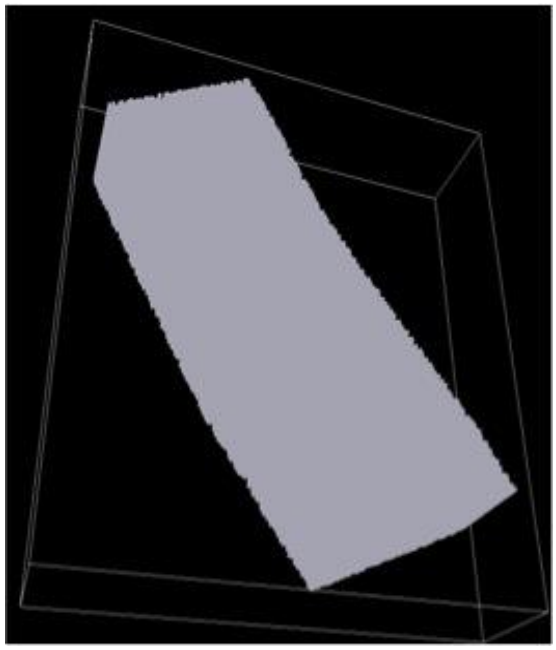

Figure 18: Blank 3D point set

3.3.4 GPS Data Acquisition

Figure 19 is an aerial map view of the field with the boundaries of the reservoir obtained by digitizing the isopach geology map (Figure 12). Additional information in Figure 19 includes GPS-derived positions of production lines, water lines, tanks, wells and valves. GPS data points, lines and polygons were obtained via direct measurement using an ultra-high precision Geo-XH GPS unit and subsequent data corrections were done using GPS pathfinder software and then imported into ArcGIS. The GPS unit and software were obtained from the University of Southern California's Spatial Sciences Institute. The Trimble GPS Geo-XH unit is an ultra-high precision data collection device, with precision to a few millimeters (GSI Works 2009*).*

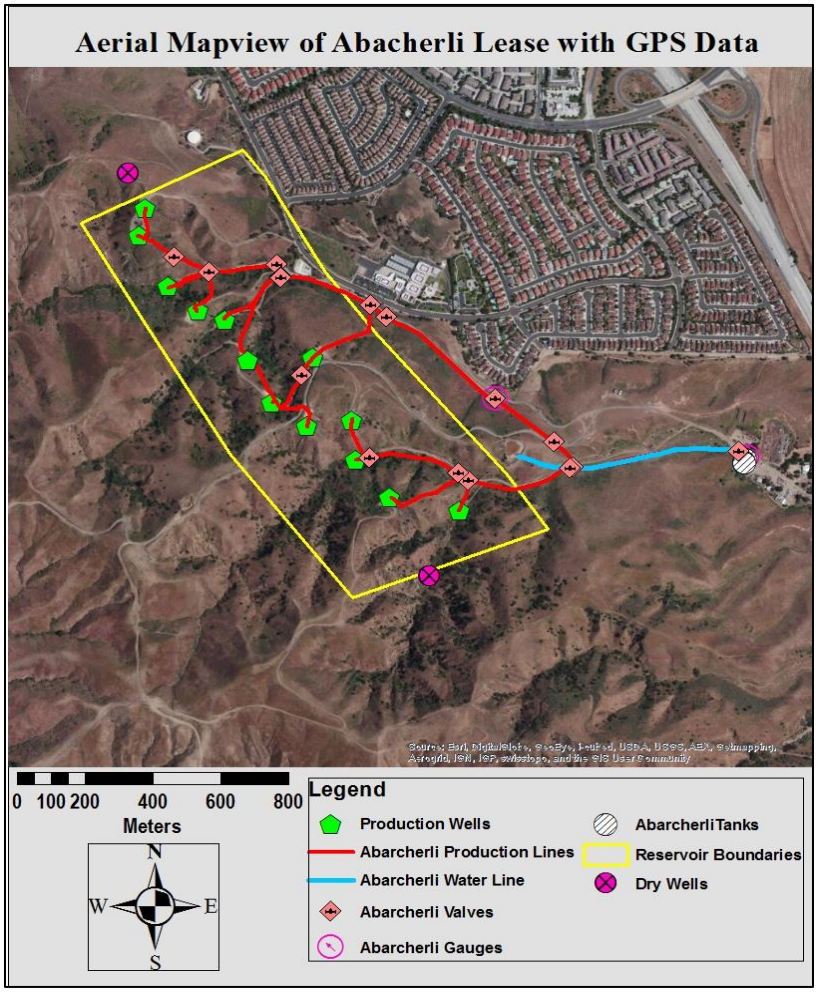

Figure 19: Mapview of study area lease (based on GPS 2013)

CHAPTER FOUR: METHODS

4.1 Data Exploration and Evaluation

4.1.1 Data Input and Transformation

Exploration of the data of the datasets allows an assessment of their suitability for the proposed analyses. An important preliminary step in the evaluation of the data is to examine the spatial distribution of the datasets. Because the kriging and conditional simulation techniques used in this study are methods for interpolating values that are modeled by a Gaussian process, it is necessary for the sample data to have a normal distribution. Simple univariate and bivariate statistical tests were performed to determine if data need transformation to become Gaussian. The well locations and log values for the thirteen active wells in the stratigraphic formation of interest in the Michelin Zone were entered into SGeMS software. A Probability Density Function (PDF), Cumulative Distribution Function (CDF) and QQ-plot of the two variables as well as a scatter plot analysis illustrating the correlation coefficient between both variables were obtained. Resulting Figures from the preliminary statistical analyses are illustrated from Figure 22 to Figure 26.

Figure 20 and 21 illustrate the spatial distribution of the wellbores, surrounded by a bounding box representing the overall volume of the field, including color-coded R and SP values and legend.

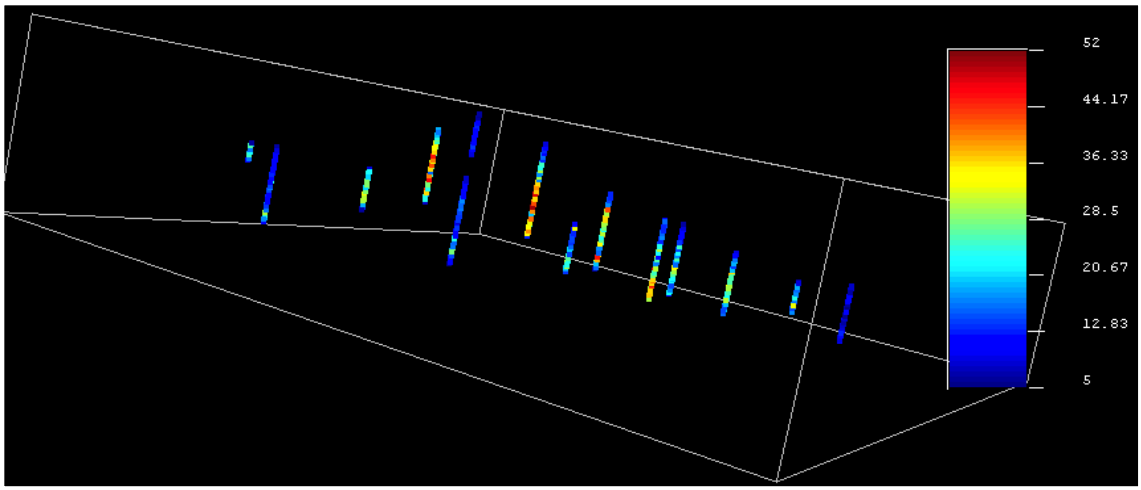

Figure 20: Resistivity Data logs

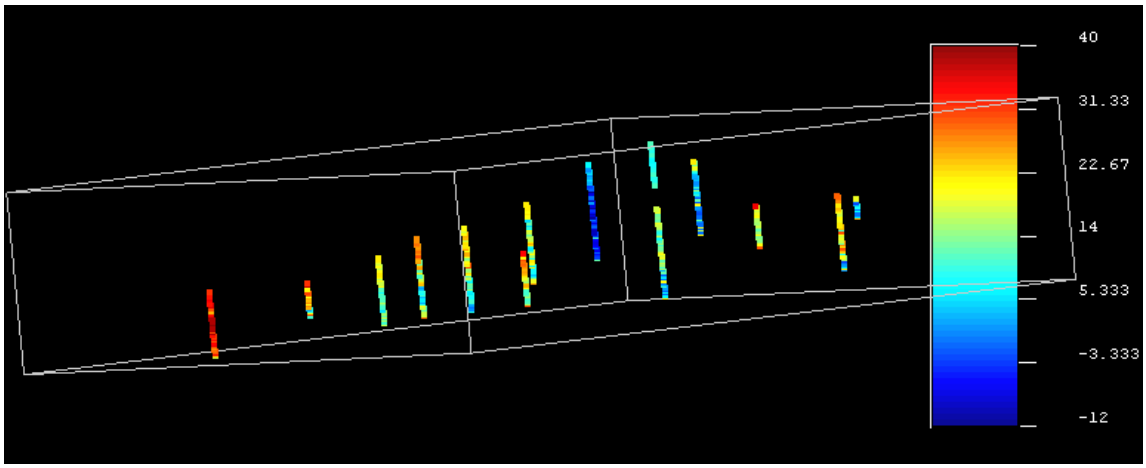

Figure 21: Spontaneous Potential Data logs

Figure 22 shows the PDF and CDF outputs of the raw SP dataset. The dataset follows an acceptable normal distribution and therefore it can be assumed that it does not need to undergo further transformation to be used in this analysis.

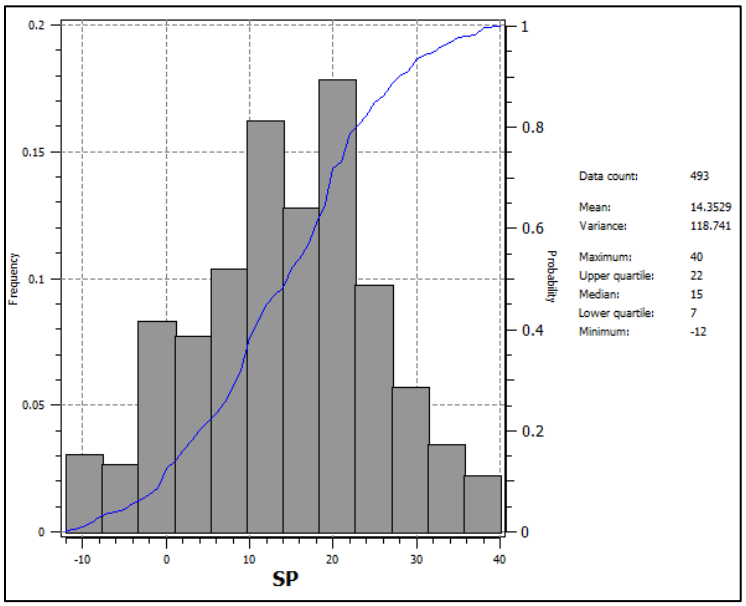

Figure 22: Spontaneous Potential CDF and PDF

Figure 23 shows the PDF and CDF of the raw R dataset. Since the data exhibit a significant positive skew to the right and thus is not normally distributed, it is therefore preferable to transform this dataset to normality.

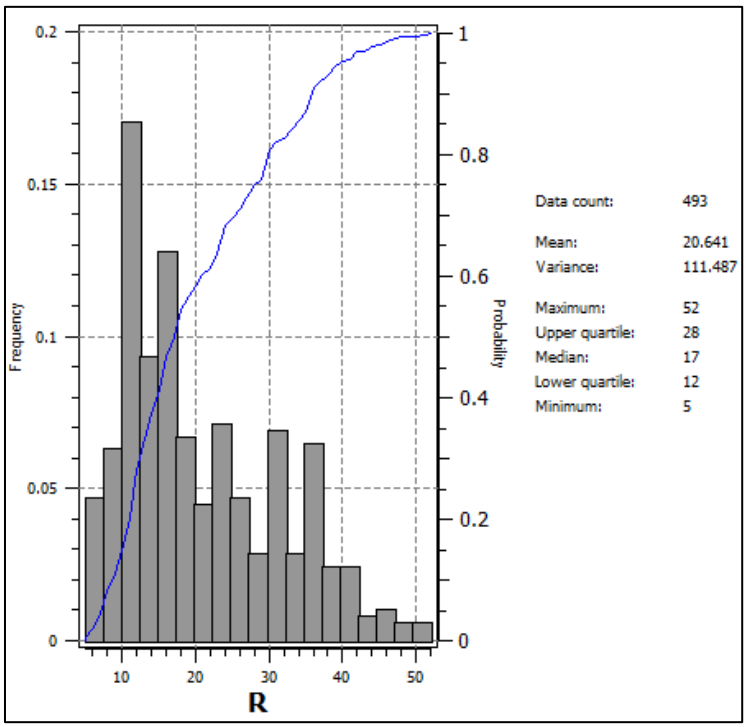

Figure 23: Raw Resistivity PDF and CDF

The R dataset was transformed to resemble a normal distribution by using the histogram transformation tool in the SGeMS utilities box. Figure 24 shows the PDF and CDF of the normally transformed R dataset.

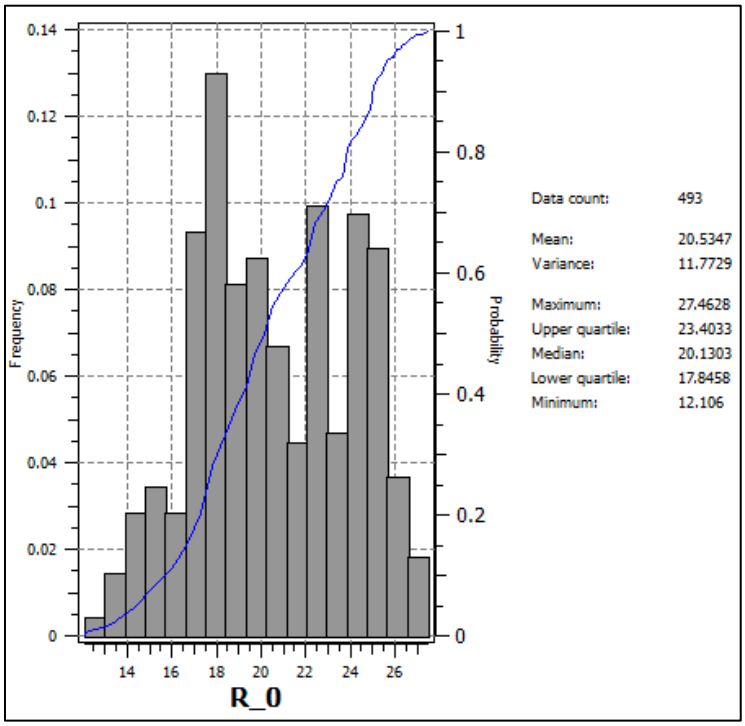

Figure 24: Transformed Resistivity PDF and CDF

Figure 25 is a Q-Q plot of both SP and R probabilities plotting their quantiles against each other. This graph compares the shapes of the two probability distributions and also allows one to better determine if the data is close to a normal distribution. For the compared probability distributions to be normal, the plotted points should lie within a straight line. The closer all points are to a straight line the closer the samples are to a normal distribution. This graph illustrates that there is a significant offset, indicating a clear deviation from normality.

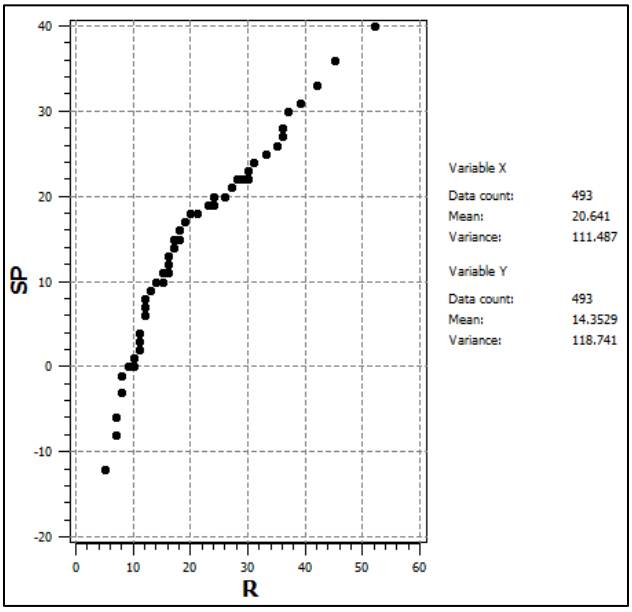

Figure 25: Raw Q-Q plot between R and SP

Figure 26 is the Q-Q plot of the SP dataset with the normally transformed R dataset. In this Figure the linear relationship between the two variables (points plotted across a straighter line) indicates a more normal distribution.

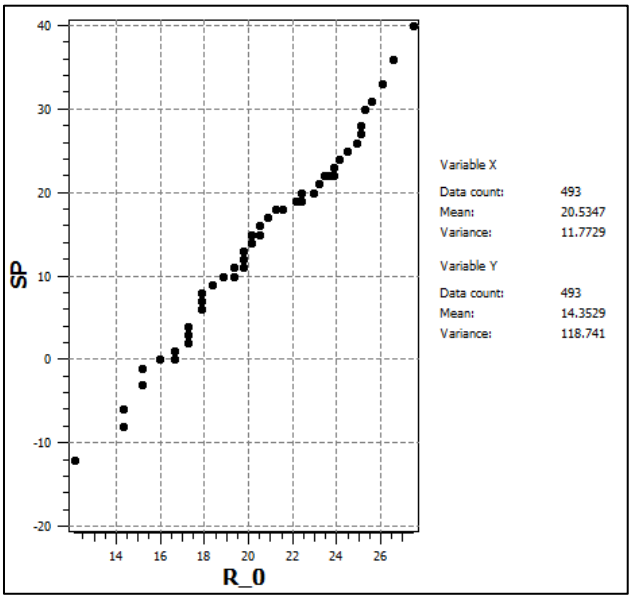

Figure 26: Transformed Q-Q plot of SP and R

Figure 27 is a scatterplot of SP and R including the linear regression line illustrating the correlation between both variables and their coefficient.

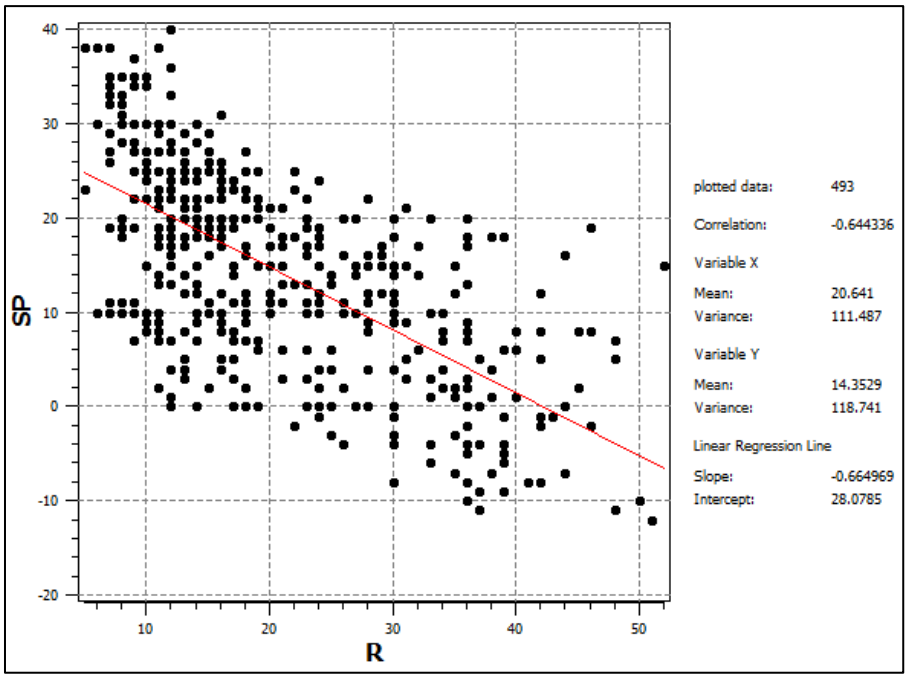

Figure 27: Scatterplot between R and SP

The correlation coefficient for SP and R is -0.665. The strong negative correlation (as SP goes up R goes down and vice versa) follows the field expectation as described in the data section. Although this correlation is not needed for ordinary kriging it provides more useful information and allows a better evaluation for potential cokriging as a future study.

4.2 Variogram

Several attempts experimenting with different parameters, conditions and components were tried in the variogram modeling for this study. Correct variogram modeling requires

practice and a fair amount of guesswork. The defined variogram model is at best an approximation of a best-fit function describing the spatial relationship of the variables in the field.

4.2.1 Variogram Parameters

A useful initial technique to help estimate the variogram is to restrict the maximum distance at which the variogram is computed to ensure sufficient pairs for a given distance while still allowing for a reliable estimate of the variogram for that given distance. A very common approach to select that restricted distance is to use around half of the maximum possible distance within the region of assumed stationarity and use it as the lag distance (Kelkar and Perez 2002). Because a variogram is symmetric this approach also ensures that all pairs on either side of a given location are included in the model, and adding 180° to a given direction provides the same variogram estimate. In addition, another common rule of thumb is to use approximately half the distance of the lag separation as the lag tolerance (Babish, G. 2000). It is important to note that these lag assumptions are not necessarily relevant for every case. The conditions (geologic structure, well geometry, depositional setting) of different oil field reservoirs can require significantly different lag parameters. However, as noted in the geology section and illustrated in Figure 19, the wells in this field are oriented or located in nearly a straight line and their spacing is consistently distributed at closely uniform intervals. In addition, the area of the field is not too large geographically so the entire reservoir system is analyzed as a whole. These factors simplify the decision-making process for defining the distance and direction of the variogram model.

Once the data is inputted into the modeling software and determined to be appropriate for the kriging analysis, an experimental variogram model can be defined. Figures 23 and 24 show the initial data input of the wells. The first step is to choose the parameters that will estimate the variogram, the lag components that define the distance and the directional components that define the direction/orientation. In SGeMS the three lag distance components are: 1) number of lags, 2) lag separation and 3) lag tolerance and the four lag direction components are: 1) azimuth, 2) dip, 3) tolerance and 4) bandwidth. Figure 28 displays the lag distance and direction parameters used.

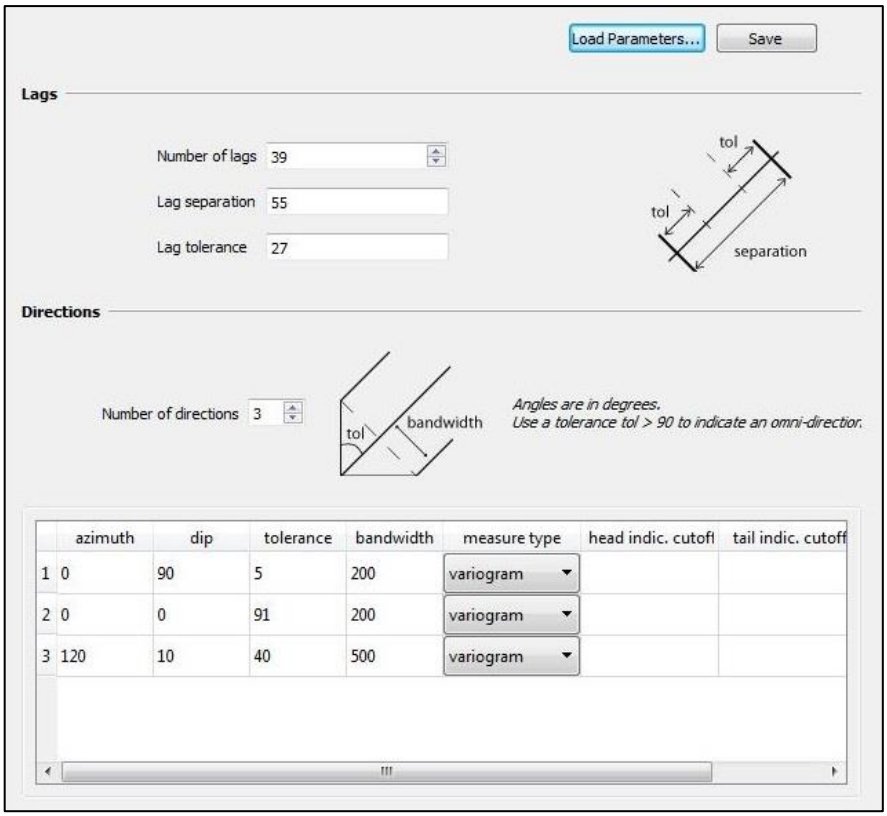

Figure 28: Variogram direction and distance parameters

Lag distance is the product of the number of lags and the lag separation, i.e. ($lag\ distance = \#\ of\ lags\ \times\ lag\ separation$). The maximum distance between any

two pairs of points in this field, for instance the distance between the two wells that are farthest apart, is 4,300'. Therefore the maximum lag distance the model was initially targeted to have is around 2,150'. After several attempts with the given directions, a lag number of 39 and a lag separation of 55 provided promising preliminary variogram plots. A lag tolerance half the value of the lag separation was targeted, so the value selected is 27 $(55 \div 2 = 27.5)$ rounded down to the nearest whole.

The variogram for a 3D model is commonly expected to include as a minimum, three directions: 1) a vertical directional component to account for variability with respect to depth in any given borehole, 2) an omni-directional component to account for global variability throughout the field, to see the overall picture, and 3) at least one horizontal directional component covering the major directions in the field.

Four components in the SGeMS software define the directionality of the variogram, including: 1) the azimuth, which corresponds to the direction on a planar surface measured in degrees from 0°-360°, 2) the dip, which corresponds to the angle of descent relative to the azimuth measured in degrees from 0°-90°, 3) the tolerance which corresponds to the angle of tolerance of the directional variogram measured in degrees from 0°-90°, and 4) the bandwidth, which corresponds to the maximum width of the area resulting from the directional variogram (Remy, Boucher and Wu 2009). The azimuth and dip, analogous to geologic strike and dip, are two important components reflecting the major axes in a 3D environment, and the tolerance and bandwidth help further refine the directions of interest to accommodate the intended directionality of the field. By manipulating the variogram azimuth, dip, tolerance and bandwidth it is possible to capture the structural geology of the field (strike, dip, rake, plunge) and hence end up

with a true volumetric (3D) estimation resembling the geology. Once a general direction, (azimuth and dip) is established then the tolerance and bandwidth choices, which are more flexible because they are based on subjective decisions, should be adjusted until an interpretable variogram structure is identified.

4.2.2 Experimental Variogram

Three variogram directions were established: a vertical direction, an omni-directional and a horizontal direction following the geological geometry (strike) of the oil field reservoir. The components for all directions are shown in Figure 28. The tolerance and bandwidth were manipulated until a clear variogram structure was obtained. Figures 29 and 30 illustrate the experimental variogram in all three directions for both datasets after a decipherable structural trend was identified.

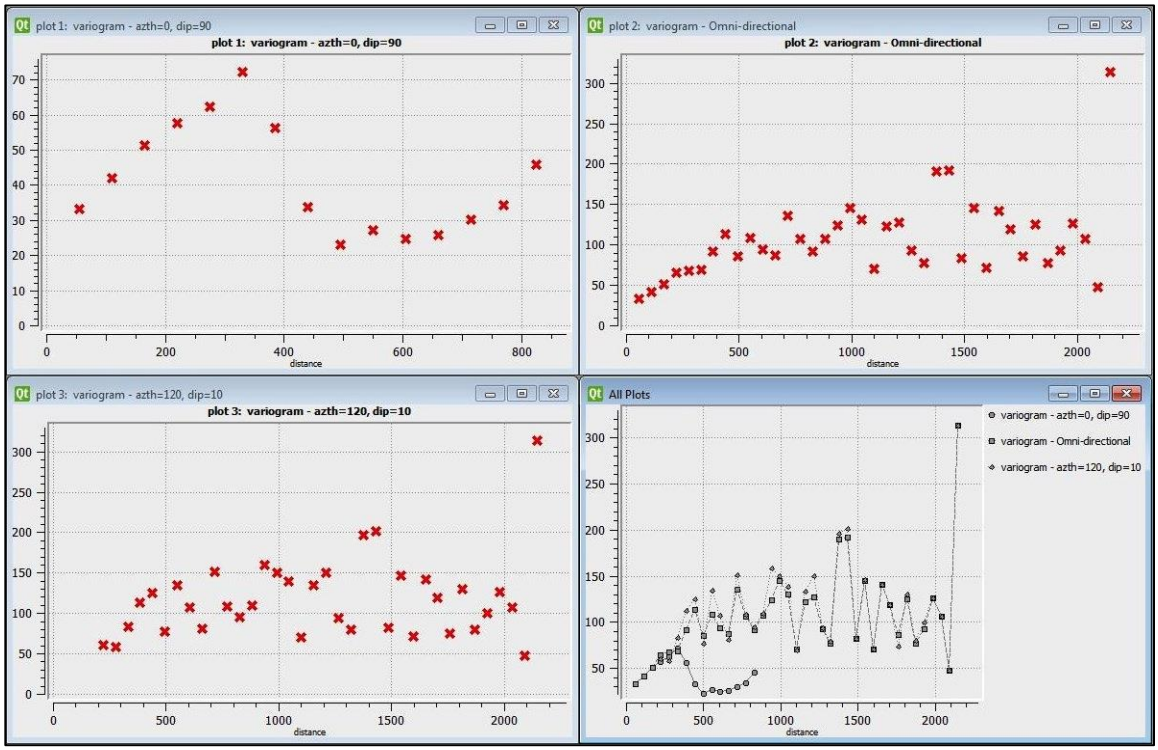

Figure 29: SP experimental variogram in all three directions

In Figures 29 and 30 if Cartesian coordinate plane orientation is assumed and the figure is divided into four separate figures, or quadrants, Quadrant I in the upper right represents the omni-direction, Quadrant II in the upper left represents the vertical direction, Quadrant III in the lower left represents the horizontal direction, and Quadrant IV in the lower right represents a plot of all the directions combined. Quadrant IV is useful to visualize the complete extent of the entire variogram.

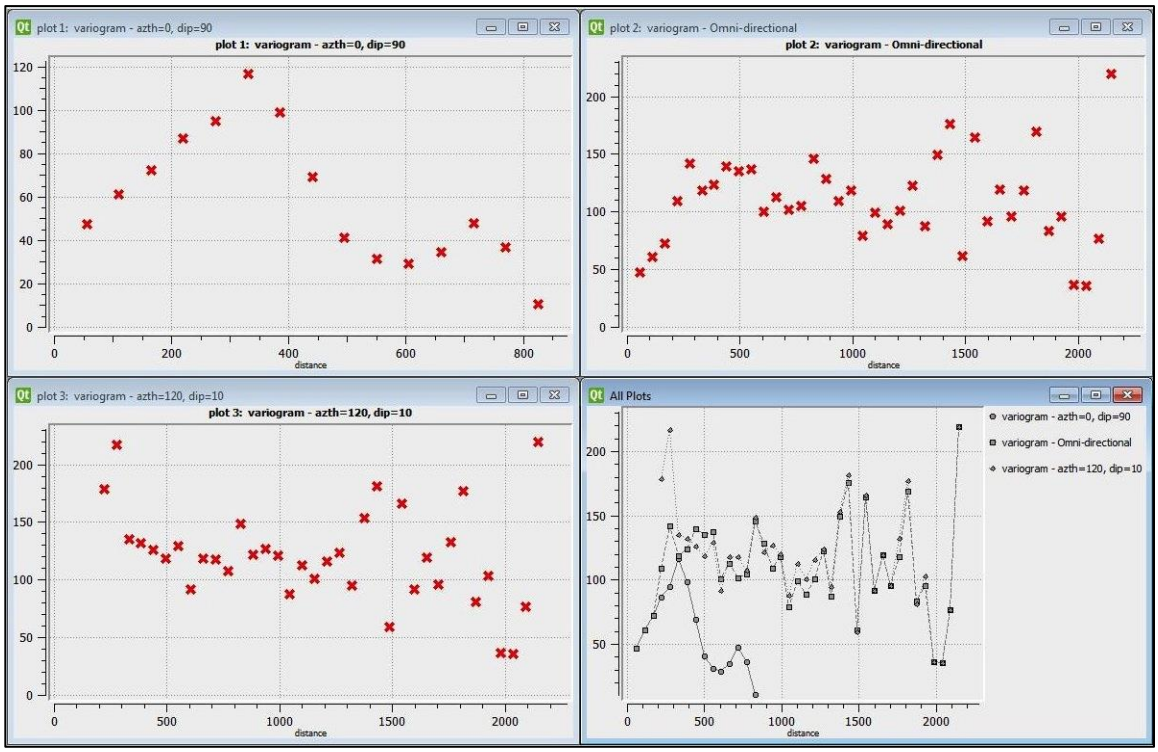

Figure 30: R experimental variogram in all three directions

The first direction established is the vertical direction with an azimuth of zero, a dip of 90°, a tolerance of 5° and bandwidth of 200 (Figure 28). The interpreted variogram

structure for each dataset in this direction as well as the fitted function is shown in Figures 31 and 32.

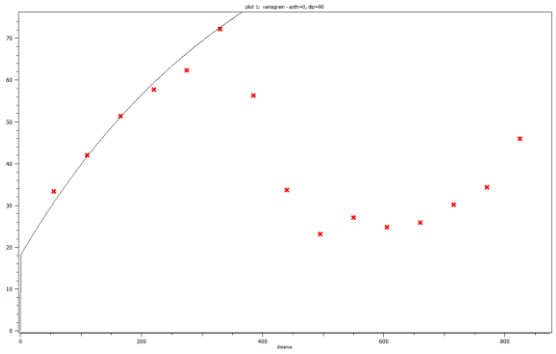

Figure 31: SP Fitted vertical variogram model

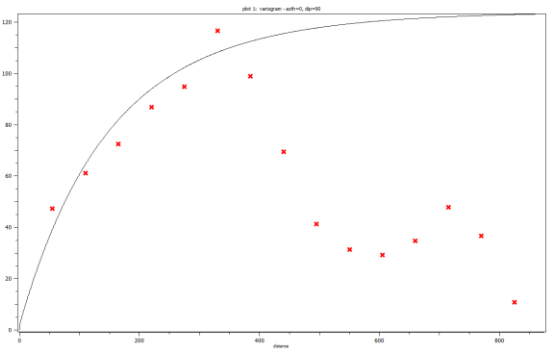

Figure 32: R Fitted vertical variogram model

The second direction established is the omni-direction with an azimuth of 0°, a dip of 0°, a tolerance of 91° and a bandwidth of 200 (see Figure 28). The interpreted variogram structure for each dataset in this direction as well as the fitted function is shown in Figures 33 and 34.

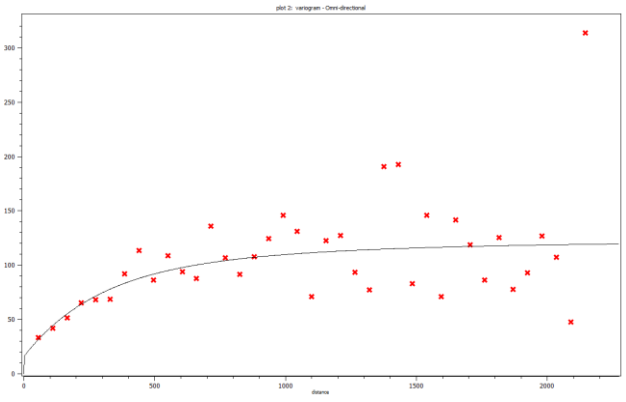

Figure 33: Fitted SP Omni-directional variogram model

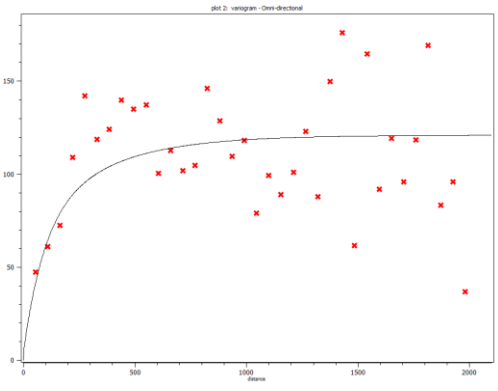

Figure 34: Fitted R Omni-directional variogram model

The third direction established is the horizontal direction aligned along the major trend of the wells with an azimuth of 120°, a dip of 10°, a tolerance of 40° and a bandwidth of 500 (see Figure 28). The interpreted variogram structure for each dataset in this direction as well as the fitted function is shown in Figures 35 and 36.

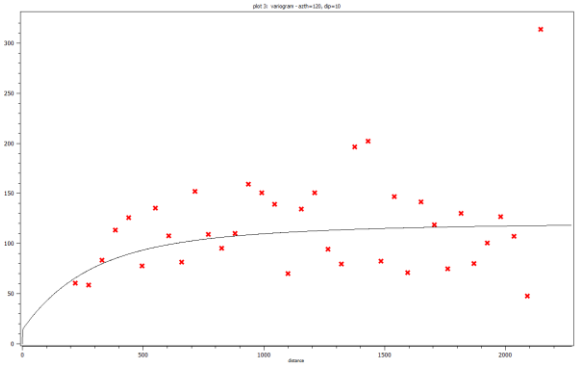

Figure 35: SP fitted horizontal variogram model

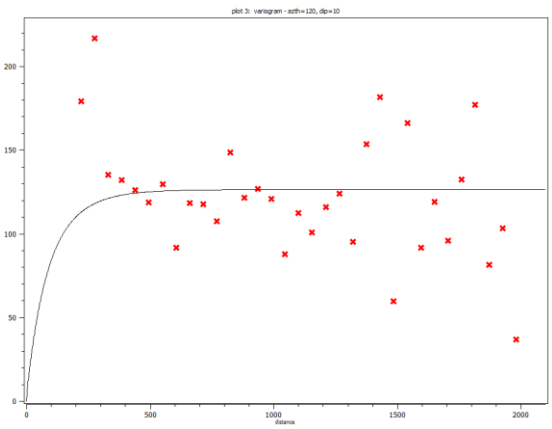

Figure 36: R fitted horizontal variogram model

4.2.3 Variogram Models

Once the distances and directions are established (see Figure 28) to get interpretable structures (Figures 29 and 30), then the variogram can be modeled to represent the statistical function. Two requirements that must be honored in modeling the variogram are: 1) the condition of positive definiteness, and 2) the use of a minimum number of parameters and models to model the variogram (Kelkar and Perez 2002). Because the model types available in the computing software (exponential, spherical, Gaussian) are already known to satisfy the condition of positive definiteness, by using any of these, or linear combinations of them, it is automatically assumed that the model is positive definite, thus satisfying condition one. As previously discussed, the variogram estimation parameters direction and distance capture the most important reservoir

structures including geologic strike and dip, and orientation or trend of wells. It is assumed that the essential spatial features of the oil field reservoir are thus included in the model, which satisfies condition two. The model types available in the software are assumed to have a sill contribution, which is a constant value after a certain lag distance called the range, as shown in Figure 37. The components in the modeling software user interface used to characterize the variogram model are described in the following table.

SGeMS Variogram Model Components	
Interface Input	*Description*
Nugget Effect	The initial abrupt jump to the first value at the beginning of the entire variogram model. Non-continuity only at the origin is due to either measurement error or variation at a scale smaller than the sampling distance.
Number of Structures	Number of (nested) variogram structures composing the variogram model. An accurate fit to a variogram model may be best constructed using a combination of multiple model functions (a.k.a. nested structures), especially to model variability at different scales.
Sill Contribution	Effect of the sill, or the maximum variance of the variogram. Sill is the limit (represented graphically as where the function flattens out) of the variogram model after a specific distance a.k.a the range.
Type	The type of variogram model. SGeMS includes only models for variograms that have a sill: Spherical, Exponential and Gaussian. The model type depends on the function used to approximate the variogram (determines the overall shape of the model).
Ranges (Max,Med, Min)	Ranges along each of the three directions of the anisotropy ellipsoid in the variogram structure (maximum, medium and minimum) used to approximate the model. Depending on the direction(s) specified these ranges help refine the shape/extent of the function.
Angles	Measurement in degrees for each of the three angles (directions) of the 3D anisotropy ellipsoid in the variogram structure: azimuth, dip and rake. Rotation of the angles along the orthogonal planes of a Cartesian coordinate system positions the 3D ellipsoid in space

Table 1: Interface input description of variogram model components

Once a nugget constant and the number of structures in the whole variogram model are selected, then each individual nested structure is further defined by the subsequent parameters listed in the table: the variance contribution (sill), the variogram function (type), and anisotropy characterized by a 3D ellipsoid defined by the ranges and angles (Remy, N., Boucher, A. and Wu, J. 2009). This 3D ellipsoid is defined by the six parameters of the ranges and angles where the three angles, azimuth, dip, and rake, represent the direction of the major, medium and minor axes, and the ranges represent the radii of the axes along the three directions. More detailed information on variogram modeling inputs and conditions is available in the following references: Chiles and Delfiner 1999, and Remy, Boucher. and Wu 2009. Figure 37 illustrates the main components of a typical variogram model, including lag distance, variance, sill, nugget and range.

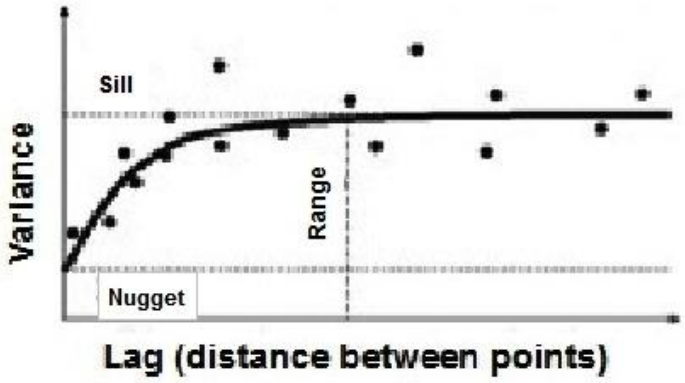

Figure 37: Illustration of main variogram model components (based on Landscape Toolbox Wiki 2014)

Several experiments with the variogram design in terms of the modeling components and variogram parameters were undertaken for both the SP and R datasets. After different options were tested, the following variogram model inputs displayed in

Figures 38 and 39 for SP and R illustrate the final variogram models used for both the interpolation functions. These variogram models were used for the subsequent ordinary kriging and conditional simulation procedures.

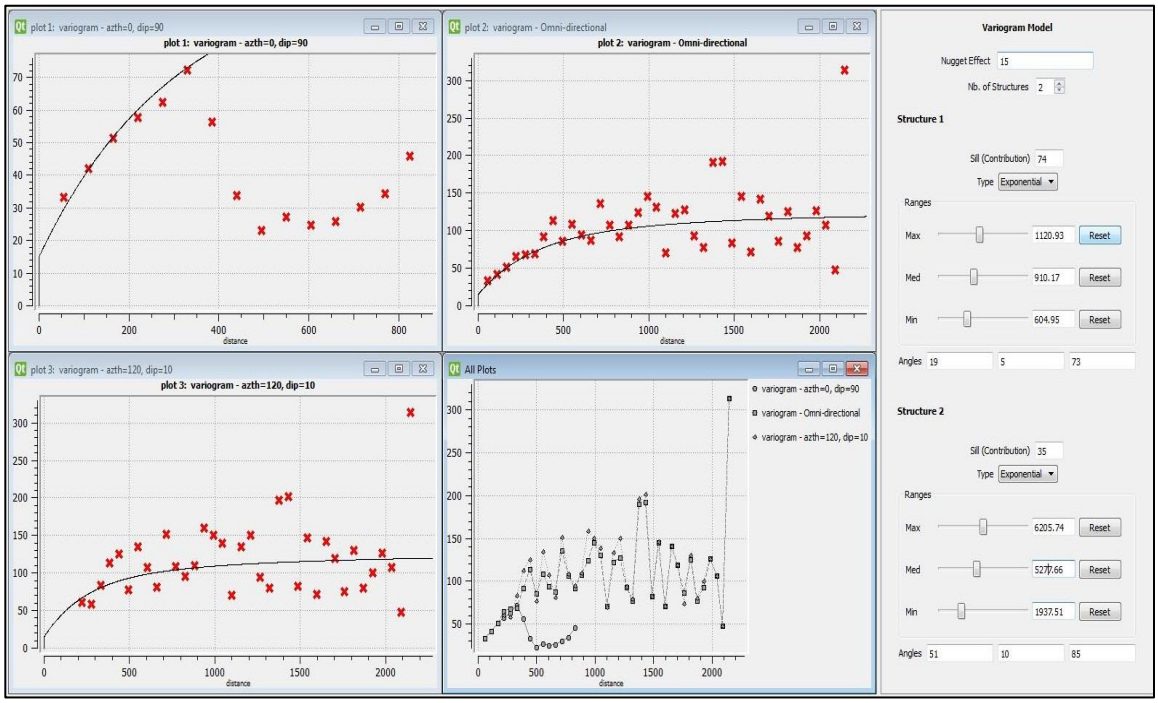

Figure 38: Complete variogram model for Spontaneous Potential

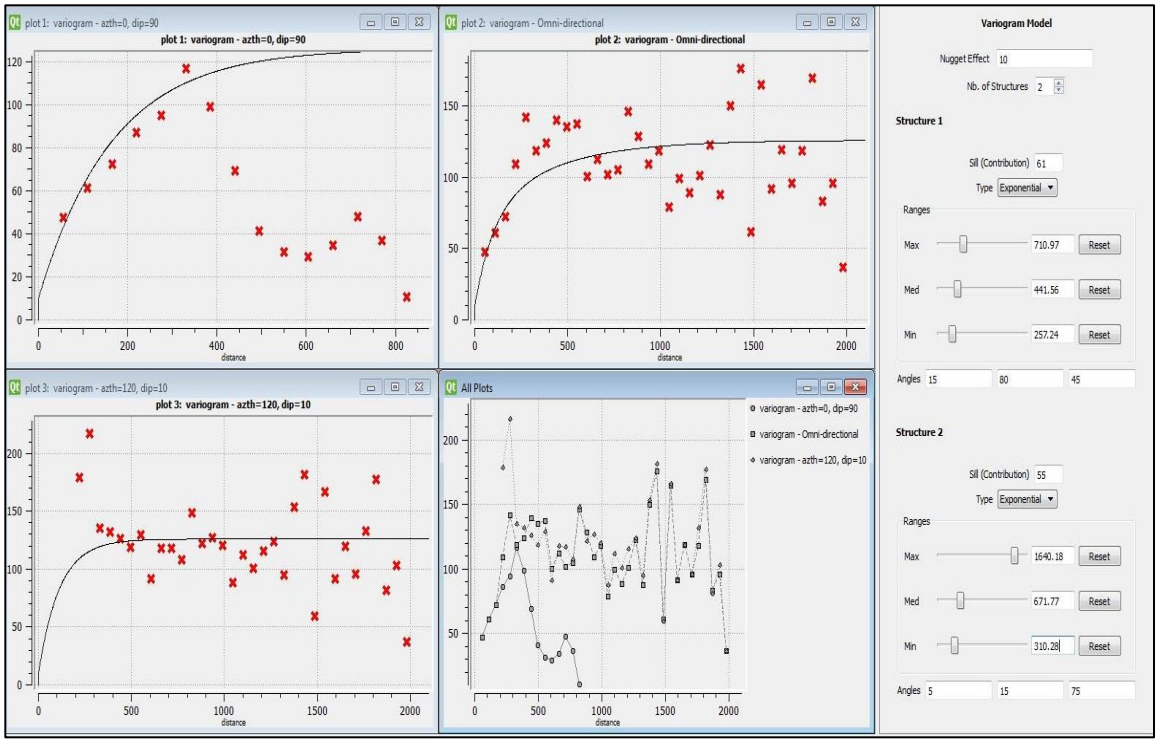

Figure 39: Complete variogram model for resistivity

4.3 Interpolation

4.3.1 Kriging Parameters

Once the variogram models are defined and saved they can be loaded into the kriging toolbox in the SGeMS program followed by simple selections of the grid, data and the type of estimation (e.g. ordinary kriging) necessary to run the analyses. Because the kriging algorithm used in the modeling software requires a 3D ellipsoid to be specified in order to represent a search volume in 3D, the only remaining task was to define the search ellipsoid (Remy, Boucher and Wu 2009). The search ellipsoid was represented by a search space surrounding the interpolation point, and only the points that fell within this search space were considered to take part in the kriging calculations, for

instance in defining the extent and volume to look for values to be used in the interpolation. The search ellipsoid, which is characterized in the same way as the variogram anisotropy ellipsoid, consists of minimum and maximum conditioning data (min/max number of data points to be included in the algorithm), max/med/min ranges and the 3-directional angles. After several experimental kriging runs were conducted, the parameters used to define the search ellipsoid for the analyses determined to be the best were selected, provided in Table 2. . These results are described in detail in Chapter 5.

Search Ellipsoid Parameters			
Conditioning Data	Min	Max	
	2	20	
Ranges	Max	Med	Min
	3000	1650	200
Angles	Azimuth	Dip	Rake
	128	2	3

Table 2: Search ellipsoid parameters used for kriging

4.4 Validation

As part of the kriging interpolation procedure the kriging variance was also calculated and the resulting models mapped the variance in the oil field reservoir. This procedure can help define the areas with higher or weaker variance in the estimation.

4.4.1 Cross-validation

To know how well the models predict the values at unknown locations in the field, in other words to test the integrity of the methods and determine their effectiveness, it was necessary to perform validation procedures on the predicted models. An appropriate technique is cross-validation which consists of leaving one data location out

(i.e. one well) and performing the estimation to predict the values at that excluded location, repeating the process by removing one different well location at a time and re-running the estimation until all the well values have been interpolated. Once the predicted values were obtained for the data at all the measured locations, they were compared to the known values to help determine the quality or accuracy of the model. The observed values, which consisted of actual values from the logs, were plotted against the estimated values predicted values from the model, then compared and contrasted to evaluate their differences. In this manner, cross-validation at each well for both datasets was performed.

4.4.2 Statistical Comparisons

By generating several realizations using the sequential Gaussian simulation algorithm based on the same kriging parameters, uncertainty can be characterized by the multiple possibilities that exhibit local variation. The uncertainty at individual locations throughout the field can be ascertained by examining the differences among several equiprobable plots which will display the local variations and distributions in the oil field reservoir. In this sense, if uncertainty at a particular location is relatively small then a number of images will display similar simulated values at that location, and conversely if uncertainty at a particular location is relatively large then a majority of images will display the differences in simulated values at that location (Kelkar and Perez 2002).

As previously stated, the primary objective of performing a stochastic simulation is to create a model for the probability distribution of the unknown variables. Because the variables are conditioned to the information provided from the field data which is

assumed to be a true representation of the subsurface geology, then their values are reasonably expected to fall within the limits of the simulated probability distribution. Summary statistics on the simulation output provide a measure of the uncertainty of the model, and specific statistical calculations on the suite of realizations provide estimated probabilities.

Calculating the median or mean of the provided multivariate distribution where the median (mean) at each cell is computed from the values of all realizations at that cell location will yield a map with the highest probability of representing the true model. This probability model can be compared to the predicted (kriged) model to provide a better assessment of the analysis. The similarity between the predicted and the probability models provides a degree of confidence in the estimated model. In addition to the median probability (i.e. P50) the P10 and P90 quantiles provide uncertainty ranges or error bars in the simulated median value, providing more confidence that the true expected mean falls within the simulated range. A total of 48 realizations for R were obtained and a total of 53 realizations for SP were obtained. These results are described in detail in Chapter 6.

CHAPTER FIVE: RESULTS

5.1 Conditional Simulation

5.1.1 Sequential Gaussian Simulation Models

In terms of final results of this thesis research, Figure 40 a-f comprises six random realizations of SP distribution across the oil field reservoir, visualized using SGS.

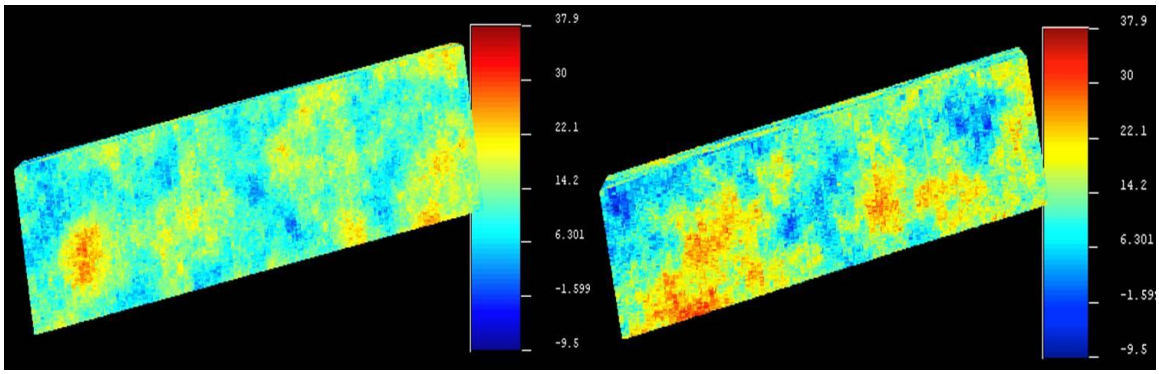

Figure 40a – SP Realization 1

Figure 40b – SP Realization 2

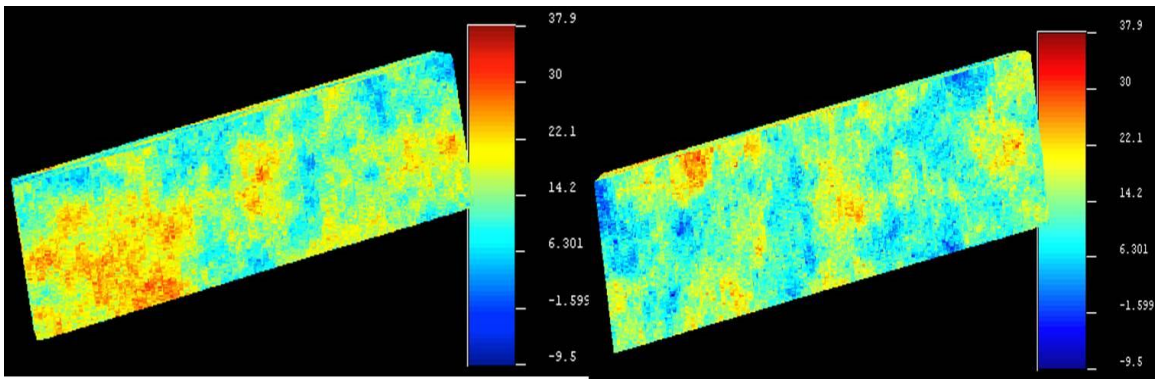

Figure 40c – SP Realization 3

Figure 40d – SP Realization 4

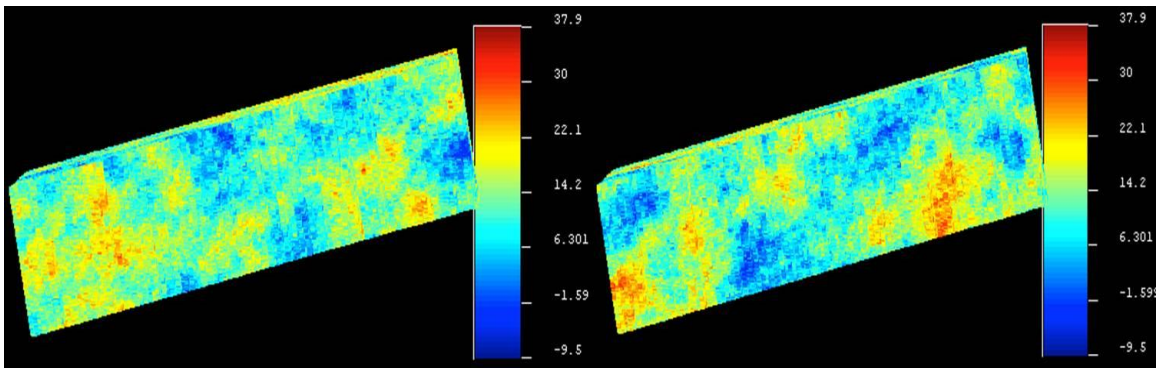

Figure 40e – SP Realization 5

Figure 40f – SP Realization 6

Figure 40 (a-f): Six random SP SGS realizations

Figure 41 (a-f) includes 6 realizations of R distribution across the oil field reservoir.

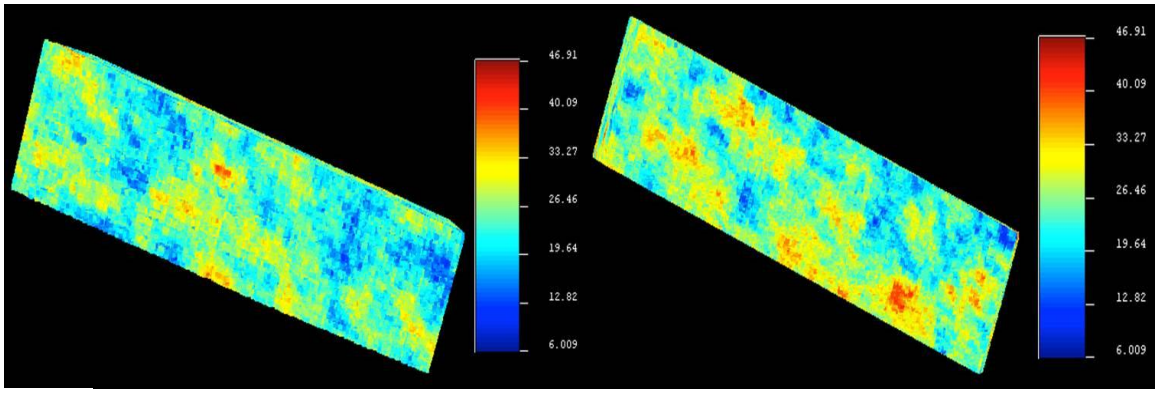

Figure 41a – R Realization 1

Figure 41b – R Realization 2

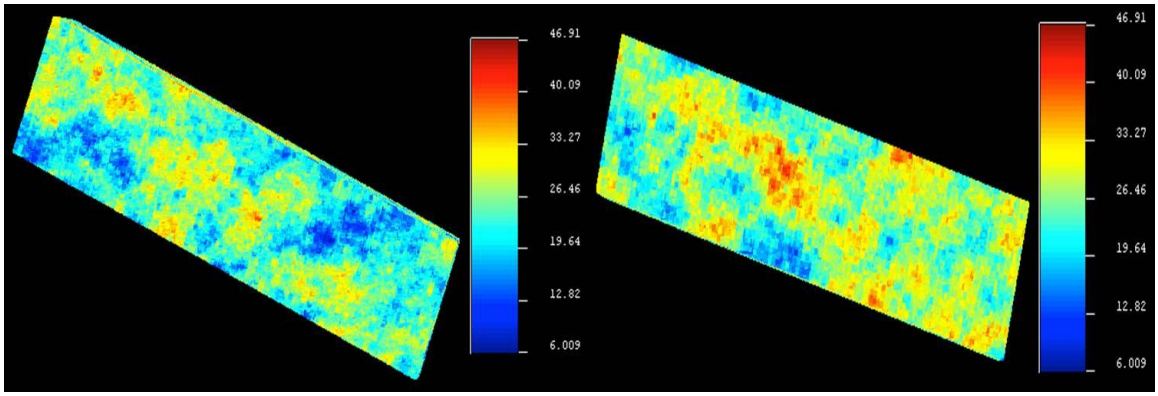

Figure 41c – R Realization 3

Figure 41d – R Realization 4

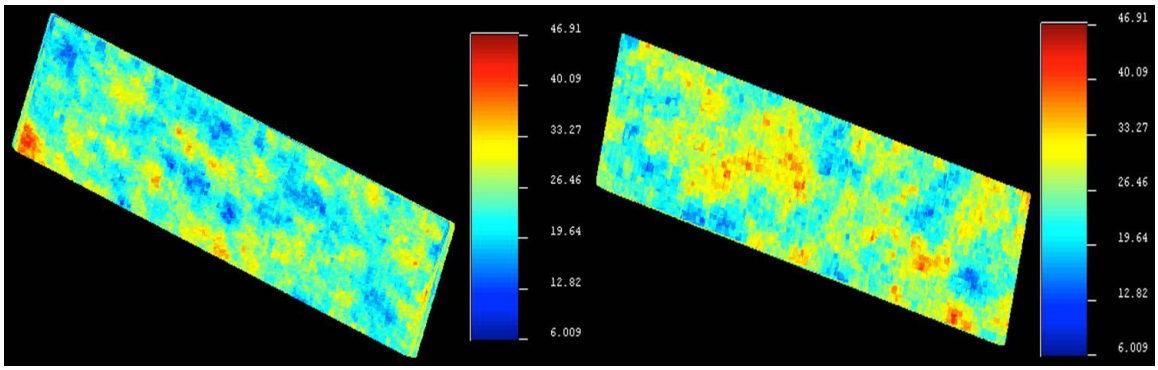

Figure 41e – R Realization 5

Figure 41f – R Realization 6

Figure 41 (a-f): Six random R SGS realizations

The calculated median (P50) as well as the P10 and P90 probability simulation models from all the realizations are also included. Figures 42-44 illustrate the P50 map as well as the P10 and P90 maps for R with designated color bars. Figures 45-47 illustrate the P50 map as well as the P10 and P90 maps for SP with designated color bars.

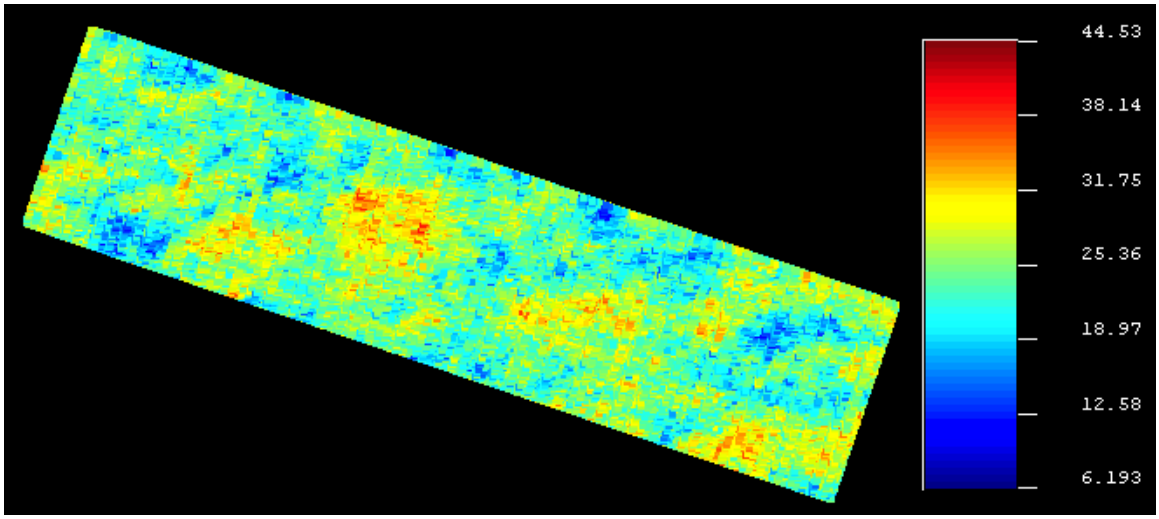

Figure 42: Resistivity P50 map

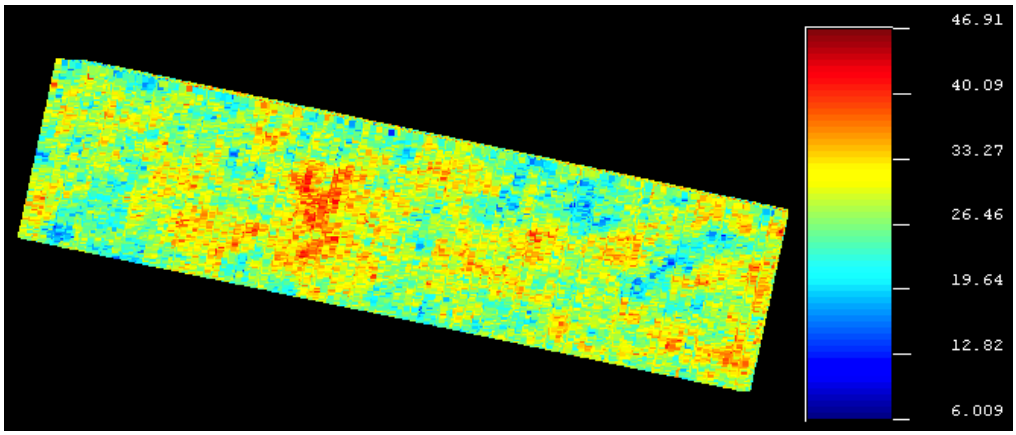

Figure 43: P10 Resistivity map

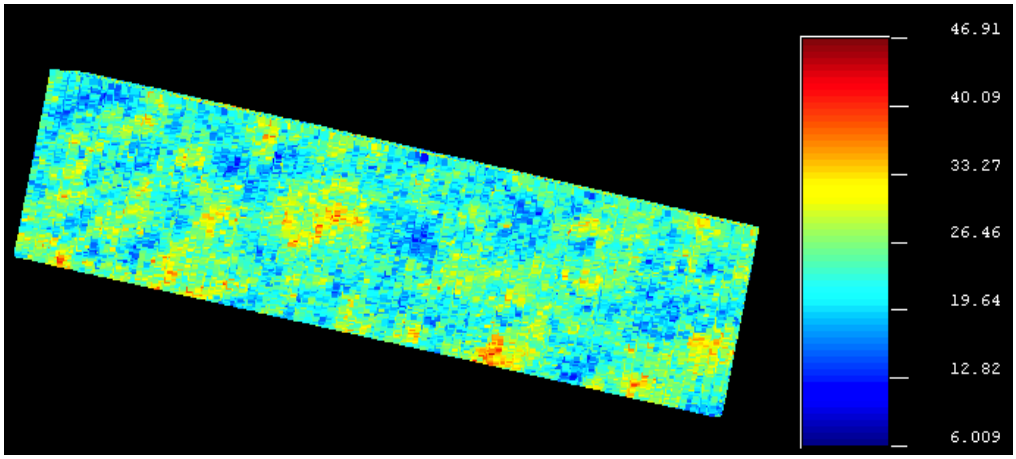

Figure 44: P90 Resistivity map

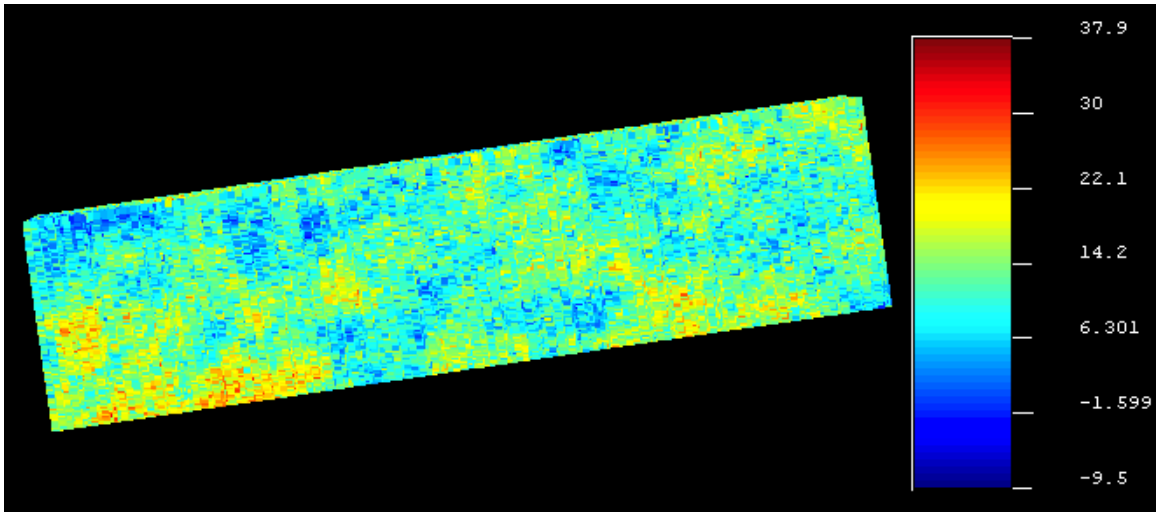

Figure 45: Spontaneous Potential P50 map

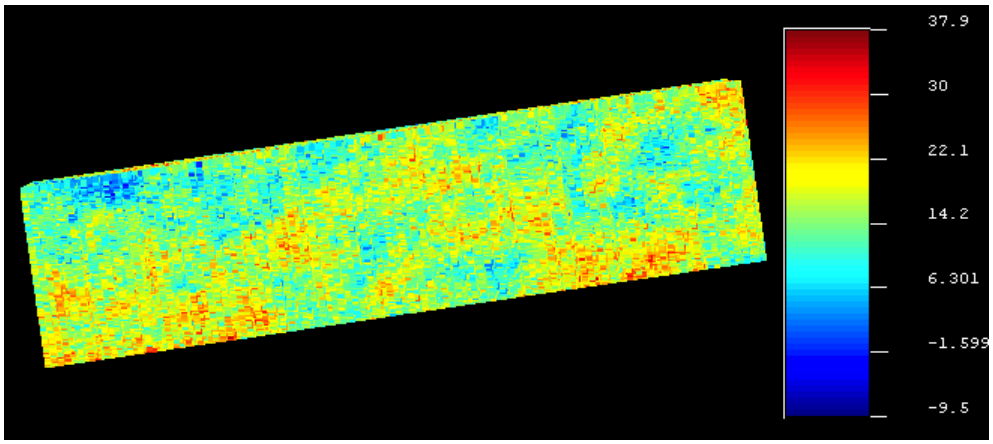

Figure 46: P10 Spontaneous Potential map

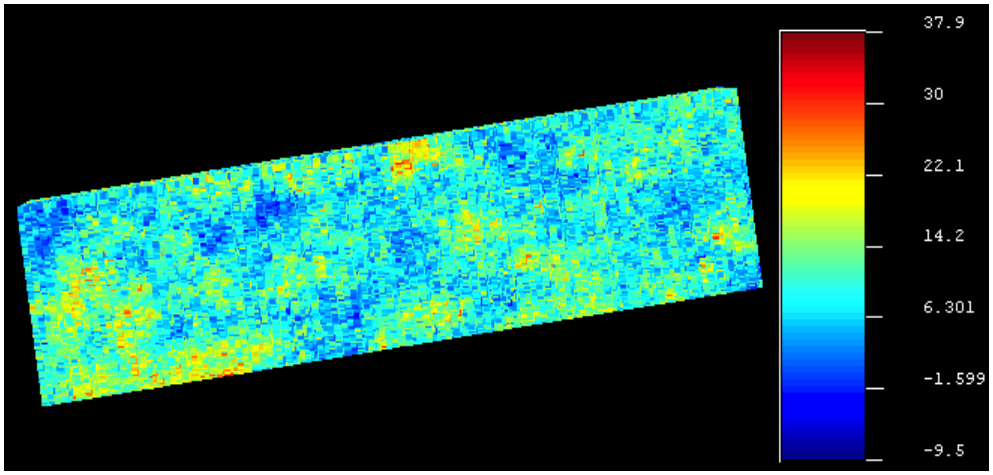

Figure 47: P90 Spontaneous Potential map

5.2 Ordinary Kriging

5.2.1 Predicted Models

The kriged model and its associated variance map for R are included as Figures 48 and 49. Figures 50 and 51 illustrate the predicted map and its associated variance map for SP.

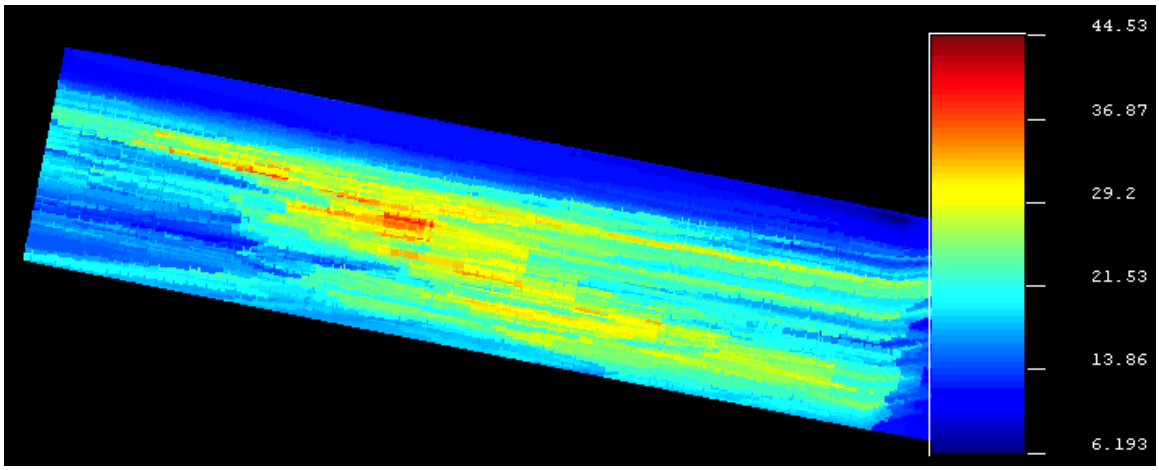

Figure 48: Resistivity ordinary kriging interpolated map

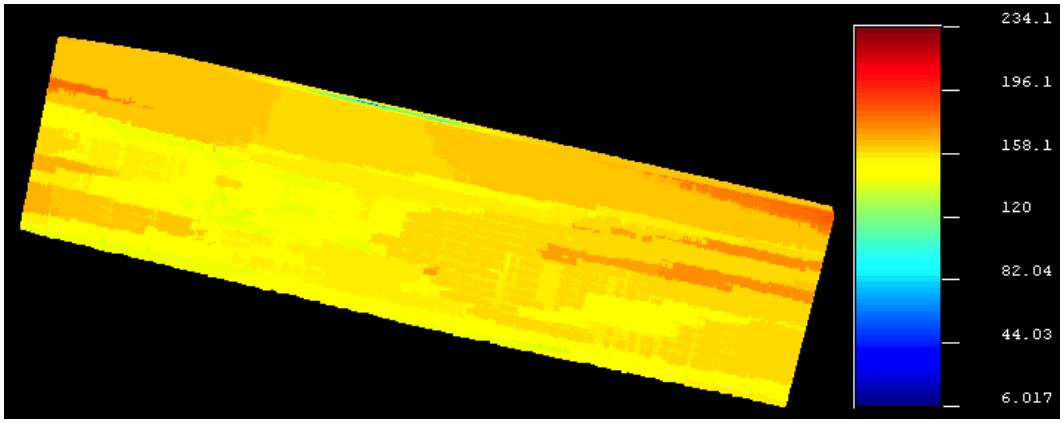

Figure 49: Resistivity variance map from ordinary kriging model

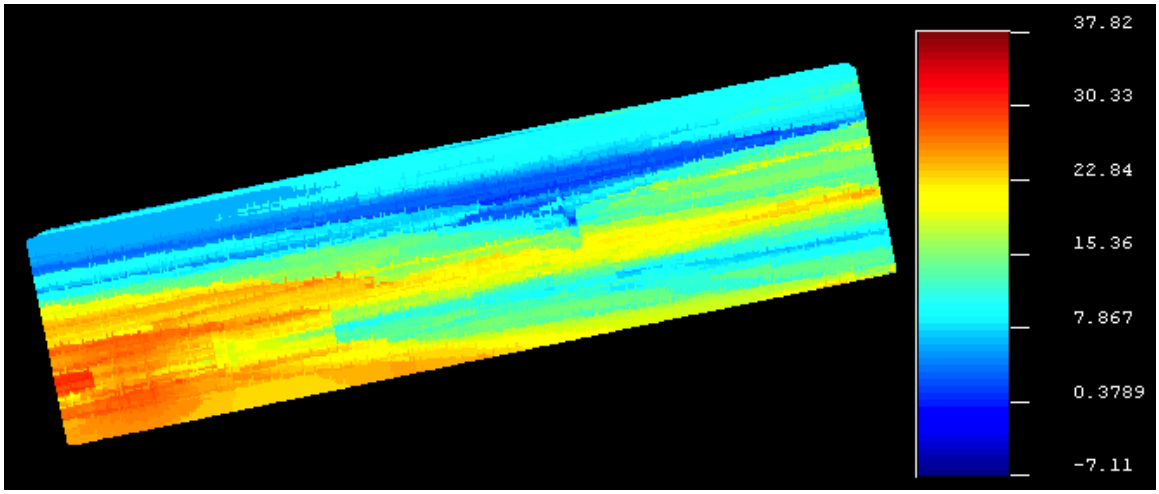

Figure 50: Spontaneous Potential ordinary kriging interpolated map

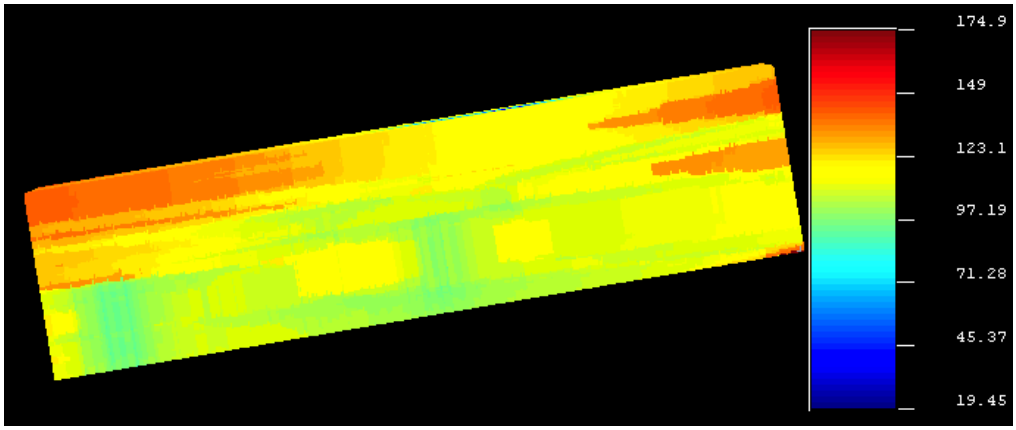

Figure 51: Spontaneous Potential variance map from ordinary kriging model

5.3 Volume Explorer

The “volume explorer” tool in the SGeMS modeling software allows exploring of the 3D distribution of properties across the estimated volume of the field. Figures 52 and 53 display a snapshot of the “inside” of the SP and R models. This is an important tool because static images mostly show the outside of a model and may not provide an

adequate representation of the entire 3D volume distribution. The scale of Figure 52 is identical to that of Figure 50 and the scale of Figure 53 is identical to that of Figure 48.

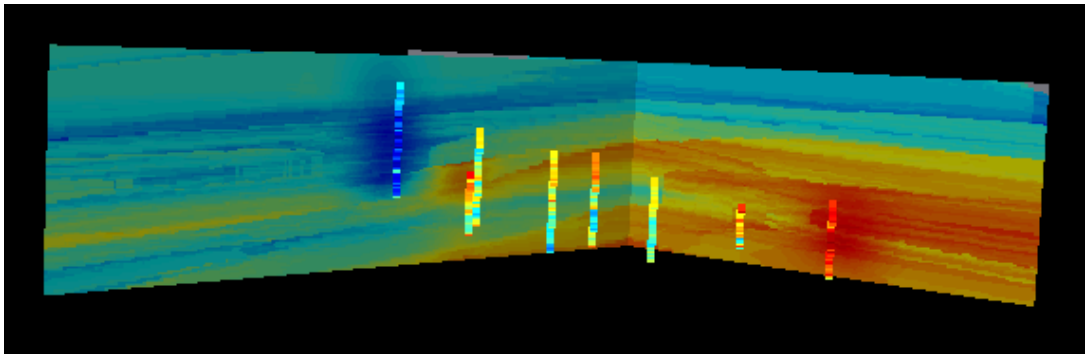

Figure 52: Spontaneous Potential 3D volume map

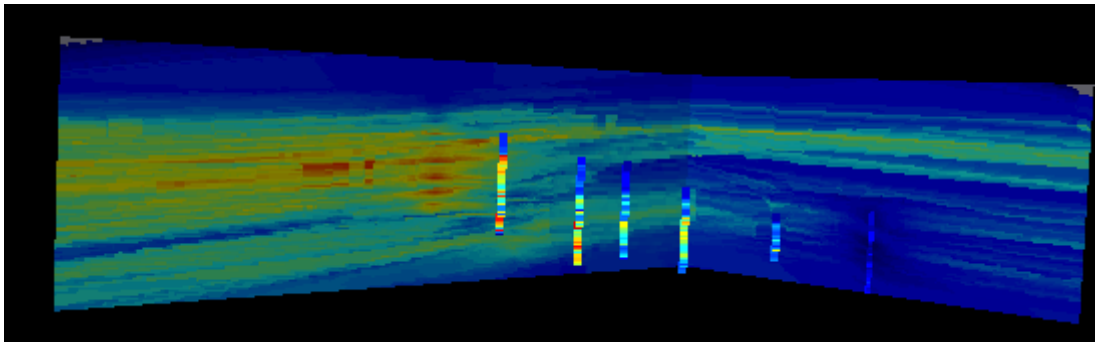

Figure 53: Resistivity 3D volume map

CHAPTER SIX: DISCUSSION AND CONCLUSION

6.1 Variogram and Simulation Model Remarks

The experimental variogram in the vertical direction (top left corner, or Quadrant I, of Figures 29 and 30) for both datasets exhibit periodic behavior, which represents cyclical geological processes. This is known as the "hole effect" in geostatistics and is typically experienced when modeling a variogram in the vertical direction. In depositional environments sediment is deposited in layers during geological events, thus this repetition of cycles will be reflected in the vertical continuity of the layers in the field. In these variograms the transition from one facies to another can be clearly defined. Interpretation from both of the vertical-directional variograms indicates that the formation is continuous in the vertical direction up to around 350' and then becomes discontinuous but regains continuity at greater distances. This trend is expected to continue throughout different depths across the field. The fitted vertical variogram functions (Figures 31 and 32) only include those values to 350' and ignore the rest because it is of most interest to only capture the extent of that continuity. In addition, the average thickness of the formation is only 378', so by modeling to 350' we are capturing all the continuity necessary for building a valid 3D model for this formation. The other two variogram directions show the overall and the horizontal continuity trends in the field, both of which exhibit very similar patterns. The fitted functions (Figures 33 through 36) were plotted in order to include most of the points. A few points which were considered as possible local outliers were neglected in order to obtain a reasonable structural function for the variogram model, discussed further in the project evaluation. Overall, the trend of the study area is well captured in both of the variogram models.

Since all of the realizations of the conditional simulations honor the same constraints because they are coming from the same data distribution, it is not possible that one realization image is more likely to occur than any other. Therefore the apparent differences between realized images is representative of the local uncertainty, and visualizing the variability between simulations provides a reasonable assessment of uncertainty. Provided the distribution is representative of the real oil field reservoir then the true reservoir values are expected to fall within the bounds of the distribution while the calculated statistical summaries of the simulations (P10, P50, P90) illustrate the probabilities of occurrence.

6.1.1 Well ID Locations

Figure 54 is a 2D map displaying the well locations of each borehole in the reservoir area, labeled by unique well identification number. The well ID numbers were assigned based on the order that the wells were drilled. The spatial configuration of wells is important to note for the discussion and interpretation of results.

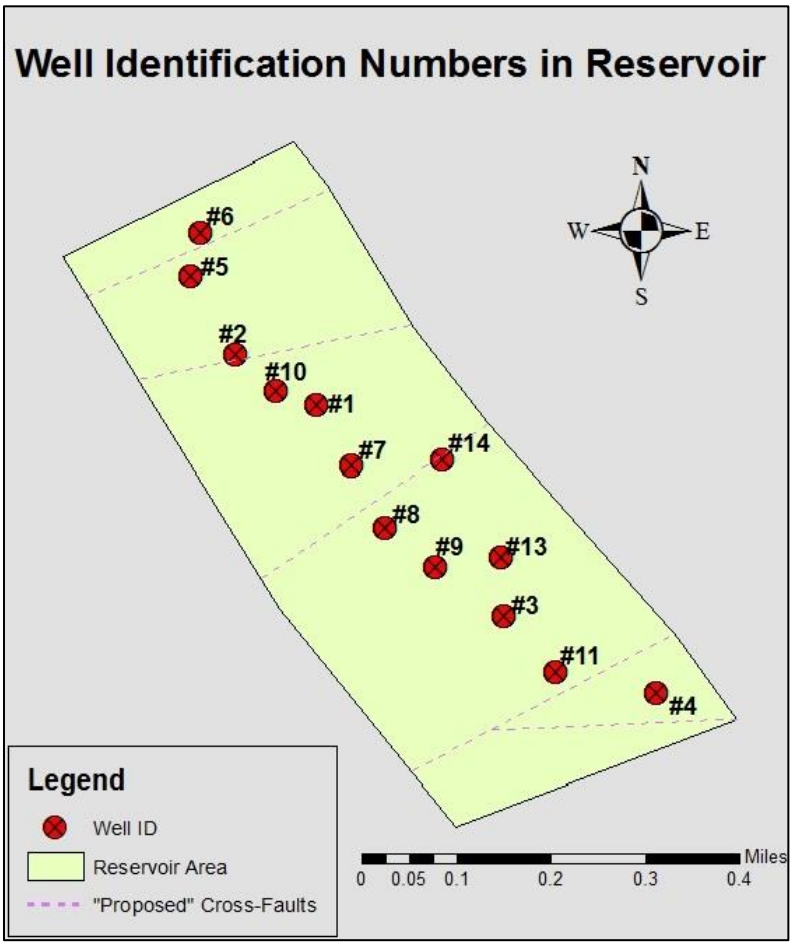

Figure 54: Well ID location map

6.2 Validation

Figures 55 and 56 (a-m) display the cross-validation results of all wells for both datasets. The well number is the well ID number (Figure 54). The results include the observed data (log values) plotted along with the estimated data (kriged values) versus subsea depth. All the plots include low, medium and high value thresholds as well as horizontal error bars of the standard deviation of the observed data for each borehole.

6.2.1 Cross-validation plots

Figure 55 (a-m) provides R cross-validation graphs which represent the differences between the observed values and the estimated values.

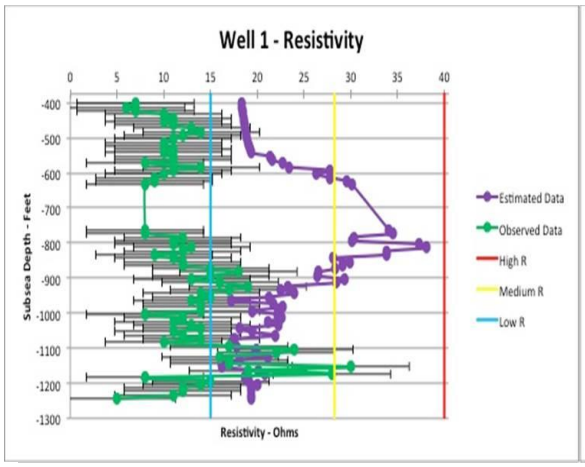

Figure 55a – R Cross-Validation Well #1

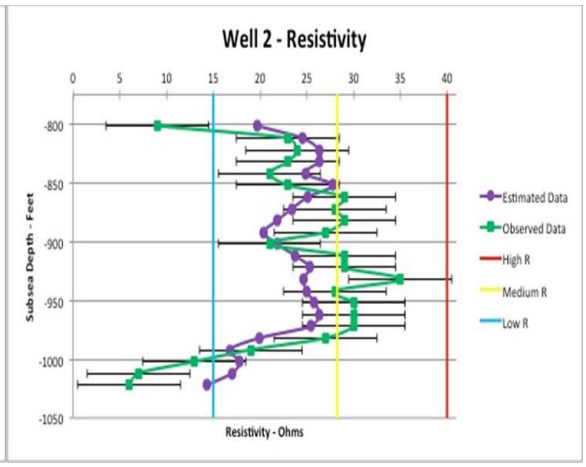

Figure 55b – R Cross-Validation Well #2

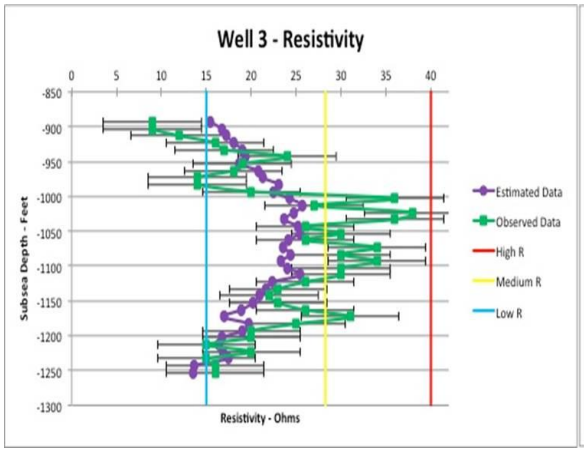

Figure 55c – R Cross-Validation Well #3

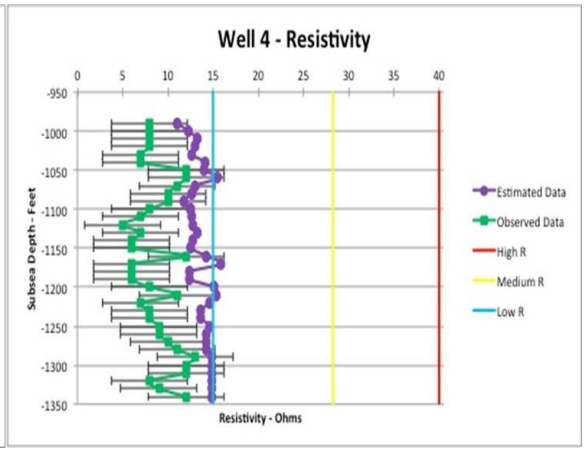

Figure 55d – R Cross-Validation Well #4

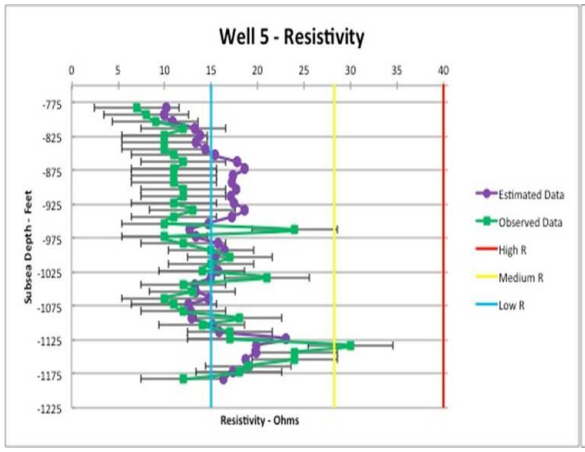

Figure 55e – R Cross-Validation Well #5

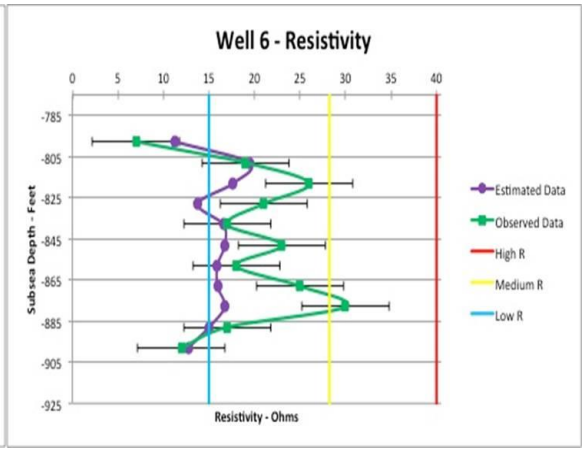

Figure 55f – R Cross-Validation Well #6

Figure 55 (a-f, continued on page 73): Resistivity cross-validation results for all wells

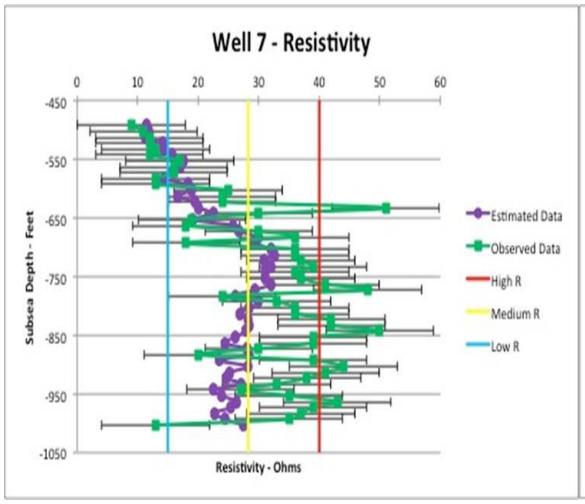

Figure 55g – R Cross-Validation Well #7

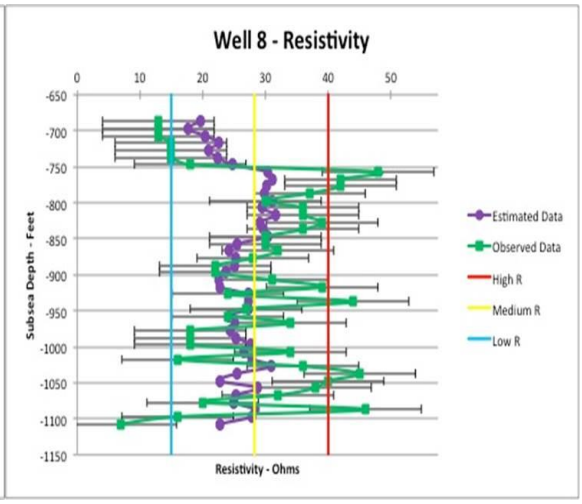

Figure 55h – R Cross-Validation Well #8

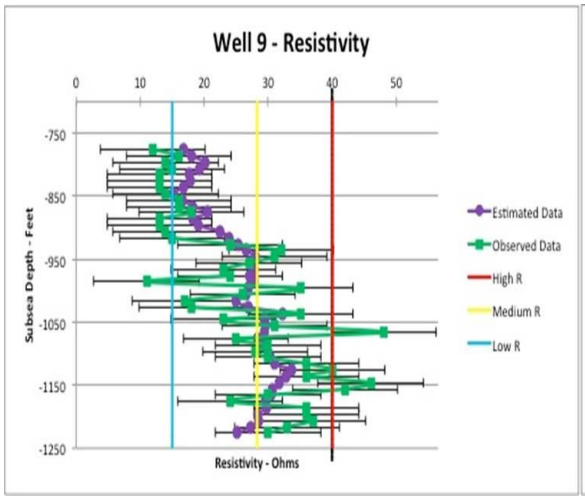

Figure 55i – R Cross-Validation Well #9

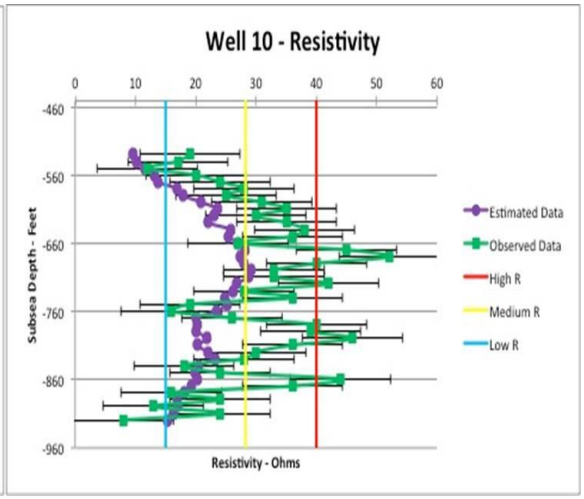

Figure 55j – R Cross-Validation Well #10

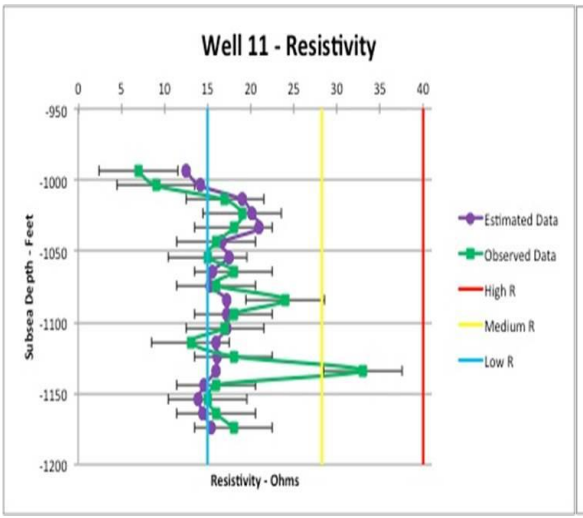

Figure 55k – R Cross-Validation Well #11

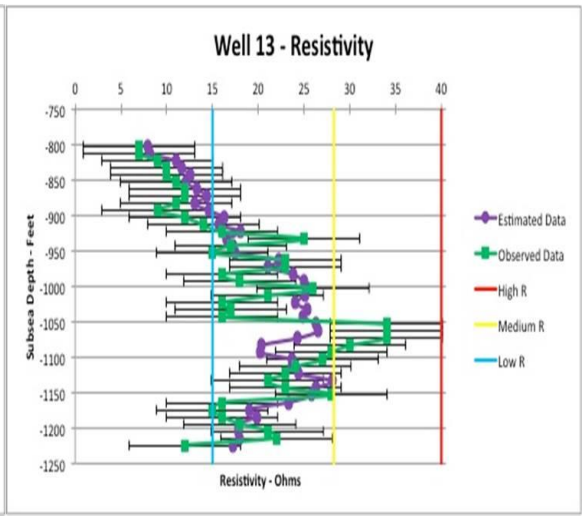

Figure 55l – R Cross-Validation Well #13

Figure 55 (g-l, continued from page 72): Resistivity cross-validation results for all wells

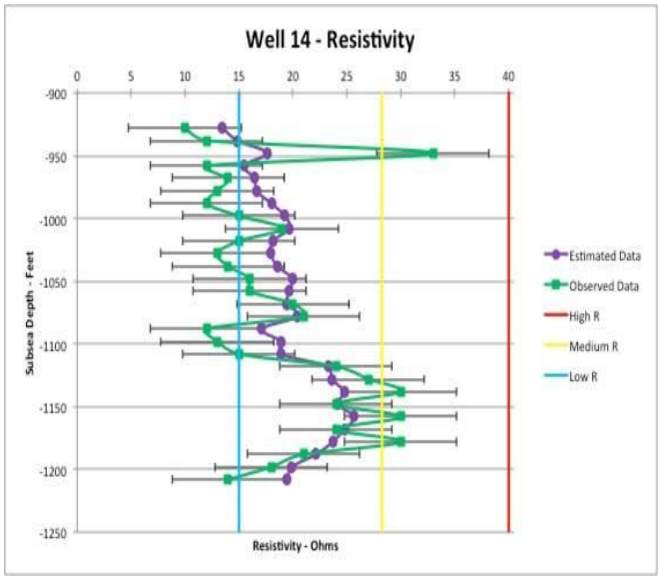

Figure 55m – R Cross-Validation Well #14

Figure 55 (m, continued from page 73): Resistivity cross-validation results for all wells

Figure 56 (a-m) displays SP cross-validation graphs, which depict the differences between observed values and estimated values.

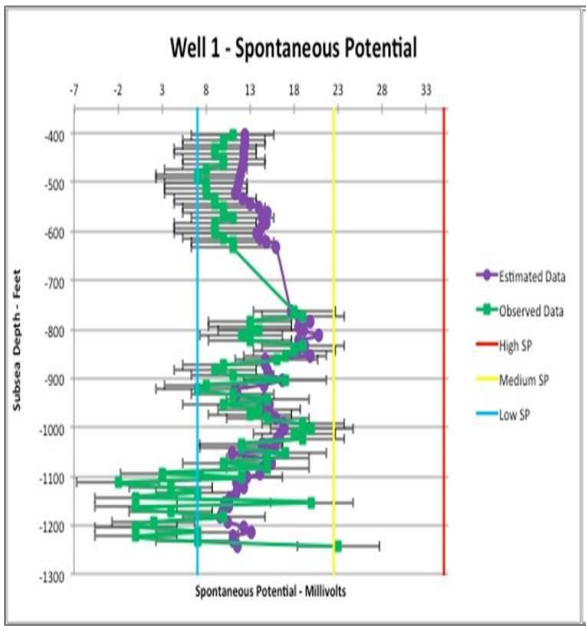

Figure 56a – SP Cross-Validation Well #1

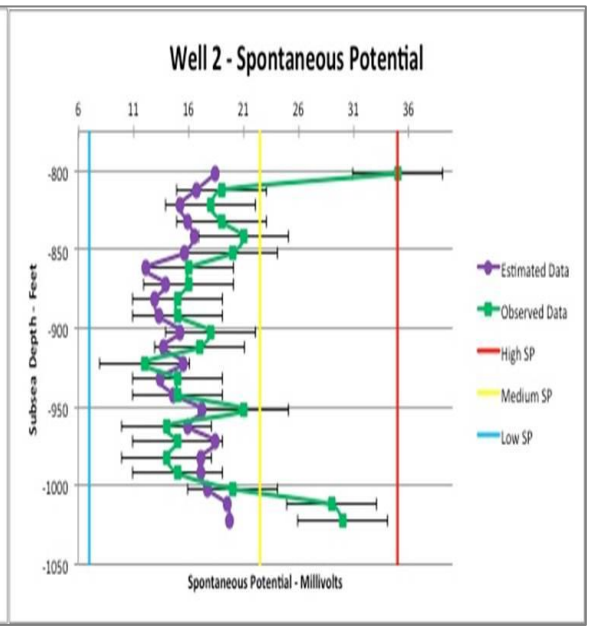

Figure 56b – SP Cross-Validation Well #2

Figure 56 (a-b, continued on page 75): Spontaneous Potential cross-validation results for all wells

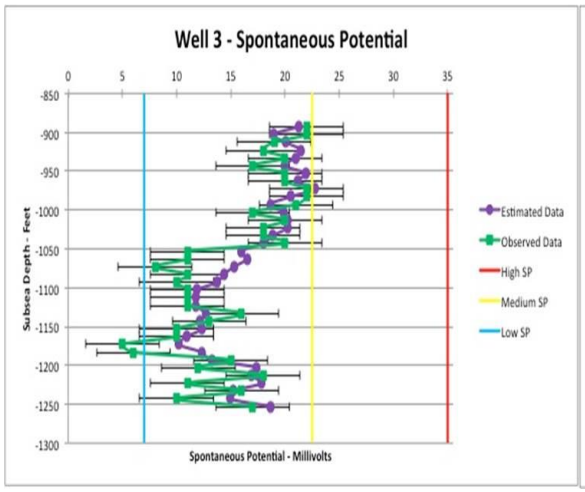

Figure 56c – SP Cross-Validation Well #3

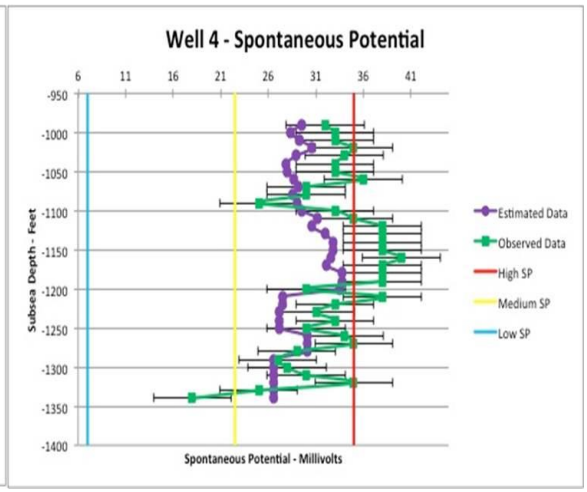

Figure 56d – SP Cross-Validation Well #4

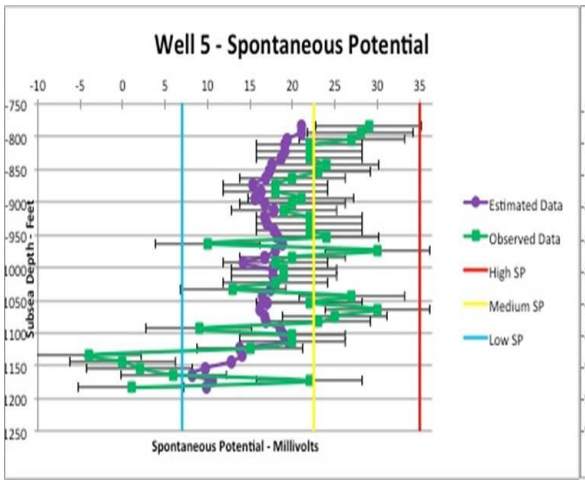

Figure 56e – SP Cross-Validation Well #5

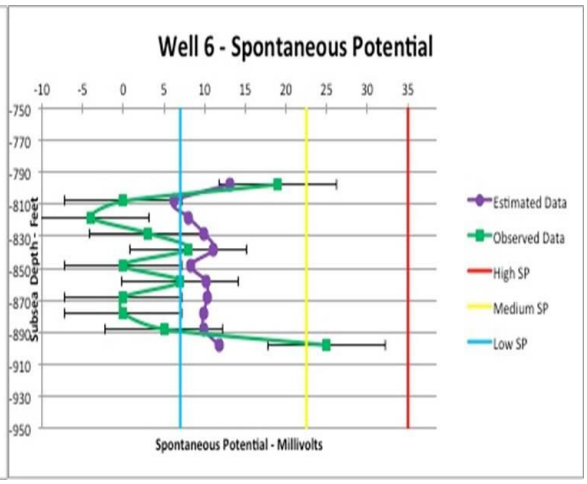

Figure 56f – SP Cross-Validation Well #6

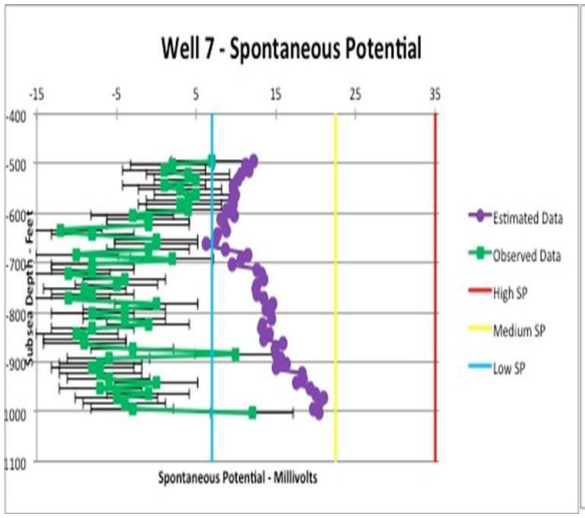

Figure 56g – SP Cross-Validation Well #7

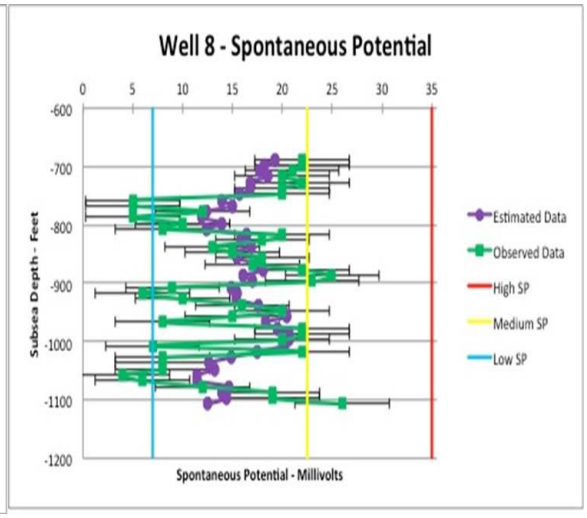

Figure 56h – SP Cross-Validation Well #8

Figure 56 (c-h, continued from page 74): Spontaneous Potential cross-validation results for all wells

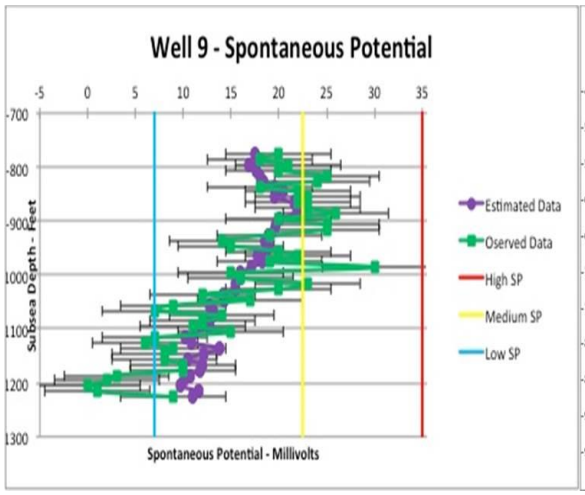

Figure 56i – SP Cross-Validation Well #9

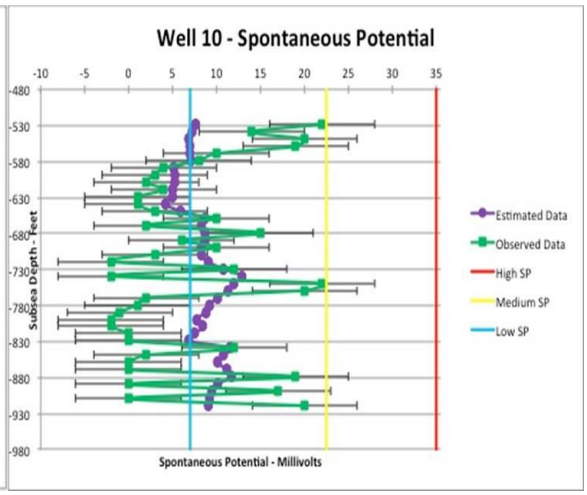

Figure 56j – SP Cross-Validation Well #10

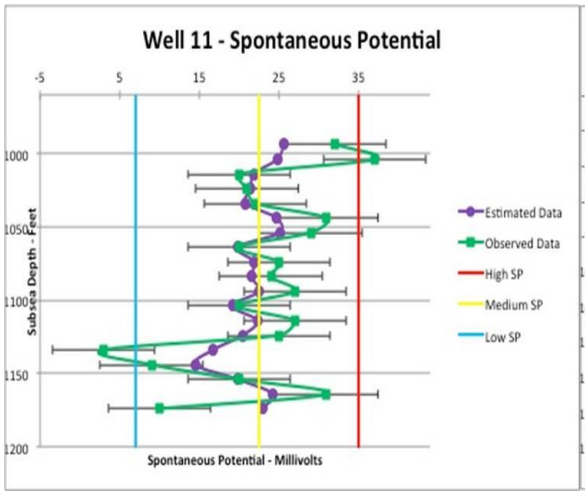

Figure 56k – SP Cross-Validation Well #11

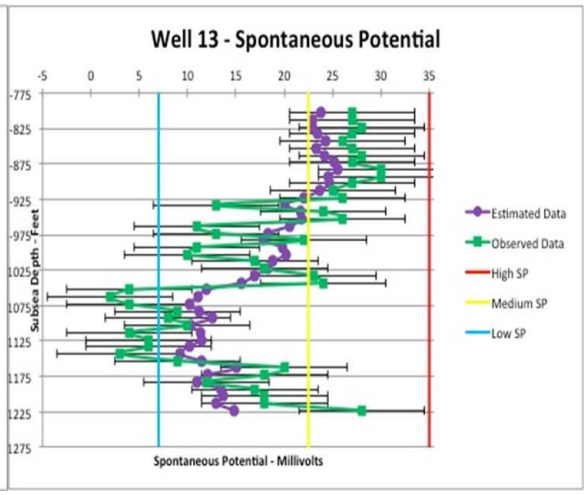

Figure 56l – SP Cross-Validation Well #13

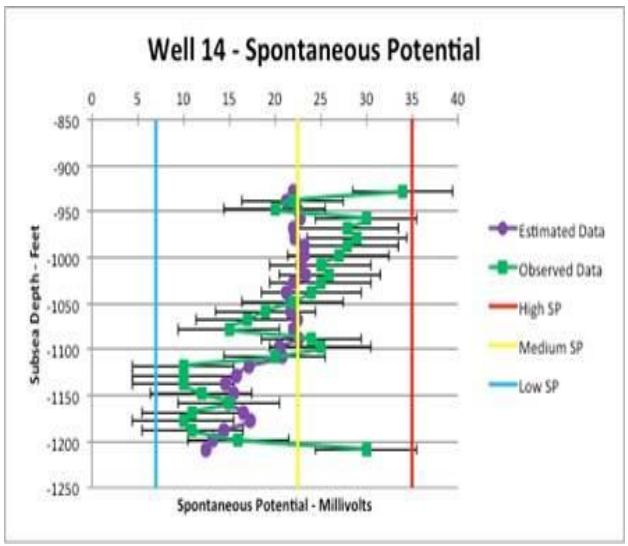

Figure 56m – SP Cross-Validation Well #14

Figure 56 (i-m, continued from page 75): Spontaneous Potential cross-validation results for all wells

6.3 Project Evaluation

Both of the kriged models illustrate static representations, in 3D, of the distribution of SP and R throughout the field. The intent of kriging interpolation is to estimate, or provide the best possible approximation of the overall continuity in this study area. The conditional simulations provide complementary information to help determine the local variation and quantify uncertainty in a probabilistic sense while providing a degree of confidence in the models. The cross-validation provides a direct measurement of the estimation accuracy.

6.3.1 Comparison of Results

Both the spontaneous potential (SP) and resistivity (R) kriged models appear to follow an expected continuity trend based on the local geology of the field, and both of their corresponding variance maps help indicate the local variance in their predictions. Both of the simulations and their calculated statistical outputs provide useful representations of the field variabilities and their probabilistic ranges. Comparing the R kriged model with the calculated R P50 simulation mean value model (Figure 48 and Figure 42), it appears that the overall trend remains generally consistent between both models with the exception of a few small areas in the upper half of the field. Comparing the SP kriged model with the calculated SP P50 simulation mean value model (Figure 50 and Figure 45) it appears that most of the continuity is also well preserved, especially in the lower half of the field. However, small to moderate dissimilarity appears within the upper half of the oil field reservoir. The dissimilarities that are most apparent occur mainly near opposite edges, which is probably due to lack of data from boreholes drilled

near the edges of the study are (i.e. no conditioning data points). In addition, the distances from the observed locations (i.e. logged wells) are larger, therefore we can expect greater uncertainty in those locations. Aside from the expected larger variances near the corners of the study area due to the edge wells being farther away from real/observed values, and some of the localized variances that can be seen from the variance maps (Figures 49 and 51), the P10 and P90 maps appear to show a modest margin of probability in the distribution in which the P50 median (or average) falls between the lower and upper quantiles (P10 and P90). The noticeable differences apparent in both datasets in the upper half of the oil field reservoir are probably related to the larger variability experienced in the upper half of the field.

From the cross-validation it is possible to gauge the accuracy of the estimation given the assumptions made in the modeling process, since the standard deviation error bars help provide a "tolerance range". Although the SP and R values obtained for the same well locations and at the same depths do show a strong (negative) correlation, the spatial relationships within each set differ significantly. The interpolation and validation procedures conducted in this study help quantify these relationships. Observance of the raw data indicates correlation trends will likely differ between both datasets due to different modest deviations within each set of wellbores. Also, the cross-validation results point out the individual wells that deviate the most.

The R well#1 is the well with the largest error in the R dataset, followed by the southernmost R well#4. Although these wells plot in a consistent manner close to the observed values, most of the calculated values fall outside the bounds of the standard

deviation (Figures 55 and 56). The estimated values for the rest of the wells in this dataset appear to plot reasonably close to the observed values. However, close examination of the results reveals that the estimations for all of the wells between R well#1 and R well #4 (i.e. wells #11, 3, 13, 9, 8 and 14 in the lower half of the field) appear to plot slightly better in terms of accuracy than all of the wells north of well #1 (i.e. wells #10, 2, 5 and 5 in the upper half of the field).

In contrast to the R data plots, the SP well#7 estimated values deviate the most from the observed data, also plotting outside the bounds of the standard deviation. Most of the other wells within this dataset plot reasonably close to the observed values, however there are some significant differences noted, including well #4 (located at the southern edge) and well #6 (located at the northern edge) which both show significant deviation. The same overall field observation noted from the R results appears to also be evident in the SP results, where all the wells in the lower half (south of the dataset outlier) provide slightly closer approximations relative to all the wells in the upper half (north of the dataset outlier). The "dataset outlier" for the SP values is well #7, and for the R values it is well #1. Also included in this observation is the significant deviation of these two wells at the boundaries, where one is located at the northern edge and one at the southern edge of the field.

6.3.2 Interpretation

In summary, the cross-validation results as well as the compared interpolation results indicate that the wells with slightly larger errors include the two wells at the

north/south edges of the field (well #4 and well #6) as well as the outlier for each dataset (well #7 for SP and well #1 for R). Also, all of the wells north of the outlier for each dataset (in upper half of field) show slightly higher errors than all of the wells south of the outlier (in lower half of field).

The apparent estimation discrepancies are probably related to the fact that well #4 is the southernmost well located in an almost isolated southeastern corner of the reservoir, and well #6 is the northernmost well and is also the thinnest borehole (100' of formation with only 10 log values). The relatively larger accuracy error of these two wells located at the study area boundaries can be attributed to their locations compared to the configuration of other wells in the field and their less than optimal proximity to the other boreholes. The clustered borehole locations have more conditioning data and so are expected to provide slightly more accurate estimates. Given a general consistency between the kriged and simulated models in addition to the same general trend expressed from the cross-validation of both electrical datasets, the assumption can be made that the spatial continuity in the lower half of the field is very strong (from well #4 up to somewhere between well #7 and well#1), and in the upper half (from well #1 to well#6) it is strong but slightly less continuous. Nevertheless, this assumption does not include the notion that the reservoir is divided into separate segments or compartments. Based on the observations discussed herein the integrity of the overall trend throughout the entire field is continuous enough to consider and treat the reservoir as a whole. Based on the results of this study, and although there a few slightly statistically deviated wells (or minor

localized zones), it is suggested that the reservoir is intact with a generally strong continuity trend mimicking the geologic attitude of the field.

It is very important to provide final clarifications on the uncertainties associated with the necessary assumptions that are expressed in the results and how it relates to the confidence that can be attributed to the models. As mentioned in Chapters 1 and 3 the assumption of stationarity for the entire reservoir must be made as a necessary subjective decision. Stationarity is assumed in order to build a single geological model for the entire study area. Also, as mentioned in Chapters 2 and 4 the wellbores are aligned along the plane parallel to the geological strike of the field. Because all of the wells are preferentially directed along this plane there is inherently more certainty in the data obtained in this direction (northwest-southeast) compared to the perpendicular direction (southwest-northeast). Due to a lack of data in the southwest-northeast direction relative to northwest-southeast, it is apparent that there is significant directional uncertainty (i.e. more uncertainty) in the model results along the lateral southwest-northeast direction. Because the assumed continuities throughout the reservoir volume are constrained to and are a direct result of the chosen variogram model parameters, the variability in the parameters for the variogram models define the global continuity in the field. As can be seen from the similarities between the variogram in the northwest-southeast trend and omni-directions the continuity in the study area is preferential in the plane parallel to the well alignment, and the uncertainty in the estimation in this direction is less significant. Similarly, because a coherent continuity trend is captured in the vertical direction for most of the thickness of the formation layer, the uncertainty in the estimation in this

direction is also less significant. According to the data in this analysis the confidence levels (i.e. from maximum continuity to minimum continuity) follow this order, from greatest to least: first the vertical direction, second the well alignment direction, and third the direction perpendicular to the orientation of the wells.

Despite the many benefits of conventional estimation techniques (as discussed in Chapter 1) one of the common weaknesses of kriging, which relies on a variogram model, is that it is completely dependent upon the input data, and because of data limitations it is necessary to make large assumptions for an entire field which typically yield results with directional uncertainty in continuities across the study area. As future work, to reduce the uncertainty in this study area along the lateral plane perpendicular to the well orientation (i.e. southwest-northeast direction), additional variogram models should be computed using available data from wellbores drilled outside of the southwestern and northeastern boundaries of the reservoir in order to determine any correlations with the continuities defined in this project.

To summarize, based on all of the assumptions discussed with regards to this specific oil reservoir, including the model parameters and directional uncertainties of the field, there are various levels of confidence. Because of the previously mentioned similarities between the simulated and predicted maps as well as the cross-validation results we can assume more confidence in the variogram and continuity results for both the trends in the vertical direction and in the direction of the wellbore alignment in the field. We can assume less confidence in the variogram and continuity results for the trend in the

direction perpendicular to the wellbore alignment because of larger uncertainties in this direction and thus weaker predictions. In addition, because of the local active geology consisting of continuous thrust faulting that extends the reservoir along its northwest-southeast plane and thins the geologic units of interest along its southwest-northeast plane, it can be expected that the trend along the plane perpendicular to the geologic strike of the study area will not be as continuous. Thus the geological representations of the field obtained from the interpolation analyses presented as the final results of this thesis appear to provide acceptable reservoir models that can be used at individual discretion for subsequent engineering analyses and field operations, as long as all of the relevant uncertainties of the field are taken into consideration.

6.3.3 Final remarks

Geostatistics is applied to several disciplines including environmental science, oceanography, geology, meteorology and epidemiology for specific operations such as petroleum production, water production, mining, weather prediction and even disease spreading. Ongoing research within this field is vast and it is likely to remain a very important modeling approach in the sciences and engineering. Although the data utilized in this study include the electrical properties of rocks and their fluids, the same (or similar) methodology can be applied to different datasets including hard data and soft data values obtained from other sources such as seismic, geochemical sampling, core sampling or remote sensing. For example, in applications to geochemistry and hydrology, geostatistical modeling using chemical and geochemical data can help quantify the flow and transport of subsurface constituents in aqueous systems (e.g. pollutants, solutes,

particles) and thus provide a better assessment of water resources including groundwater quantity and quality (e.g. remediation of contaminant plumes and aquifer productivity).

The discipline of geostatistics is a core component of reservoir characterization and is a necessary step to obtain an adequate geological model of the reservoir that can be integrated into a fluid-flow numerical simulator to predict hydrocarbon production, then further formulated into an inverse model and adjusted to match field responses. The whole reservoir characterization-simulation-engineering process is a dynamic and continuous process that allows scientists, engineers and operators to understand, predict and to some extent control the reservoir in order to achieve optimal field performance.

6.4 Conclusion

The use of geostatistics provides an effective way to integrate earth science and spatial science with engineering. This research project has demonstrated the necessary steps to develop a geological model that characterizes the distribution of subsurface properties using a two-point geostatistics approach. Additionally this study has directly exemplified how GIS tools can be combined with engineering techniques based on geological concepts and use genuine field data to solve complex real-world problems with the aid of software interoperability. The oil field represents a conventional petroleum reservoir and preliminary evaluation of the hard data obtained from direct subsurface field measurements presents ordinary kriging and sequential Gaussian simulation as valid methods for the aforementioned analysis and modeling. A satisfactory variogram was defined incorporating geological and statistical assumptions, and used for

the kriging and conditional simulation interpolations to map the field properties in a volumetric extent. The procedures taken to construct the variogram as well as the major aspects and the different components of these techniques including the variogram parameters, kriging parameters and interpolation conditions are discussed throughout the report. Results include 3D static models and multiple possible realizations of the spatial distribution of electrical properties of rocks and their fluids throughout the field domain. And because of the direct relationship of SP and R with additional reservoir properties and their associated characteristics (such as permeability, porosity, water saturation) the geostatistical outputs provide useful information that can be used for further field modeling including numerical and inverse modeling. With the information provided and especially with the addition of subsequent engineering analyses such as reservoir simulation and history matching, it is possible to make more informed decisions for field operations aimed at improving petroleum development and management, including activities such as drilling and waterflooding.

Validation procedures included statistical calculations to assess local uncertainty and variability, as well as direct measurement comparisons. By way of comparing and evaluating the analyses the interpretable conclusion is that the modeling techniques performed do indeed provide a proper approach for reservoir characterization. Although the structural continuity of the reservoir appears to retain general consistency throughout the entire field, there is an apparent continuity trend (based on keen observations) where the upper half of the reservoir becomes slightly less continuous relative to the lower half. This small to modest apparent change reflected from the field continuity is probably due to geological phenomena attributed to the major thrusting experienced in the area.

Moreover, the confidence level in the models and interpreted results and the associated uncertainties due to the inherent variability and limitations in modeling subsurface geological formations always need to be taken into consideration. The interoperability of this project between GIS, engineering and geology alike is expected to promote the growing field of geoinformatics and thus help bridge the gap in interdisciplinary collaboration for data intensive research in the natural and applied sciences.

REFERENCES

AAPG UGM SC. One day course review: Hydrocarbon prospect in western indonesia | *AAPG UGM - SC. in American Association of Petroleum Geologists* (database online). 2011 (cited 03/18 2014). Available from http://ugmsc.wordpress.com/2011/03/30/one-day-course-review-hydrocarbon-prospect-in-western-indonesia/.

Alvarado, Vladimir, and Eduardo Manrique. 2010. Enhanced oil recovery: An update review. *Energies* 3 (9): 1529-75.

Awange, Joseph L., 1969, and John B. Kyalo Kiema. 2013. *Environmental geoinformatics: Monitoring and management*. Berlin ;New York: Springer Berlin Heidelberg.

Babish, Gregg. 2000. Geostatistics without tears: A practical guide to geostatistics, variograms and kriging. *Environment Canada, Ecological Research Division, Environmental Conservation Branch.*

Bell, Julia. IPAA ranks top 10 U.S. oil and natural gas records. in Independent Petroleum Association of America (database online). Washington, D.C., 2014 (cited March/04 2014). Available from http://www.ipaa.org/2013/07/30/ipaa-ranks-top-10-u-s-oil-natural-gas-records/.

Burrough, P. A. 2001. GIS and geostatistics: Essential partners for spatial analysis. *Environmental and Ecological Statistics* 8 (4): 361-77.

California State Parks. Geography. in State of California Department of Parks and Recreation (database online). Sacramento, CA, 2013 (cited March/05 2014). Available from http://www.parks.ca.gov/?page_id=21971.

Caumon, Guillaume. 2010. Towards stochastic time-varying geological modeling. *Mathematical Geosciences* 42 (5): 555-69.

Chiles, Jean-Paul, and Pierre Delfiner. 1999. *Geostatistics: Modeling spatial uncertainty*. New York: Wiley.

CIPA. About CIPA - california independent petroleum association. in California Independent Petroleum Association (database online). Sacramento, CA, 2014 (cited March/05 2014). Available from http://www.cipa.org/i4a/pages/index.cfm?pageid=91.

Coats, K. H. 1969. Use and misuse of reservoir simulation models. *Journal of Petroleum Technology* 21 (11): 1391-8.

Delshad, Mojdeh. 2013. Using soap to revive mature oil fields. *The Way Ahead, Society of Petroleum Engineers* 9 (3): 28-9.

Deutsch, C. 2006. What in the reservoir is geostatistics good for? *Journal of Canadian Petroleum Technology* 45 (4).

Division of Oil, Gas and Geothermal Resources (DOGG). 1992. *CALIFORNIA OIL and GAS FIELDS volume II – southern, central coastal, and offshore california oil and gas fields.* Sacramento, CA: State of California Department of Conservation, TR12.

Dorsey, Ridgely. 1993. *Geologic review abacherli lease mahala field: Eastern puente hills san bernardino, california.* KMT Oil Company, .

Dubrule O, and Damsleth E. 2001. Achievements and challenges in petroleum geostatistics. *Petroleum Geoscience* 7 (SUPP): 1-.

Durham, D. L., and R. F. Yerkes. 1964. Geology and oil resources of the eastern puente hills area, southern california. *United States Geological Survey* 420 (B): 1-62.

Enhanced Oil Recovery Institute (EOIR). Enhanced oil recovery institute: Fall 2013 newsletter. in University of Wyoming (database online). Laramie, WY, 2013 (cited March/05 2014). Available from http://www.uwyo.edu/eori/news-and-updates/fall2013newsletter.pdf.

ESRI. Desktop help 10.0 - working with ArcGlobe and ArcScene. in esri.com [database online]. Redlands, CA, 2012 [cited March, 2014]. Available from http://help.arcgis.com/en/arcgisdesktop/10.0/help/index.html#//00q8000000sv000000.

Gorell, Sheldon B. 1995. Using geostatistics to aid in reservoir characterization. *The Leading Edge* 14 (9): 967.

GSI Works. Trimble handhelds. in Geospatial Innovations, Inc. (database online). 2009 (cited March/05 2014). Available from http://www.gsiworks.com/Handhelds.pdf.

Journel, Andre G. 2000. Geostatistics and petroleum geology. *Mathematical Geology* 32 (1): 139-41.

Kelkar, Mohan, and Godofredo Perez. 2002. *Applied geostatistics for reservoir characterization*. Richardson, TX: Society of Petroleum Engineers Inc.

KMT Oil Company, Inc., 2014. Mr. James Kellogg. Owner and operator. Conversation. http://owr.conservation.ca.gov/WellSearch/WellSearch.aspx

Krivoruchko, Konstantin. 2012. Empirical bayesian kriging: Implemented in ArcGIS geostatistical analyst. *Arcuser, Esri* 15 (4): 6-10.

Landmark Software. Sequential gaussian simulation. in Halliburton (database online). Houston, TX, 2011 (cited March/05 2014). Available from http://esd.halliburton.com/support/LSM/DSD/DSD/5000/5000_8/Help/mergedProjects/dsem/sequential_gaussian_simulation.htm.

Landscape Toolbox Wiki. Semivariogram analysis: Rangeland methods guide. in The Nature Conservancy and the USDA Agricultural Research Service (database online). Las Cruces, NM, (cited 03/2014 2014). Available from: http://wiki.landscapetoolbox.org/doku.php/spatial_analysis_methods:semivariogram_analysis.

Lowrie, William,. 2007. Geoelectricity. In *Fundamentals of geophysics.*, 252-259. Cambridge: Cambridge University Press, http://books.google.com/books?id=h2-NjUg4RtEC&pg=PA254#v=onepage&q&f=false .

Madden, Christopher, and Robert Yeats. 2008. *Paleoseismic and structural investigations to determine late quaternary slip rate for the chino fault, southeastern los angeles basin, california.* Santa Ana, CA: National Earthquake Hazards Reduction Program, 04HQGR0107.

McCammon, Richard B. ed. 1975. *Concepts in geostatistics*. New York: Springer-Verlag.

Myers, Donald. What is geostatistics**?**. in University of Arizona, Department of Mathematics (database online). 2013 (cited March/04 2014). Available from http://www.u.arizona.edu/~donaldm/homepage/whatis.html (accessed Tucson, AZ).

National Stripper Well Association. Stripper well facts. in National Stripper Well Association (NSWA) (database online). Oklahoma City, OK, 2014 (cited March/04 2014). Available from http://nswa.us/custom/showpage.php?id=25.

Nobre, M. M., and J. F. Sykes. 1992. Application of bayesian kriging to subsurface characterization. *Canadian Geotechnical Journal* 29 (4): 589-98.

Olea, Ricardo, Ronald Charpentier, Troy Cook, David Houseknecht, and Christopher Garrity. 2012. Geostatistical population-mixture approach to unconventional-resource assessment with an application to the woodford gas shale, arkoma basin, eastern oklahoma. *SPE Reservoir Evaluation & Engineering* 15 (5): 554-61.

Olson, Larry J. 1977. *Mahala oil field and vicinity.* Sacramento, CA: California Division of Oil & Gas, no. TR18, ftp://ftp.consrv.ca.gov/pub/oil/publications/tr18.pdf.

Optima Conservation Resources, 2014. Dr. Alberto Vasquez. President. Conversation. http://www.ioilexchange.com

PetroWiki. Geostatistical conditional simulation. in Society of Petroleum Engineers (database online). Richardson, TX, 2013 (cited March/05 2014). Available from http://petrowiki.org/Geostatistical_conditional_simulation.

———. Glossary:Conditional simulation. in Society of Petroleum Engineers (database online). Richardson, TX, 2013 (cited March/05 2014). Available from http://petrowiki.spe.org/Glossary%3AConditional_simulation.

———. Kriging and cokriging. in Society of Petroleum Engineers (database online). Richardson, TX, 2013 (cited March/05 2014). Available from http://petrowiki.org/Kriging_and_cokriging.

———. Spontaneous (SP) log. in Society of Petroleum Engineers (database online). Richardson, TX, 2013 (cited March/05 2014). Available from http://petrowiki.org/Spontaneous_%28SP%29_log.

PolitiFact. A vast majority of the production in the united states comes from small independent oil and gas companies. in Tampa Bay Times (database online). St. Petersburg, FL, 2014 (cited March/04 2014). Available from http://www.politifact.com/truth-o-meter/statements/2011/may/03/dan-boren/rep-dan-boren-says-most-domestic-oil-produced-smal/.

Radhakrishna, I., and T. Gangadhara Rao. 1990. Evaluation of hydrogeochemical parameters with spontaneous potential logs. *Journal of Hydrology* 114 (3): 245-57.

Ranken Energy. Useful information: A partial list of products made from petroleum (144 of 6000 items). in Ranken Energy Corporation (database online). Edmon, OK, (cited March/05 2014). Available from http://www.ranken-energy.com/Products%20from%20Petroleum.htm.

Remy, Nicolas, Alexandre Boucher, and Jianbing Wu. 2009. *Applied geostatistics with SGeMS: A User's guide*. Paperback ed. New York, NY: Cambridge University Press.

Schechter, David. Formation evaluation and the analysis of reservoir performance**.** chapter 9: Spontaneous potential. in Department of Petroleum Engineering, Texas A and M University (database online). College Station, TX, 2014 (cited March/05 2014). Available from http://www.pe.tamu.edu/blasingame/data/z_zCourse_Archive/P663_10B/P663_Schechter_Notes/SP%20Log.PDF.

Schlumberger. Oilfield glossary: Wireline log. in Schlumberger Limited (database online). Houston, TX, 2014 (cited March/05 2014). Available from http://www.glossary.oilfield.slb.com/en/Terms/w/wireline_log.aspx.

Schoenherr, Allan A. 1992. *A natural history of california*. Vol. 56. Berkeley: University of California Press.

Sinha, A. Krishna, Ian Jackson, Peter Fox, Deborah McGuinness, Dogan Seber, Herman Zimmerman, Zaki Malik, et al. 2010. Geoinformatics: Transforming data to knowledge for geosciences. *GSA Today* 20 (12): 4-10.

Sinha, A. Krishna, David Arctur, Ian Jackson, and Linda and Gundersen. 2011. *Societal challenges and geoinformatics*. Boulder, CO: Geological Society of America.

Stags, H. M., and E. F. Herbeck. 1971. Reservoir simulation models an engineering overview. *Journal of Petroleum Technology* 23 (12): 1428-36.

Thomas L. Wright. 1987. Structural geology and tectonic evolution of los angeles basin. *AAPG Bulletin* 71 , http://archives.datapages.com/data/specpubs/basinar3/images/a135/a1350001/0000/chapter3.pdf.

Thompson, Mark. U.S. to become biggest oil producer and energy independent. in Cable News Network (CNN Money) (database online). London, UK, 2012 (cited March/04 2014). Available from http://money.cnn.com/2012/11/12/news/economy/us-oil-production-energy/.

Tzimas, E., A. Georgakaki, C. Garcia Cortes, and S. D. Peteves. 2005. *Enhanced oil recovery using carbon dioxide in the european energy system.* Petten, Netherlands: Institute for Energy, European Commission Directorate-General Joint Research Centre, EUR 21895 EN.

U.S. Energy Information Administration. How much oil does the united states consume per year?. in U.S. Department of Energy (database online). Washington, D.C., 2012 (cited March/04 2014). Available from http://www.eia.gov/tools/faqs/faq.cfm?id=33&andt=6.

United States Geological Survey, 2014. http://nationalmap.gov/viewer.html

United States Geoscience Information Network. 2011. *California active faults*. Geothermal data project., ed. United States Geological Survey, Association of American State Geologists, Arizona Geological SurveyArcGIS Online, Open Geospatial Consortium.

Wilson, John P. 1955- (John Peter), and A. Stewart Fotheringham. 2008. *The handbook of geographic information science*. Vol. 7. Malden, MA: Blackwell Pub.

APPENDIX I: Cross-section with stratigraphic log of adjacent reservoirs in Mahala

Obtained from CA DOGGR 1992 Report #TR12

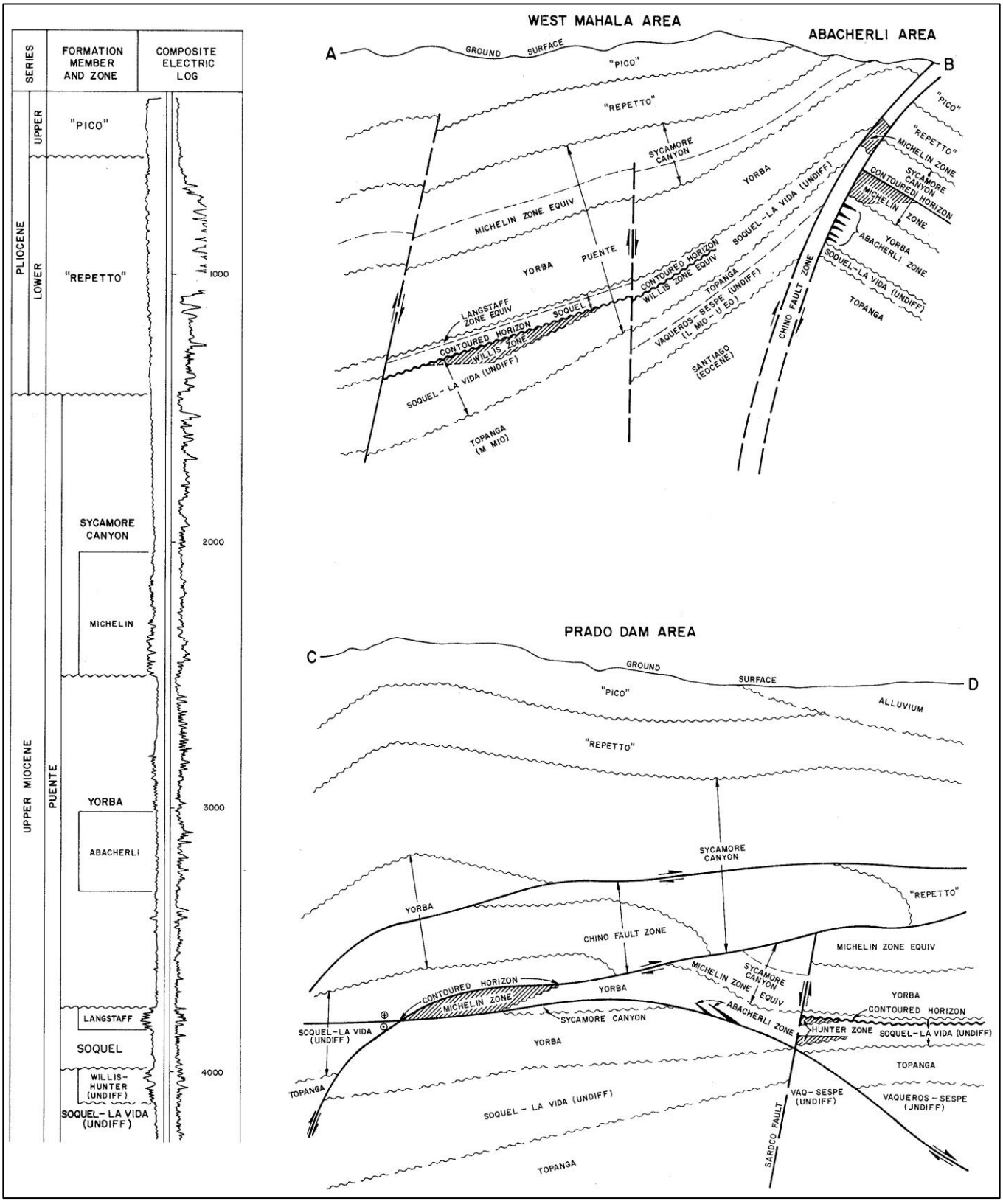

APPENDIX II: Stratigraphic Column of Mahala Oilfield

Obtained from DOGG Report #TR18

Series		Formation	Member / Producing Zone	Approximate thickness (feet) — Abacherli area	Mahala area	West Mahala area	Prado Dam area	Lithology
Holocene–Pleistocene		alluvium–terrace deposits		0	0	0	0–500	Silt, sand, clay and gravel, light-gray to reddish-brown; a few cobbles and boulders. Contains fresh water. Nonmarine.
		(unconformity)						
Pliocene	upper	"Pico"		0–500	1,300	300–900	0–500	Sandstone and conglomerate, white-to-brown, poorly consolidated; sandy siltstone and shale. Contains fresh water. Marine.
		(unconformity)						
	lower	"Repetto"		0–600	700	300–800	400–600	Shale, sandstone and conglomerate, buff-to-gray, poorly consolidated. Contains fresh water. Marine.
Miocene	upper	Puente	Sycamore Canyon	900	1,000	1,200	1,100	Sandstone, conglomerate (predominant at base), siltstone and shale, buff- to dark-brown, white-to dark-gray, thin-bedded, hard, calcareous to poorly consolidated. Contains fresh water. Marine.
			Michelin	400			250	
			Yorba	700	1,000	1,300	600	Shale and siltstone, dark-brown, locally dark-gray, laminated, fossiliferous, fish scales common, commonly fractured, interbedded with hard, thin-bedded, calcareous shale and 4-inch to 5-foot beds of fine- to coarse-grained white-gray sandstone. Marine.
			Abacherli	600	900		100	
			Soquel	200	250	250	200	Sandstone, gray or buff-to-brown, silty, very fine-grained; siltstone, yellowish-brown, interbedded with shale. Marine.
			Langstaff		50			
			Soquel–La Vida	0	50	200	50	Sandstone, interbedded with shale. Marine. Willis zone: turbidite, fine- to coarse-grained sandstone, interbedded with shale. Hunter zone: gray-to-buff, fine- to coarse-grained sandstone and conglomerate
			Willis		0–50	0–200		
			Hunter				50	
			La Vida	300	400	500	300	Shale and siltstone, dark-brown or gray-to dark-gray, fossiliferous, fish scales and phosphatic nodules common, interbedded with thin-bedded, hard, calcareous shale, and thin-bedded sandstone. Marine.
	middle	(unconformity)						
		Topanga		350	50 +	50 +	400	Sandstone, gray-to-buff, pebbly, very hard, interbedded with conglomerate; siltstone and shale, gray-green. Marine.
	lower +							
Oligocene	upper ↑	Vaqueros–Sespe		300			300 +	Sandstone and conglomerate, reddish-brown, clayey; siltstone, greenish-gray. Marine and nonmarine.
Eocene	upper	(unconformity)						
	middle	Santiago		600				Interbedded sandstone, conglomerate and siltstone, gray-to-buff, green and red volcanic clasts. Marine.
		(unconformity)						
Paleocene		Silverado?		200 ±				Sandstone, gray-to-buff, gritty, with basal red shale; conglomerate and siltstone. Marine and nonmarine.
		(unconformity)						
Upper Cretaceous		Ladd?		100 ±				Siltstone, gray-to-black; sandstone, greenish-gray. Marine.
		Trabuco?		100 ±				Conglomerate, cobble-to-boulder, buff-to gray-green, red granite clasts. Nonmarine.
		(unconformity)						
Upper Cretaceous or older		Plutonic basement rocks						Quartz diorite and granodiorite?

APPENDIX III: Structural Contour Map of Chino Fault Zone
Obtained from *USGS NEHRP 2008 report # 04HQGR0107*

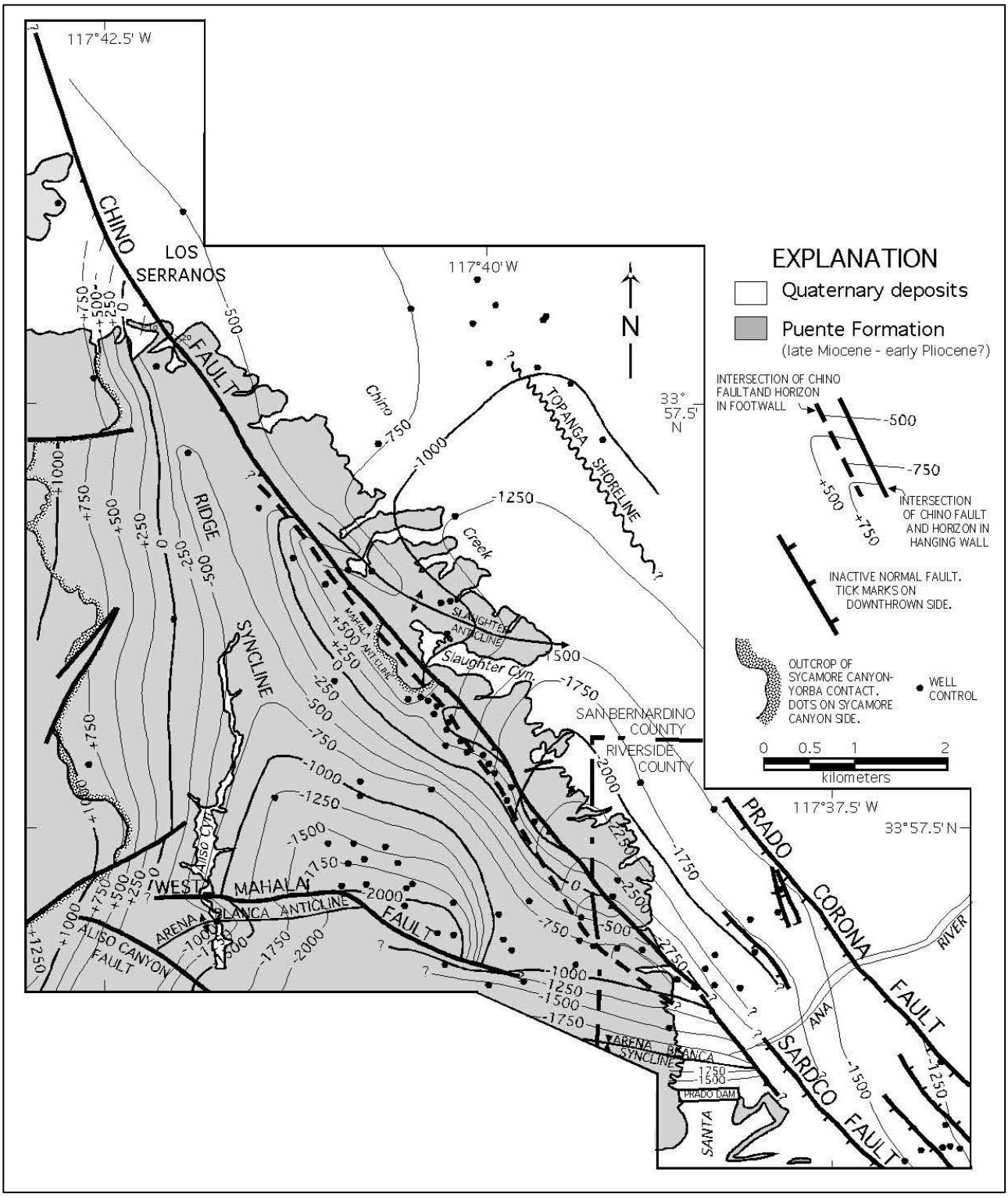

APPENDIX IV: Geological Contour Map
Obtained from DOGG Report #TR18

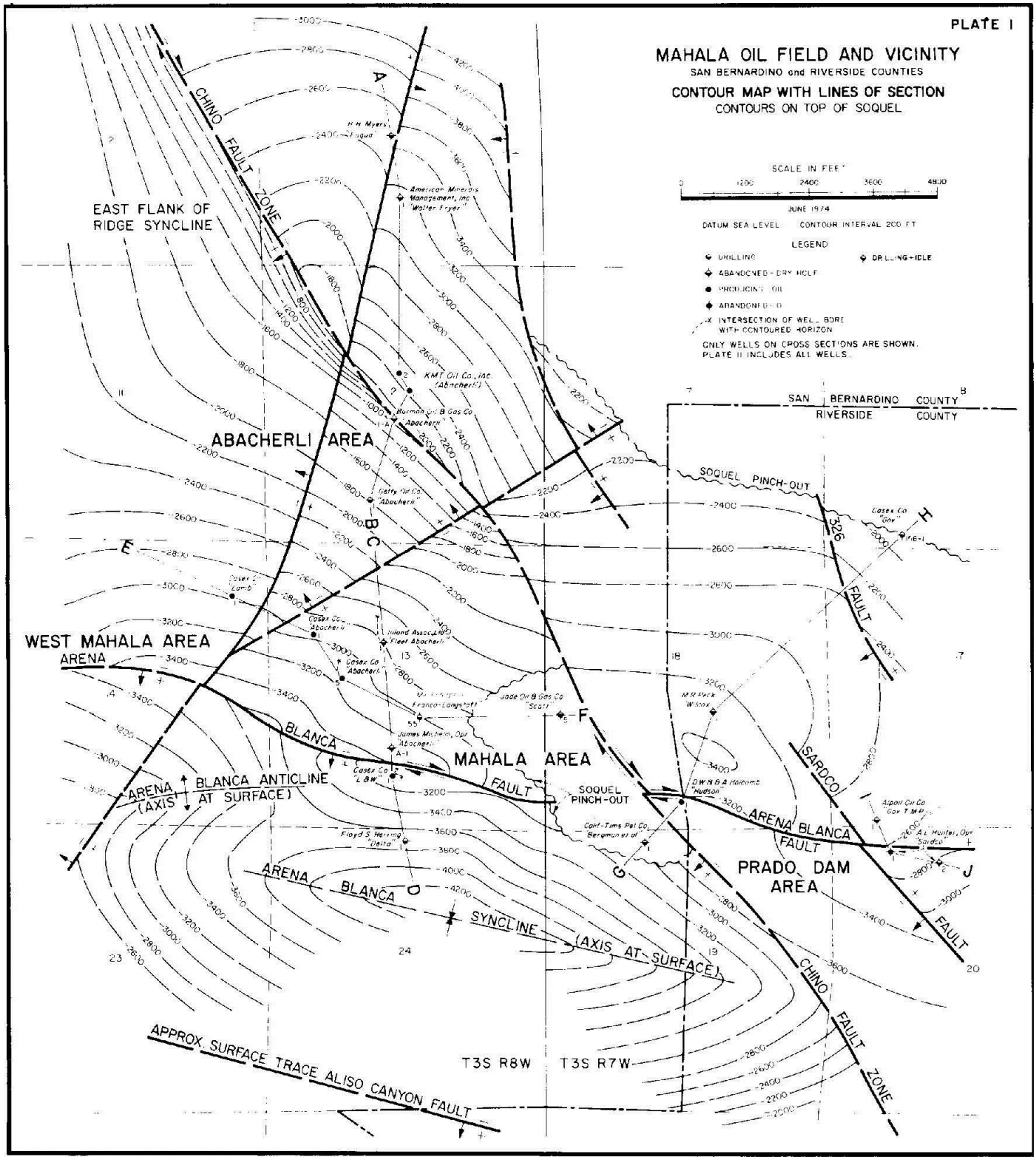

APPENDIX V: Structural Contour/Isopach Map of Mahala and West Mahala Fields

Obtained from CA DOGGR 1992 Report #TR12

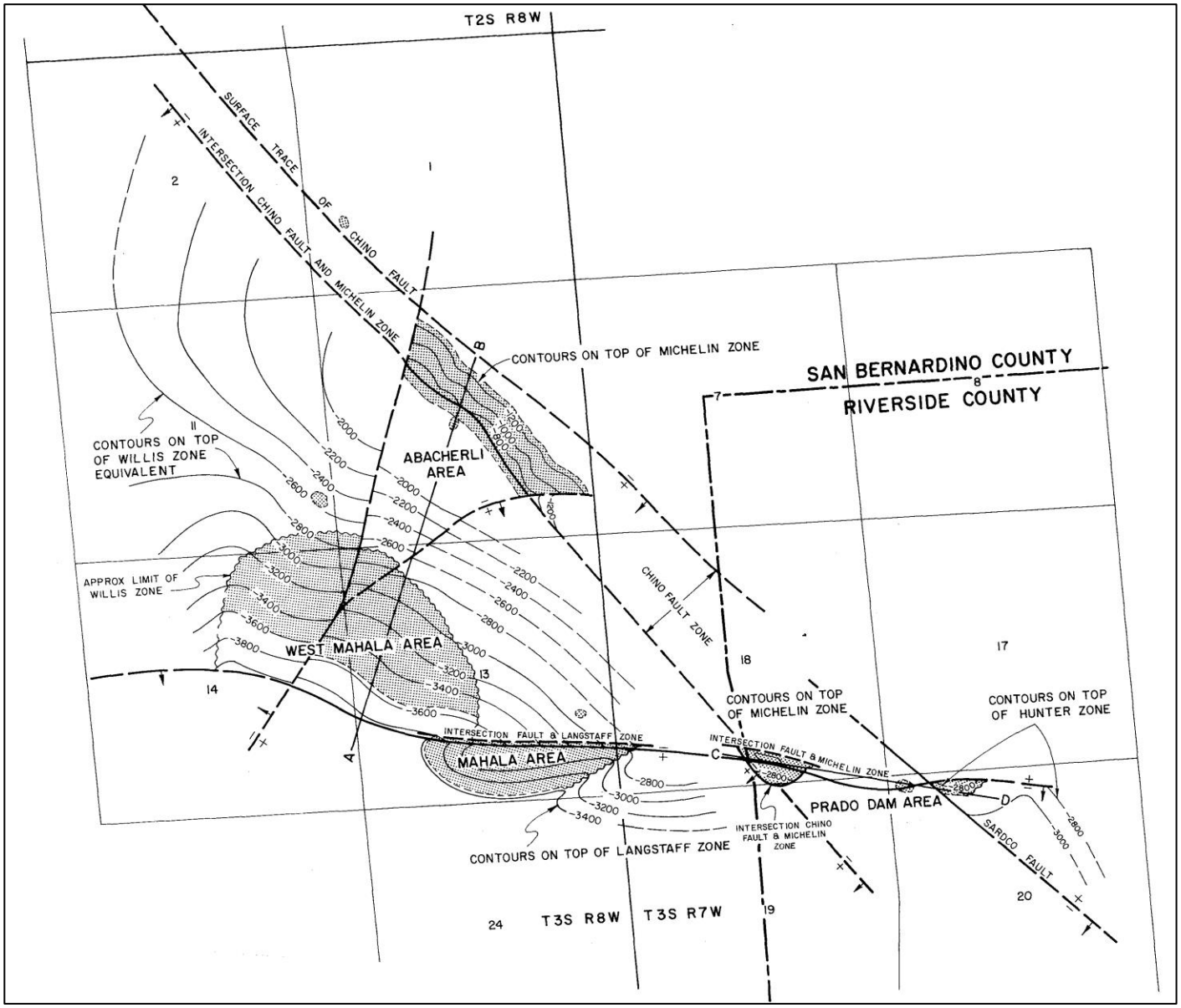

APPENDIX VI: INTEGRATED VOLUMETRIC AND NUMERICAL MODELS

Obtained from combining Matlab, SGeMS, Excel and ArcGIS using Reservoir Data